Heat-Air-Moisture Transport

Measurements on Building Materials

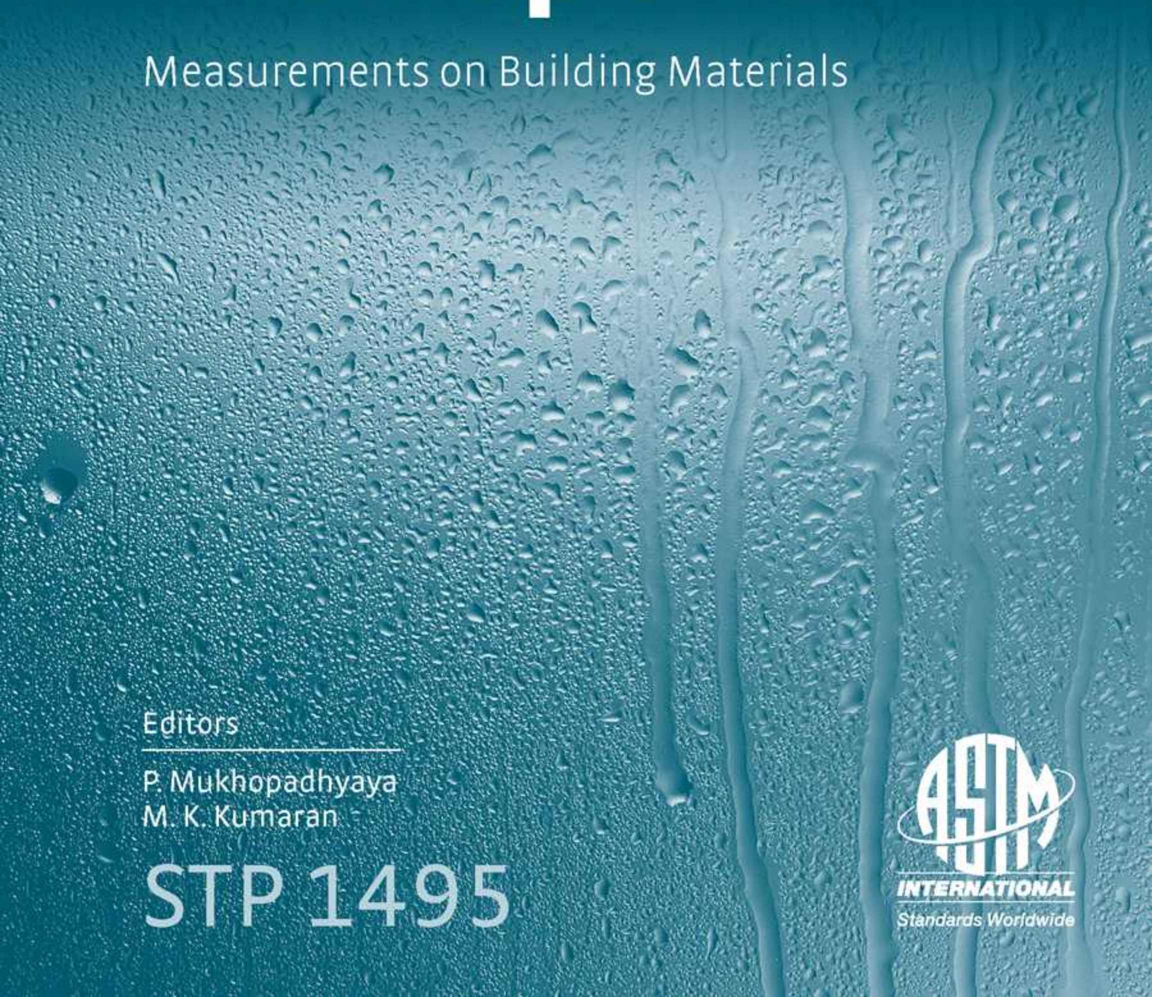

Editors

P. Mukhopadhyaya
M. K. Kumaran

STP 1495

STP 1495

Heat-Air-Moisture Transport: Measurements on Building Materials

Dr. P. Mukhopadhyaya and Dr. M. K. Kumaran,
editors

ASTM Stock Number: STP1495

ASTM
100 Barr Harbor Drive
PO Box C700
West Conshohocken, PA 19428-2959

INTERNATIONAL
Standards Worldwide

Printed in the U.S.A.

Library of Congress Cataloging-in-Publication Data

Heat-air-moisture transport : measurements on building materials /
Phalguni Mukhopadhyaya and Mavinkal Kumaran, editors.
p. cm.
ISBN 978-0-8031-3422-5
1. Dampness in buildings. 2. Heat--Transmission. I. Mukhopadhyaya,
Phalguni. II. Kumaran, Mavinkal.

TH9031.H43 2007
693.8' 93--dc22

2007040740

Photocopy Rights

Peer Review Policy

Each paper published in this volume was evaluated by two peer reviewers and at least one editor. The authors addressed all of the reviewers' comments to the satisfaction of both the technical editor(s) and the ASTM International Committee on Publications.

The quality of the papers in this publication reflects not only the obvious efforts of the authors and the technical editor(s), but also the work of the peer reviewers. In keeping with long-standing publication practices, ASTM International maintains the anonymity of the peer reviewers. The ASTM International Committee on Publications acknowledges with appreciation their dedication and contribution of time and effort on behalf of ASTM International.

Printed in the USA
November 2007

Foreword

The First Symposium on Heat-Air-Moisture Transport: Measurements on Building Materials was held in Toronto, Ontario, Canada on 23 April 2006. ASTM Committee C-16 on Thermal Insulation served as its sponsor. The symposium chairs and co-editors of this publication were Phalguni Mukhopadhyaya and Mavinkal K. Kumaran of the National Research Council, Ottawa, ON, Canada.

Contents

Overview

Since the inception in 1938, ASTM Committee C16 has been working on various aspects concerning the development of standards, promotion of knowledge, and stimulation of research pertaining to the heat-air-moisture transport through building materials (e.g. thermal insulation materials, products, systems, and associated coatings and coverings). During this time the committee has seen many changes and challenges in the building construction industry and invariably responded effectively to address the pressing concerns of the time.

In recent years, the building construction industry is making increased use of sophisticated computer based design tools for moisture design of building envelopes. These design tools invariably require well-defined heat-air-moisture transport properties of component building materials. The basics for heat-air-moisture transport through building materials had been researched upon for a long-time all over the world. However, there is a glaring lack of unifomity in the ways these transport processes are measured in various laboratories all over the world. The results coming out from various test methods are also presented in many different ways. This leads to a very confusing scenario for the end users of these material properties. Globally there is a great need to resolve this issue urgently so that the measured material properties are reliable, consistent and meaningful irrespective of the laboratory and personnel involved in the process.

The primary goal of the 1st symposium of "Heat-Air-Moisture Transport: Measurements on Building Materials," held in Toronto, Canada on April 23, 2006 was to provide a forum to discuss the state-of-the-art research and development activities on the measurement of heat-air-moisture transport through building materials, related to international standards. This STP presents selected peer reviewed papers from the symposium authored by renowned international experts. The STP starts with a paper that outlines the importance and necessity of reliably measured hygrothermal material properties, and the papers that follow deal with the individual material properties. Some of them identify the need for improvement in existing standards and others point towards new measurement techniques and corresponding standards.

Finally, the editors would like to acknowledge that this STP is a product of tremendous diligent efforts of many people. In particular, the editors would like to thank ASTM symposium organizing committee, all of the authors and paper reviewers who devoted their time for this endeavor. Special thanks are due to Dorothy Fitzpatrick and Timothy Brooke at ASTM for their support, timely assistance, and efficient handling of all minute details.

Dr. P. Mukhopadhyaya
National Research Council
Ottawa, ON, Canada

Dr. M. K. Kumaran
National Research Council
Ottawa, ON, Canada

Journal of ASTM International, Vol. 4, No. 2
Paper ID JAI100460
Available online at www.astm.org

Hugo S. L. C. Hens[1]

Modeling the Heat, Air, and Moisture Response of Building Envelopes: What Material Properties are Needed, How Trustful Are the Predictions?

ABSTRACT: The physical models which form the basis for the different software tools used to predict heat, air, and moisture response of building envelopes seem quite diverse. For example, various "potentials" are used, and each individual potential demands apparently different properties. Anyhow, when digging into the physics and confronting the theory with what is measurable, then an array of eight basic material characteristics appear, all backed by an experimental rationale. Adapting that array to the potentials in use is not a question of creating new properties but of implementing the basic ones into potential-adapted expressions. A different problem, however, is that these basic properties are macroscopic in nature, i.e., represent the complexity of a material at the micro-scale by one single "average" number. That introduces restrictions as to the use of the property values measured experimentally. Hence, those restrictions are typically mixed up with the inability of the actual software packages to represent reality in full detail. Too many times, assumed incorrectness of the property values are blamed for causing the differences found between the predicted and real heat, air, moisture response of envelope parts. That inability, instead, should convince researchers and building engineers that the way to gain a well balanced understanding of the heat, air, and moisture response of envelopes is not by modeling only but by combining modeling with testing and field experience.

KEYWORDS: heat, air and moisture transfer, models, material properties, application

Introduction

In Europe, the history of full heat, air, and moisture modeling goes back to 1932 when Hirsch published his book on drying technology [1]. That book was reworked in 1956 by Krischer and Kröll [2]. In his book, Krischer treats the basics of combined heat and mass transfer and applies it to industrial drying. The chapter on moisture transport sees the water vapor resistance factor and the moisture diffusivity introduced as main material properties that govern drying by vapor diffusion and capillary suction. Krischer anyhow was not the only one digging in the field of knowledge. In 1955, a German translation of a book written by a Russian scientist, Lykow, was published by VEB Verlag Technik in the DDR [3]. Like Krischer, Lykow also analyzed drying and came up with analogous properties. De Vries was the last of the founding fathers, with his theory of combined heat and moisture transfer in porous materials, published in 1958 [4].

In 1958–1959, Glaser advanced a simple method to control interstitial condensation in cold store walls [5–7]. As most materials used in cold stores are noncapillary, as the walls are airtight and as the temperature and vapor pressure difference are close to constant, steady state vapor diffusion remained as the only moisture transport mechanism involved. Thus, the method gave quite good results for those types of envelopes. That motivated other authors to extend the Glaser rationale to building envelopes, which was a step too far [8]. None of the conditions fulfilled by cold store walls in fact are typical for building envelopes. Transiently loaded, air-tightness not guaranteed, many materials capillary active, gravity not negligible, etc., though the Glaser approach was charming by its simplicity. In North America, a method analogous to the Glaser rationale was adapted, based on research done during the 1930s [9].

In the years that followed the 1950s, some authors upgraded the Glaser method [10–12] while others returned to the work by de Vries, trying to measure some of the material properties he introduced, and translating the PDEs into numerical models and computer software [13–24].

Manuscript received February 13, 2006; accepted for publication January 19, 2007; published online February 2007. Presented at ASTM Symposium on Heat-Air-Moisture Transport: Measurements on Building Materials on 23 April 2006 in Toronto, Canada; P. Mukhopadhyaya and M. Kumaran, Guest Editors.

[1] Professor at the K. U. Leuven, Department of Civil Engineering, Laboratory of Building Physics–Kasteelpark Arenberg 40, B-3001 Leuven, Belgium.

Combined Heat, Air, and Moisture Models

Combined heat, air, and moisture modeling is based on the paradigms of energy and mass conservation, in combination with diffusive and convective flow equations and a few equations of state. One should thus expect that all models look the same and use identical material properties. On first sight, however, in the models actually commercialized, the heat and moisture balances look quite different. The Match® software for example is based on the following PDEs [25]

Air balance not considered

$$\textit{Heat balance} \quad \rho c_p \frac{\partial \theta}{\partial t} = \nabla(\lambda \, \nabla \, \theta) + h_v \, \nabla \, (\delta_v \, \nabla \, p) \tag{1}$$

$$\textit{Moisture balance} \quad \rho \frac{\partial X}{\partial t} = \nabla(\delta_v \, \nabla \, p + k_w \, \nabla \, s) \tag{2}$$

with ρ density of the moist material (kg/m^3), θ temperature (°C), ∇ the nabla operator reflecting a divergence when applied on a vector and a gradient when applied on a scalar, λ thermal conductivity (W/(m.K)), X moisture ratio (kg/kg), h_v heat of evaporation (J/kg), δ_v vapor permeability (s), p partial water vapor pressure (Pa), k_w water permeability (s) and s capillary suction (Pa). Potentials in the moisture balance are vapor pressure and capillary suction.

The Wufi® software in turn uses as PDEs [26]:

Air balance not considered

$$\textit{Heat balance} \quad \frac{\partial H}{\partial \theta}\frac{\partial \theta}{\partial t} = \nabla(\lambda \, \nabla \, \theta) + h_v \, \nabla \, (\delta_v \, \nabla \, (\phi p_{\text{sat}})) \tag{3}$$

$$\textit{Moisture balance} \quad \frac{dw}{d\phi}\frac{\partial \phi}{\partial t} = \nabla(\delta_v \, \nabla \, (\phi p_{\text{sat}}) + D_\phi \, \nabla \, \phi) \tag{4}$$

with H enthalpy in J/K, p_{sat} partial water vapor saturation pressure at a temperature θ (Pa), ϕ relative humidity (-) and w moisture content (kg/m^3). Potentials in the moisture balance are the product of relative humidity and partial water vapor saturation pressure, which equals partial water vapor pressure and relative humidity.

To compare with, in his article on simultaneous transfer of heat and moisture in porous media, De Vries [4] proposed as equations for combined heat and moisture transport:

$$\textit{Heat balance} \quad \frac{\partial H}{\partial t} = \rho_w \, \nabla \, (D_{T,T} \, \nabla \, \theta + D_{T,\Psi} \, \nabla \, \Psi) \tag{5}$$

$$\textit{Moisture balance} \quad \frac{\partial w}{\partial t} = \rho_w \, \nabla \, (D_{\Psi,T} \, \nabla \, \theta + D_{\Psi,\Psi} \, \nabla \, \Psi) \tag{6}$$

the potentials being temperature and volumetric moisture ratio (Ψ).

Properties Involved

Heat and Moisture

The right-hand side of all equations represents transfer of heat or moisture. Seven different material properties and five different (pseudo?) potentials are used to quantify the flows. While the potentials temperature, partial water vapor pressure, relative humidity, capillary suction and moisture ratio are well known, only two of the seven properties are evenly well known: thermal conductivity λ and water vapor permeability δ_v. The left-hand side of the equations models storage. Normally that side should contain as many storage defining characteristics as the number of potentials intervening at the transfer side. All except one in both the heat and the moisture balance are so tiny that they may be overlooked. Match®

specifies the characteristic that governs heat storage: volumetric specific heat capacity, the product of specific heat capacity at constant pressure (c_p) and density (ρ). Hence, sensible enthalpy used in Wufi® and by De Vries may be written as $H = \rho c_p \theta$, meaning that the thermal balances in the De Vries equation, Wufi® and Match® are identical. Also the moisture storage in the two models does not differ. In fact, $\rho\,\partial X/\partial t$ can be written as $\partial w/\partial t$, which in turn may be transformed into $(dw/d\phi)(\partial\phi/\partial t)$ with the derivative $dw/d\phi$ equal to the slope of the sorption/desorption curve of the capillary porous material. That slope is called the specific moisture content ξ_ϕ^w, a property which mirrors the specific heat capacity. Instead, a derivative for suction can also be used $((dw/ds)(\partial s/\partial t))$, giving as specific moisture content: ξ_s^w.

In both Wufi® and Match® partial water vapor pressure activates vapor transfer. Liquid transfer, however, is mobilized by capillary suction in Match® and relative humidity in Wufi®. That choice in Wufi® is based on Künzel's simplification that Fickian-like diffusion is governed by the geometry of the porous system only, tuning vapor permeability as a constant to be measured in a dry cup test, while the increase in apparent vapor permeability at high relative humidity is caused by surface flow in the adsorbed water layers covering the pore walls. That flow goes in a direction opposite to the gradient in relative humidity.

Can both liquid parts be unified? The answer is yes. A gradient in relative humidity is easily rewritten as $\nabla\phi = (d\phi/ds)\nabla s$, which means that the transport properties k_m and D_ϕ are linked by:

$$D_\phi = k_w \frac{ds}{d\phi} \tag{7}$$

In moist capillary porous materials, capillary suction close to equilibrium now obeys Thompson's law:

$$s = \rho_w RT \ln(\phi) \tag{8}$$

meaning that the derivative $ds/d\phi$ is changeable into a function of relative humidity, which makes the moisture transfer coefficient D_ϕ transposable into a moisture permeability k_w. Thus, Wufi® and Match® use essentially the same equations and demand the same material properties. Besides, in noncapillary porous materials, suction does not exist. Anyhow, once interstitial condensation has brought the moisture ratio close to saturation, external pressures and gravity become the movers.

Is a same unification doable with the De Vries equations? Let us return to the basics. Moisture transport above freezing combines two flows: vapor and liquid. The vapor flow is typically described by a Fickian-like diffusion equation:

$$g_v = -\delta_v \nabla p \tag{9}$$

That equation is easily transformed into a two potentials expression:

$$\begin{aligned} g_v &= -\delta_v \nabla (p_{\text{sat}}\phi) = -\delta_v\left(\phi \frac{dp_{\text{sat}}}{d\theta}\nabla\theta + p_{\text{sat}}\nabla\phi\right) = -\rho_w\left(\delta_v \frac{\phi}{\rho_w}\frac{dp_{\text{sat}}}{d\theta}\nabla\theta + \delta_v \frac{p_{\text{sat}}}{\rho_w}\frac{d\phi}{d\Psi}\nabla\Psi\right) \\ &= -\rho_w\left(D_{\Psi,\theta}^v \nabla\theta + D_{\Psi,\Psi}^v \nabla\Psi\right) \end{aligned} \tag{10}$$

with:

$$D_{\Psi,\theta}^{\text{v}} = \delta_v \frac{\phi}{\rho_w}\frac{dp_{\text{sat}}}{d\theta}$$

$$D_{\Psi,\Psi}^v = \delta_v \frac{p_{\text{sat}}}{\rho_w}\frac{d\phi}{d\Psi} = \delta_v \frac{p_{\text{sat}}}{\xi_\phi^w} = \delta_v \frac{d\phi}{ds}\frac{p_{\text{sat}}}{\xi_s^w} \tag{11}$$

or, the vapor part of the strange moisture properties De Vries uses, combines quantities of state (partial water vapor saturation pressure as a function of temperature) with two typical vapor-related material properties: vapor permeability and specific moisture content.

The liquid part stands for capillary flow:

$$g_l = -k_m \nabla s \tag{12}$$

As for vapor, that equation could be rewritten as:

$$g_1 = -\rho_w\left(\frac{k_m}{\rho_w}\frac{ds}{d\theta}\nabla\theta + \frac{k_m}{\rho_w}\frac{ds}{d\Psi}\nabla\Psi\right) = -\rho_w\left(0.17\ 10^{-3}\frac{k_m}{\rho_w}\nabla\theta + \frac{k_m}{\rho_w}\frac{ds}{d\Psi}\nabla\Psi\right) = -\rho_w(D^{\mathrm{l}}_{\Psi,\theta}\nabla\theta + D^{\mathrm{l}}_{\Psi,\Psi}\nabla\Psi) \tag{13}$$

with

$$D^{\mathrm{l}}_{\Psi,\theta} = 0.17\ 10^{-3}\frac{k_m}{\rho_w}$$

$$D^{\mathrm{l}}_{\Psi,\Psi} = \frac{k_m}{\rho_w}\frac{ds}{d\Psi} = \frac{k_m}{\xi^w_s} \tag{14}$$

Again, the two typical material properties appear: moisture permeability and specific moisture content.

When combining liquid and vapor, parallel flow is assumed, meaning that each cut through a material crosses pores where vapor mitigates and pores where liquid moves. Summing up both flow equations gives:

$$g = -\rho_w[(D^v_{\Psi,T} + D^{\mathrm{l}}_{\Psi,T})\nabla\theta + (D^v_{\Psi,\Psi} + D^{\mathrm{l}}_{\Psi,\Psi})\nabla\Psi] = -\rho_w(D_{\Psi,T}\nabla\theta + D_{\Psi,\Psi}\nabla\Psi) \tag{15}$$

with

$$D_{\Psi,\theta} = \frac{1}{\rho_w}\left(\delta_v\phi\frac{dp_{\mathrm{sat}}}{d\theta} + 0.17\ 10^{-3}k_m\right)$$

$$D_{\Psi,\Psi} = \frac{1}{\rho_w}\left(\rho_w\delta_v\frac{d\phi}{ds}\frac{p_{\mathrm{sat}}}{\xi^w_s} + \frac{k_m}{\xi^w_s}\right) \tag{16}$$

Match® and Wufi® do not consider the temperature driven liquid flow, arguing that it is minimal compared to the vapor part. With that simplification in mind, the De Vries moisture balance transforms into the Match®/Wufi® moisture equation.

In the thermal balance, three flows intermix: heat conduction, vapor related sensible enthalpy mitigation, and liquid related sensible enthalpy mitigation. The last two are typically set zero, which is acceptable as long as both mass flows are very small. As heat source or sink we have a change of state from vapor to liquid and vice versa. That change is governed by the divergent of the vapor flow, or:

$$\begin{aligned}
\rho c\frac{\partial\theta}{\partial t} &= \rho_w\left[\nabla\left(\frac{\lambda}{\rho_w}\nabla\theta\right) + \nabla\left(\frac{\delta_v}{\rho_w}\nabla p\right)\right] \\
&= \rho_w\left[\nabla\left(\frac{\lambda}{\rho_w}\nabla\theta\right) + \mathrm{l}_b\nabla\left(\delta_v\frac{\phi}{\rho_w}\frac{dp_{\mathrm{sat}}}{d\theta}\nabla\theta + \delta_v\frac{p_{\mathrm{sat}}}{\xi^w_\phi}\nabla\Psi\right)\right] \\
&= \rho_w\left[\nabla\left[\left(\frac{\lambda}{\rho_w} + \mathrm{l}_b\delta_v\frac{\phi}{\rho_w}\frac{dp_{\mathrm{sat}}}{d\theta}\right)\nabla\theta\right] + \nabla\left(\mathrm{l}_b\delta_v\frac{p_{\mathrm{sat}}}{\xi^w_\phi}\nabla\Psi\right)\right] = \rho_w\nabla(D_{\theta,\theta}\nabla\theta + D_{\theta,\theta}\nabla\Psi)
\end{aligned} \tag{17}$$

with

$$D_{\theta,\theta} = \frac{1}{\rho_w}\left(\lambda + \mathrm{l}_b\delta_v\phi\frac{dp_{\mathrm{sat}}}{d\theta}\right)$$

$$D_{\Psi,\Psi} = \mathrm{l}_b\delta_v\frac{p_{\mathrm{sat}}}{\xi^w_\phi} \tag{18}$$

Again the De Vries equation is nothing else but a different way of writing the same balance as Match® and Wufi® do. Anyhow, the potential "volumetric moisture ratio" is not a real one as its value changes at each interface between materials. Real potentials, instead, should be continuous at interfaces, except if that interface itself forms a resistance.

Clearly, the De Vries model demands the same six basic material properties as Match® and Wufi®.

TABLE 1—*Array of basic material properties.*

	Storage	Transport
General	Density (ρ)	
Heat	Specific heat capacity (c_p)	Thermal conductivity (λ)
Air		Air permeability (k_m) or Air permeance coefficient (a) and flow exponent (n)
Moisture	Specific moisture content (ξ)	
Vapor		Vapor permeability (δ_v) or vapor resistance factor (μ)
Liquid		Moisture permeability (k_m)

Air

None of the three models scrutinized considers air flow. Some models already do. We refer to Janssens [27] and the recent versions of hygIRC [24], Latenite [19], and Delphin [22]. In general, air mitigation per unit of surface and time through an open-porous material is governed by:

$$g_a = -\,k_a \,\nabla\, (P_a - \rho_a g z \bar{u}_z) \tag{19}$$

with k_a air permeability, g acceleration by gravity, z height above a zero level, and $\bar{u}_z$ the unit vector in vertical direction. As air is hardly compressible under small pressure differences and storage barely plays, except when very fast air pressure changes are imposed which is the case when sound waves pass, the divergent of the flow may be set zero, giving as a balance:

$$\nabla[k_a \,\nabla\, (P_a - \rho_a g z \bar{u}_z)] = 0 \tag{20}$$

To describe air flow in cavities, air layers, cracks, joints, holes, voids, and fractionated layers, a flow equation of the form $g_a = -a\Delta(P_a - \rho_a g z \bar{u}_z)^n$ may be used with a the air permeance coefficient ($\mathrm{kg/(m^2.s.Pa}^n)$) and n the flow exponent. With those two flow equations, solving a problem of air mitigation means transforming the building detail under scrutiny into a hydraulic network and applying continuity in each of the nodes in the network. Hence, air flow adds a seventh (and eighth) material property to the list: air permeability or the air permeance coefficient and the flow exponent.

That hydraulic network methodology works fine as long as the air spaces are not too wide. If so, CFD should be used to describe the complex air flows which may develop in wide air spaces.

Property Array

Table 1 summarizes the material properties needed to describe combined heat, air, and moisture transfer in building parts. For most of them, appropriate measuring methods exist [28–30].

Anyhow, before a full hygrothermal evaluation can be done, also all equations of state, the exact geometry, the composition of the part or detail and some specific characteristics such as contact resistances between layers, the network of cracks, air layers, voids a.o. in the part when present, etc., have to be known.

What Do These Properties Reflect?

In General

Most models transform materials into a continuum that mixes up matrix and pores. Real materials, however, may consist of granules, bound by an intermediary paste. They may form a continuous, perforated mass, have a bubble-like structure or consist of fibers glued together in the contact points. Heat is conducted by the matrix and the air in the pores; the last in combination with radiation and sometimes convection in medium and larger voids. The fact that matrix and pores contribute together, explains why the thermal properties typify a material quite nicely. Round robin tests fit well and, if deviations are detected, they practically always are a consequence of inaccuracies or errors in measurement.

Mass flows instead develop in the pores. Their magnitude is shaped by the geometry of the porous system. As that geometry may differ between specimens of a same material, the air and moisture properties show large standard deviations and do not univocally typify a material. Results of round robin tests are

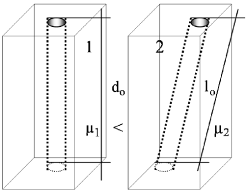

FIG. 1—*Path length.*

quite disappointing, even when the samples distributed come from the same batch. The spread encountered cannot be explained by measuring inaccuracies only, also differences in pore structure are responsible.

Water Vapor Permeability and Water Vapor Resistance Factor

Further discussion is restricted to the water vapor permeability and water vapor resistance factor. For a dry porous material, the water vapor permeability depends on two parameters: water vapor permeability of stagnant air and geometry of the porous system. Krischer and Kröll [2] differentiated between both by introducing the water vapor resistance factor, symbol μ. Scientifically, the water vapor resistance factor represents the ratio between the water vapor permeability of a layer of stagnant air and the water vapor permeability of the material:

$$\mu = \frac{\delta_{v,a}}{\delta_v} \tag{21}$$

As such, its value is shaped by the pore geometry. In fact, the only thing that counts in the case of Fickian-like diffusion is the open surface available for the water molecules to pass through. For straight pores with constant section, orthogonal to the surface and parallel to the gradient in partial water vapor pressure, the water vapor resistance factor therefore equals the inverse of open porosity (Ψ_o):

$$\mu = \frac{1}{\Psi} \tag{22}$$

If the straight pores make an angle α with the normal on the surface, then the path length increases and the water vapor resistance factor augments to:

$$\mu = \frac{1}{\Psi}\left(\frac{1}{\cos\alpha}\right) \tag{23}$$

with α the angle between the orthogonal and the inclined path (=d_o/l_o, see Fig. 1). When the section of the straight pores changes along the path of diffusion, the water vapor resistance factor becomes:

$$\mu = \frac{1}{\Psi}\left\{\frac{\Psi}{\cos\alpha}\sum_{i=1}^{n}\left[\sum_{j=1}^{m}\left(\frac{d_j}{A_j}\right)\right]\right\} \tag{24}$$

The part between the brackets { } in the formulas is called the tortuosity of the porous system with a symbol Ψ_T. For pores crossing each other perpendicularly, transverse diffusion develops as soon as the pores in the main direction change in shape along the path length. If shape distribution is stochastic and pores cross the material in all directions, isotropic behavior could be expected if the representative volume of the material under scrutiny is infinitesimally small and equal in pore system. Such material, however, does not exist. Typically, equal representative volumes will not be found and isotropic, homogeneous behavior will figure as an assumption, not as reality. Brick, timber, concrete, and aerated concrete are examples of that. They all show a large spread in values for different samples of a same batch of material, as is shown in Fig. 2. That figure gives the results of a dry cup measurement on 30 brick samples of a same production batch.

For calculations, typically the average value of all water vapor resistance factors, measured at a same relative humidity on several samples of a material, is used. If the sample thickness equals the layer thickness, then the number of samples, divided by the harmonic average of all data is a better choice. One

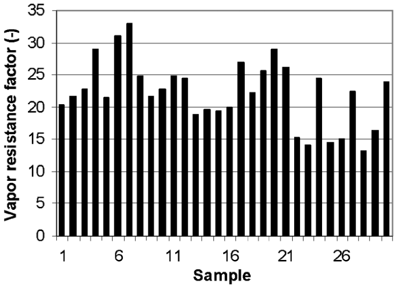

FIG. 2—*Dry cup water vapor resistance factor for handmade bricks. Results for 30 samples from a same batch (from Roels et al. [30]).*

in fact may expect the same diversity as found between the samples along the surface of a layer of the tested material, which means that the vapor will traverse a mosaic of sample large surfaces in parallel. For the brick of Fig. 1, the arithmetic mean totals 22.1 while the harmonic mean equals 21, a difference of 5.3 %. If the sample thickness differs from the layer thickness then calculating a correct average becomes a random exercise. The main consequence of that diversity in water vapor resistance factors for a same material is that one-dimensional vapor flow through a flat layer is nonexisting. One will always have spots where more and less water vapor diffuses through than the average.

If the water vapor diffusion resistance factor is a geometric characteristic of the pore system, one should expect it to be constant, independent of relative humidity. Remarkably, this is not true. Even at low relative humidity, the molecule thick layers, adsorbed against the pore walls of a sorption-active material, already reduce open porosity. That reduction anyhow is so small that hardly any increase in water vapor diffusion resistance factor will be seen. But, once capillary condensation starts, diffusion in the pores shifts from an unhampered process to a jump from water island to water island. As a result, the path length shortens, which is translated in a decrease of the water vapor diffusion resistance factor with increasing relative humidity, as measured data on sand-lime stone clearly show, see Fig. 3.

But, jumping from water island to water island only does not explain the sharpness of the decrease at very high relative humidity. Also a relative humidity driven parallel flow of absorbed water intervenes, driving moisture back to the low relative humidity locations. In an isothermal diffusion test, relative humidity and vapor pressure both point in the same direction, resulting in that sharp decrease of the water vapor resistance factor. That pointing in the same direction is no longer true in a nonisothermal situation. There, they may oppose. That fact was to some extend accounted for by the upgraded Glaser tool of the 1970s. That introduced the concept of critical moisture content. Below, only vapor moved in capillary porous materials. Above, vapor and liquid moved, with the liquid taking the lead and displacing from higher to lower relative humidity. Anyhow, if the above theory holds, noncapillary, hardly hygroscopic materials should be characterized by a water vapor resistance factor independent of relative humidity. Measurements on cork and polystyrene are proof of that as shown in Figs. 4 and 5.

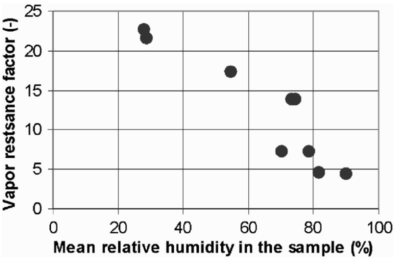

FIG. 3—*Water vapor resistance of sand-lime brick as a function of relative humidity (from Hens [12]).*

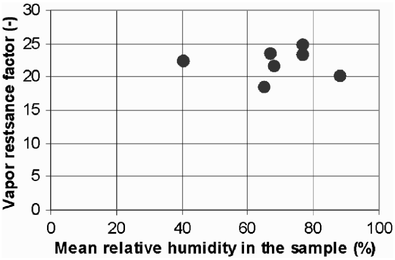

FIG. 4—*Water vapor resistance of cork as a function of relative humidity (from Hens [12]).*

But, the water vapor resistance factor not only depends on relative humidity. Also temperature intervenes. In pores, which are thinner than the free path length of the water molecule, Fickian diffusion changes into friction diffusion, also called Knudsen diffusion. While the Fickian vapor permeability of stagnant air increases with temperature to an exponent 0.81, the Knudsen vapor permeability in a fine pore decreases with temperature to an exponent 0.5:

$$\delta_{v,K} \div \sqrt{\frac{1}{T}} \quad \text{versus } \delta_{v,F} \div \left(\frac{T}{273.15}\right)^{0.81} \tag{25}$$

Traditionally, fine-porous materials are evaluated as if Fickian diffusion does the job. In reality, Knudsen diffusion may have quite some impact, turning the water vapor resistance factor into an upward function of temperature. Also temperature related changes in porous structure may have an impact on the temperature dependency of the water vapor resistance factor.

Usage?

In the hygroscopic region, mass flows are assumed to engage water vapor only, be it by diffusion or by advection, the combination of diffusion and bulk flow of vapor within moving air. Advection is mostly neglected in massive walls composed of fine-porous materials, which leaves diffusion as the only mover. So, mass flow calculations are performed, using measured water vapor resistance factors and measured specific moisture ratios for the materials involved, which are all considered as perfectly homogeneous and isotropic, while ideal diffusion contacts between layers is taken for granted.

In the capillary region, where liquid flow as a consequence of suction overwhelms diffusion in capillary active porous materials, the same hypotheses are advanced: all materials homogeneous and isotropic, ideal suction contact between layers.

Does all this fit with reality? Of course not. To start with, massive layers such as masonry, roof covers, and lathed finishes are not homogeneous in nature. They consist of blocks and mortar joints, tiles and overlaps, timber laths with groove and tongue joints. Mortar joints for example include voids at random

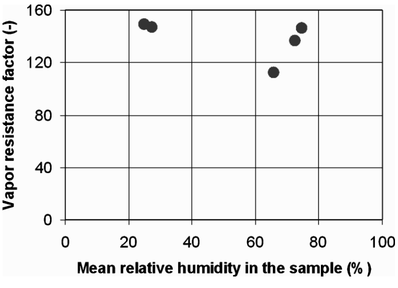

FIG. 5—*Water vapor resistance of extruded polystyrene as a function of relative humidity (from Hens [12]).*

TABLE 2—*Water vapor diffusion resistance factor of massive concrete blocks and veneer walls, brick-laid with the blocks ($l \times b \times h = 0.29 \times 0.09 \times 0.19$ m^3, density 2153 kg/m^3, mortar joints 10-mm wide, from Hens [31]).*

Concrete Blocks	Veneer Wall, Brick-laid with the Blocks		
		RH	Eq, Water Vapor Resistance Factor
μ_{50}[a]	Wall	%	μ_{eq}
50	1	59	3.0
50	2	57	3.2

[a] Water vapor diffusion resistance for a relative humidity of 58 %.

and the head joints show microscopic cracks at the interfaces with the blocks. These voids and cracks lower the equivalent water vapor diffusion resistance of veneer walls, inside leafs and massive walls considerably compared to the water vapor diffusion resistance of the blocks used, as is shown in Table 2 [31].

At the same time, the veneer's air permeability cannot be neglected, while capillary suction will be dominated by the cracks. Cracks and voids may also activate gravity flow at the cavity side when rain runs off. The wall should only have a cavity between the fill and the veneer but may in reality contain two air layers, one where it should be and one between the fill and the inside leaf, activating air looping around the insulation if containing leaks up and down. All block are perforated, which creates as many air flow paths as there are perforations when the horizontal joints are badly filled (Fig. 6). All that should withhold modelers from tackling that type of wall with today's advanced tools, which all assume homogeneity and isotropy. As a consequence, measured data may deviate substantially from simulated results, a reality which is overlooked by many authors, who blame the material property data to be the reason for the discrepancies. They call them unreliable. The same holds for cathedralized roofs with tiled or slated decks and a groove and tongue timber lathed inside lining [27].

Things are even more complicated. Future weather is unknown. So, one has to use weather files from the past to predict things that are coming. The inside climate is a random variable, especially in relation to indoor humidity. Its ever moving value will depend on future outside climate, building usage, and ventilation habits, on the vapor sources present indoors, on interior buffering, etc. Contacts between materials in a part are never ideal. As long as two layers only contact one another, continuity of diffusion is granted but not continuity of suction. In case layers are poured together or in case a layer is pargetted against another, a contact may be formed with sometimes quite different properties than the two layers in separate. Real contacts may mix up both cases. Some work has been done on that [32].

Actual models also have problems with wind-driven rain. How rain touches a surface is quite well predictable, at least under steady state wind pressure differences [33]. As long as the impinging droplets are absorbed, models master things quite well [34]. However, when run-off starts, preferential paths are formed and the water moving down may get concentrated or diluted and stick on horizontal surfaces, where it may move inward through random leaks and cracks by gravity and air pressure differences. This

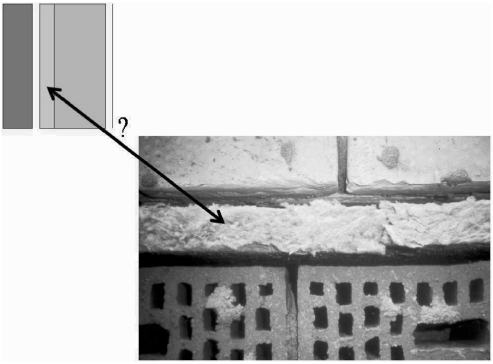

FIG. 6—*Difference between a virtual cavity wall, as calculated by a 1D heat, air, and moisture model, and a real cavity wall!*

is not tractable with the actual 1D or 2D heat, air, moisture models, as one never knows in advance where the cracks, open joints, voids, unexpected air layers, etc. will be, and as no model counts for these random gravity and pressure effects.

A weak point is also that most models are deterministic in nature. They calculate an assumed situation, with geometry, material properties, in and outside climate, contact conditions, initial conditions all well known. As said, this is fiction. Models should evaluate probability and risk, rather than a fixed scenario.

In other words, the material properties as defined and measured, do not allow simulation of how real constructions will behave under combined heat, air, and moisture loading, except in some very specific cases of extremely simple parts.

Conclusions

Today, many so-called full models are available to simulate heat, air, and moisture response of envelope parts. On first sight, the balance equations used and the materials properties needed seem sometimes quite different. When digging in the basics behind, however, it becomes clear that all use the same basic material properties. While the thermal properties are quite representative for a given material, the mass transfer properties may show large standard deviations for a same material. This is due to the fact they do not characterize the material but the porous system, which may be quite variable between samples of a same batch of material samples and interacts intensively with the relative humidity in the surrounding air, giving rise to adsorption and capillary condensation.

Things even become more complicated when looking to real envelope parts. They do not behave as the idealized constructions, models simulate, composed of homogeneous materials, with ideal diffusion and suction contacts in between. Simulating their heat, air, and moisture response with the models available today may show results which deviate largely from the actual response. Blaming the quality of the material data for these discrepancies is not correct. One should instead critically scrutinize the models and work on upgrades which include material heterogeneity, account for air transport, consider gravity and external pressure induced flow through cracks, voids and air layers, take real initial conditions into account and evaluate probability and risk.

All this proves we need a healthy mix between modeling, experiment, and field experience in combined heat, air, and moisture work. Modeling helps in gaining insight, experiments allow validating some of the steps in modeling and understanding how complex even a simplified test reality is, while field experience is needed to gain a reliable, well balanced knowledge of hygrothermal facts and figures.

References

[1] Hirsch, M. , 1932, Trocknungstechnik, Springer Verlag, Berlin/Gýttingen/Heidelberg

[2] Krischer, O., and Kröll, K., *Die wissenschaftlichen Grundlagen der Trocknungstechnik*, Springer Verlag, Berlin/Göttingen/Heidelberg, 1957.

[3] Lykow, A. W., *Transporterscheinungen in kapillarporösen Körpern*, Akademie Verlag, Berlin, 1955.

[4] De Vries, D. A., “Simultaneous Transfer of Heat and Moisture in Porous Media,” *EOS Trans. Am. Geophys. Union*, Vol. 39, No. 5, October 1958.

[5] Glaser, H., Wärmeleitung und Feuchtigkeitsdurchgang durch Kaltraumisolierungen, *Kältetechnik*, Vol. 3, 1958, pp. 86–91.

[6] Glaser, H., Vereinfachte Berechnung des Dampfdiffusion durch geschichtete Wände bei Ausscheiden von Wasser und Eis, *Kältetechnik*, Vol. 11, 1959, pp. 358–364, *Kältetechnik*, Vol. 12, 1959, pp. 386–390.

[7] Glaser, H., Grafisches Verfahren zur Untersuchung von Diffusionsvorgénge, *Kältetechnik*, Vol. 10, 1959, pp. 345–349.

[8] Seiffert, K., *Wasserdampfdiffusion im Bauwesen*, Bauverlag, Wiesbaden/Berlin, 1967.

[9] Rowley, F. B., “A Theory Covering the Transfer of Vapor Through Materials,” *ASHVE Transactions*, No. 1134, July 1938.

[10] Vos, B. H., “Internal Condensation in Structures,” *Build. Sci.*, Vol. 3, 1969, pp. 191–206.

[11] Vos, B. H., “Condensation in Flat Roofs Under Nonsteady State Conditions,” *Build. Sci.*, Vol. 7, 1971, pp. 7–15.

[12] Hens, H., "Theoretical and Experimental Study of the Hygrothermal Behavior of Building and Insulating Materials During Interstitial Condensation and Drying, with Application on Flat Roofs," Ph.D. Thesis, K. U. Leuven (in Dutch), 1975.

[13] Van der Kooi, J., "Moisture Transport in Cellular Concrete Roofs," Ph.D. Thesis, Uitgeverij Waltman, Delft, 1971.

[14] Nielsen, A. F., "Moisture Distribution in Cellular Concrete During Heat and Moisture Transfer," Ph.D. Thesis, Thermal Insulation Laboratory, Technical University of Denmark, 1974.

[15] Kießl, K., "Kapillarer und dampformiger Feuchtetransport in mehrschichtigen Bauteilen," Ph.D. Thesis, Universität und Gesamthochschüle Essen, 1983.

[16] Crausse, P., "Etude fondamentale des transfers couples de chaleur et d'humidité milieu poreux non-saturé," Thèse de doctorat, ENSEEIHT, Toulouse, 1983.

[17] Kohonen, R., "A Method to Analyze the Transient Hygrothermal Behavior of Building Materials and Components," Technical Research Center of Finland (VTT), Publication 21, 1984.

[18] Duforestel, T., "Bases métrologiques et modèles pour la simulation du comportement hygrothermique des composants du bâtiment," Thése de doctorat, Ecole Nationale des Ponts et des Chaussées, Paris, 1992.

[19] Karagiozis, A., "Overview of the 2-D Hygrothermal Heat-moisture Transport Model Latenite," Internal IRC/BPL report, IRC/NRC, 1993.

[20] Hens, H., "Heat, Air and Moisture Transfer in Insulated Envelope Parts, Modeling," Vol. 1 of the final report of the IEA-ECBCS Annex 24. ACCO, Leuven, 1996.

[21] Matsumoto, M. and Nagai, H., "An Analysis of Moisture Variations in Building Walls by Quasi Linearized Equations for Nonlinear Heat and Moisture Transport," *Proceedings of the CIB-W40 Meeting*, Borås, Sweden, 1985.

[22] Grünewald, J., "Diffusiver und konvektiver Stoff- und energietransport in Kapillar-porösen Baustoffen," Ph.D. Thesis, Technische Universität Dresden, 1997.

[23] Hagentoft, C. E., "Hamstad-Modelling," final report EU Hamstad Project, 2002.

[24] Maref, W., Kumaran, M. K., Lacasse, M. K., Swinton, M. C., and Van Reenen, D., "Advanced Hygrothermal Model-HygIRC, LMBF," *Proceedings of the 12th International Heat Transfer Conference*," , Grenoble, 2002, pp. 1–6.

[25] Rode, C., "Combined Heat and Moisture Transfer in Building Constructions," Thermal Insulation Laboratory, Technical University of Denmark, 1990.

[26] Künzel, H. M., "Verfahren zure in- und zweidimensionalen Berechnung des gekoppelten Wärme-Und Feuchtetransports in Bauteilen mit einfachen Kennwerte," Ph.D. Thesis, Universität Stuttgart, 1994.

[27] Janssens, A., "Reliable Control of Interstitial Condensation in Lightweight Roof Systems," Ph.D. Thesis, K. U. Leuven, 1998.

[28] Krus, M., "Feuchtetransport- Und Speicherkoeffizienten poröser mineralischer Baustoffe. Theoretische Grundlagen und neue Meßtechniken," Ph.D. Thesis, Universität Stuttgart, 1995.

[29] Descamps, F., "Continuum and Discrete Modeling of Isothermal Water and Air Transport in Porous Media," Ph.D. Thesis, K. U. Leuven, 1997.

[30] Roels, S., Carmeliet, J., and Hens, H., "Moisture Transfer Properties and Material Characterization," EU Hamstad Project, Final Report WP1, 2002.

[31] Hens, H., "The Vapor Diffusion Resistance and Air Permeance of Masonry and Roofing Systems," *Buildings and Environment*, Vol. 41, June 2006, pp. 745–755.

[32] Qiu, X., "Moisture Transport Across Interfaces Between Building Materials," Ph.D. Thesis, Concordia University, 2003.

[33] Blocken, B., "Wind-Driven Rain on Buildings: Measurements, Numerical Modeling and Applications," Ph.D. Thesis, K. U. Leuven, 2004.

[34] Janssen, H. and Carmeliet, J., "Hygrothermal Simulation of Masonry Under Atmospheric Excitation," *Research in Building Physics and Building Engineering*, P. Fazio, H. Ge, J. Rao, and G. Desmarais, Eds., Taylor and Francis, London/Leiden/New York/Philadelphia/Singapore, 2006, pp. 77–83.

Journal of ASTM International, Vol. 4, No. 1
Paper ID JAI100335
Available online at www.astm.org

Lisbeth G. Thygesen[1] *and Kurt K. Hansen*[1]

Improved Suction Technique for the Characterization of Construction Materials

---

ABSTRACT: The suction technique is a method from soil science that is used for the study of moisture storage capacity in porous construction materials at high relative humidity levels (above approximately 93 %). The samples to be studied are placed in a pressurized container (an extractor) on a water saturated ceramic disk or membrane. The pressure corresponding to a certain relative humidity level is established and moisture is expelled from the samples until moisture equilibrium is reached. This paper presents two adjustments to this method and their applicability. The first adjustment is a new procedure for determining the equilibrium moisture content of samples during the experiment. The method (referred to as the balance method) is to simply keep track of all water entering and leaving the system and use these data to estimate the moisture content of the samples. The advantage of this approach is that the experiment does not need to be stopped and restarted for each relative humidity level tested. The main disadvantage of the method is that the estimation of the moisture content in the samples depends on a correct estimation of the moisture content of the ceramic disk. The second adjustment is the development of a pressure regulation system that keeps the pressure constant (±0.015 bar) within an extractor for weeks.

KEYWORDS: suction technique, porous construction materials, moisture storage capacity, moisture content

Nomenclature

φ = Relative humidity $[-]$
M = Molar mass of water $[\mathrm{kg\,mole^{-1}}]$
σ = Surface tension of water $[\mathrm{N\,m^{-1}}]$
θ = Contact angle [rad]
r = Radius [m]
ρ = Density of water $[\mathrm{kg\,m^{-3}}]$
R = Universal gas constant $[\mathrm{J(K\cdot mol)^{-1}}]$
T = Absolute temperature [K]
s = Suction, i.e., the pressure difference between the pore water pressure and the ambient total pressure [Pa]

Introduction

The suction technique is an experimental method for studying the relationship between the relative humidity and the equilibrium moisture content of porous materials at very high relative humidity levels. Typically, the purpose is to establish the upper part of the sorption isotherm (i.e., above approximately 93 % relative humidity), but it could also be to produce samples with a high moisture content to be studied using other techniques. At humidity levels above approximately 96–97 %, climate chambers are normally not an option. When exposed to rain, construction materials may, however, experience such conditions

---

Manuscript received January 30, 2006; accepted for publication November 8, 2006; published online December 2006. Presented at ASTM Symposium on Heat-Air-Moisture Transport: Measurements on Building Materials on 23 April 2006 in Toronto, Canada; P. Mukhopadhyaya and M. Kurmaran, Guest Editors.

[1] Associate Professors, Technical University of Denmark, Department of Civil Engineering, Building 118, DK-2800 Kgs. Lyngby, Denmark, e-mail: lgt@byg.dtu.dk, kkh@byg.dtu.dk

during their service life, and it is consequently of interest to study materials at these high humidity levels. The equilibrium moisture contents of porous materials, such as brick or wood, at high moisture contents may also be of importance during drying. Within basic research, the structure or properties of porous materials at high moisture contents are interesting per se.

The suction technique was originally developed to study soil samples [1,2], but the method has been adapted to both inorganic and organic construction materials . The technique implies that one or more water saturated samples are placed in a container (an extractor). Pressure is applied, and moisture is forced out of the samples through a water conductive medium and collected outside the extractor. Equilibrium has been reached when no more water leaves the samples. The equilibrium relative humidity is calculated from the applied pressure (the higher the pressure, the lower the corresponding relative humidity) using the Kelvin and la Place equations (Eqs 1 and 2, respectively).

$$\ln \varphi = -\frac{2 \cdot \sigma \cdot M \cdot \cos \theta}{r \cdot \rho \cdot R \cdot T} \tag{1}$$

$$s = -\frac{2 \cdot \sigma \cdot \cos \theta}{r} \tag{2}$$

The Kelvin equation gives the relationship between the relative humidity and the meniscus radius (identical to the pore radius), while the la Place equation gives the relationship between the applied pressure and the pore radius. Thus, by combining the two equations the relationship between the applied pressure and the relative humidity may be established:

$$s = \frac{\ln \varphi \cdot \rho \cdot R \cdot T}{M} \tag{3}$$

Since the suction technique implies that moisture is removed from initially water saturated samples, only the desorption isotherm may be studied.

Equipment for suction studies is intended for certain pressure ranges, for example, three different types of extractors relevant for construction materials are available from SOILMOISTURE®[2]: Up to 5 bar (above 99.7 % RH), up to 15 bar (above approximately 99 % RH), and 100 bar (above approximately 93 % RH). The water conductive medium, which connects the sample pore system to the tube for expelling water out of the pressurized container, depends on the pressure range of the system. For the 100 bar system the samples are placed on a water saturated cellulose membrane, while the other two systems use a water saturated ceramic disk covered by a layer of wet kaolin and a wet textile cloth. The cloth is meant to prevent kaolin from entering the samples.

This paper describes two improvements to the way suction experiments are normally performed. The first improvement is an alternative way of registering whether the equilibrium moisture content has been reached. The new procedure was only tested for 5 and 15 bar systems. The second improvement is a new pressure regulation system that keeps the pressure constant in a 100 bar extractor.

The Balance Method

The traditional method for determining when equilibrium has been reached is described in a Nordtest method for suction analysis [7]. This method measures only the change in the volume of water leaving the sample. The expelled water is led into a burette, and when there has been no change for at least 48 h the pressure is released, and samples are removed and weighed. To obtain the moisture content at a higher pressure level the samples are put back into the extractor. Studies have demonstrated that it is necessary to use a fresh layer of kaolin and a new water saturated ceramic disk to ensure the hydraulic contact between the porous system of the sample and the kaolin layer [8,9]. This method is referred to here as the volume method.

The newly developed method instead uses the weight of the water that has left the system to monitor whether equilibrium has been reached. By applying strict control of the amount of water in the system it is possible to calculate the moisture content of the sample without stopping the experiment and removing

---

[2] Soilmoisture, Santa Barbara, CA.

the samples. To switch to a higher pressure (i.e., a lower RH level) the pressure is simply raised without having to stop and restart the experiment. This method is refered to as the balance method.

Characteristics of the volume method:

- The method is an established test method.
- Values for individual samples may be obtained also when they are placed on the same disk/membrane. Samples of different materials may thus be placed on the same disk, if needed.
- Control of the amount of water entering the system is not needed.
- No estimation of the water content in the disk/membrane is needed.

Characteristics of the balance method:

- The experiment does not need to be stopped and restarted to measure the moisture content of the samples corresponding to a certain pressure level, eliminating possible hysteresis effects from cycles of increasing and releasing pressure. Additionally, the samples remain in the extractor and therefore are not exposed to laboratory conditions which cause the samples to lose moisture as soon as the pressure is released. This exposure makes it difficult to obtain correct weight measurements, and implies that the samples, in a worst case scenario, risk losing so much moisture that their moisture content falls below the next equilibrium moisture content level.
- The weight of the water that has left the system may only be recorded for a whole disk/membrane. Therefore, if data are needed for individual samples, only one sample may be placed on each disk/membrane. However, if the mean characteristics of a given material is sought, a number of similar samples may be placed on the same disk/membrane and their mean moisture content may then be found (but not the standard deviation between the individual samples).
- Complete knowledge of all water entering and leaving the system is a requirement. This means that during setup of the system, the dry and wet weights of all components need to be measured (disk, kaolin, cloth, etc.).
- The balance method requires a "blank" disk/membrane to be tested in order to estimate the amount of water present within the system but outside the sample(s) at different pressure levels. Provided that the same kaolin layer thickness is used for all runs these estimates need only be established once, and may then be used henceforth.

Once established in the laboratory the balance method is less time consuming, as switching from one relative humidity level to the next is simply a matter of raising the pressure. However, initially the method requires collection of some background data. The most important background data are an estimate of the equilibrium moisture content in the water conductive system inside the extractor, i.e., in the membrane or in the disk, kaolin layer, and the cloth. Without the estimation, it is not possible to determine how much of the water in the extractor is contained by the sample(s). Another estimate needed is the rate of evaporation of water from the container that collects the water outside the extractor. The rate of evaporation is needed to estimate the amount of water leaving the system through evaporation and to ensure the experiment is stopped at the right time. If evaporation is ignored there is a risk of stopping the experiment prematurely. The following two subsections describe these two estimations.

Estimation of the Moisture Content Within the Ceramic Disk, Kaolin Layer, and Cloth

The balance method calculates the amount of water within the samples by monitoring the amount of water entering and exiting the system. Consequently, the amount of water inside the extractor that is not contained by the samples (i.e., within the disk, kaolin, or cloth) must be known. This can be estimated by performing experiments without samples. In order to verify estimates based on the balance method the suction experiments were stopped at each equilibrium moisture content level and the ceramic disks (including kaolin layer and cloth) were removed from the extractor, wrapped in plastic to prevent evaporation, and weighed. The results are given in Tables 1 and 2.

Tables 1 and 2 show that individual ceramic disks have different equilibrium moisture contents. Even those intended for the same pressure range vary. This means that the equilibrium moisture content of a particular disk must be estimated in order to use the balance method. The tables also show that the estimates from the balance method are a little higher than corresponding measurements from the volume method. The differences are up to 3.4 %. The cause of the systematic error on the estimates is unknown, but on several occasions drops of condensed water were observed on the inside of the extractor lid. Also the disks will undoubtedly start losing moisture as soon as the pressure is released, and will continue doing

TABLE 1—*Five bar extractor: moisture contents (MC) of ceramic disks (including kaolin layer and cloth) according to the volume method (V) and the balance method (B) at five different relative humidity levels.*

s	φ	Disk I MC [%]		Disk II MC [%]		Disk III MC [%]		Disk IV MC [%]	
[bar]	[%]	V	B	V	B	V	B	V	B
1.0	99.93	19.3	19.4	18.4	18.4	21.4	21.6	18.6	18.8
1.4	99.90	19.2	19.4	18.4	18.4	21.1	21.4	18.5	18.8
2.0	99.85	18.9	19.1	18.3	18.4	20.9	21.3	18.3	18.7
2.7	99.80	18.6	18.9	18.2	18.3	20.7	21.3	18.1	18.6
3.4	99.75	18.6	18.9	18.1	18.3	20.6	21.3	18.0	18.6

so while the extractor lid is unscrewed. This implies that the balance method most likely gives better estimates of the total amount of water inside the extractor but outside the samples. However, when compared to the moisture content of the disk, kaolin, and cloth determined directly from weighing, the estimates from the balance method appear to be too high.

The moisture present in the water conductive system inside the extractor is distributed between the ceramic disk, the kaolin layer, and the cloth that make up the sandwich on which the sample is placed. This implies that unless the exact same amount of kaolin and the same size and type of cloth is used for every experiment, the estimates from Tables 1 and 2 are useless. In order to minimize the differences between runs, the setup procedure needs to be standardized. For example, a special spatula with a 2 mm gap is used to apply the kaolin layer to ensure that the layer thickness is the same every time a disk is prepared.

Evaporation of Water through a Floating Lid of Hexadecane

The criterion for equilibrium is the same for the two methods, i.e., no change in the amount of expelled water for at least 48 h. However, initial tests showed that one cannot ignore the amount of water that evaporates from the container in which it is collected. A floating lid of *n*-hexadecane was used to reduce evaporation; however, evaporation was not completely eliminated. In order to be able to correct the weight of the expelled water for the evaporation it was thus necessary to quantify the evaporation through the hexadecane lid. Four different layer thicknesses were tested (approximately 5, 10, 12, and 20 mm) in a room with a temperature of 20 °C and a relative humidity of 65 % from cylindrical containers with a surface area of 100 cm^2. Figure 1 shows that a few days after the water has penetrated the lid, the evaporation rate is surprisingly independent of the layer thickness. It appears that only the interface between the water and the hexadecane layer reduces the evaporation from the water. Hexadecane does not evaporate under the conditions used here (no weight loss for two months). From Fig. 1 the evaporation rate was estimated to be approximately 0.045 g per 100 cm^2 per day regardless of the lid thickness, which was utilized in the experiments using the balance method.

Results from Sandstone Samples

The balance method was tested for two different types of sandstones (white and green). Prior to the experiment the ceramic disks were wetted using capillary saturation, while the samples were water saturated using vacuum saturation. The results are shown in Figs. 2 and 3. The figures show that the balance

TABLE 2—*Fifteen bar extractor: moisture contents (MC) of ceramic disks (including kaolin layer and cloth) according to the volume method (V) and the water balance method (B) at five different relative humidity levels.*

s	φ	Disk I MC [%]		Disk II MC [%]		Disk III MC [%]		Disk IV MC [%]	
[bar]	[%]	V	B	V	B	V	B	V	B
3.3	99.76	18.9	19.2	18.8	18.9	19.6	19.7	18.9	19.0
5.3	99.61	18.7	19.2	18.5	18.6	19.2	19.5	18.5	18.6
9.5	99.30	18.1	18.6	18.0	18.2	18.8	19.1	17.9	18.0
10.0	99.26	18.0	18.6	17.8	18.0	18.6	19.1	17.7	17.9
13.4	99.01	17.8	18.6	17.0	17.3	18.5	19.1	17.0	17.3

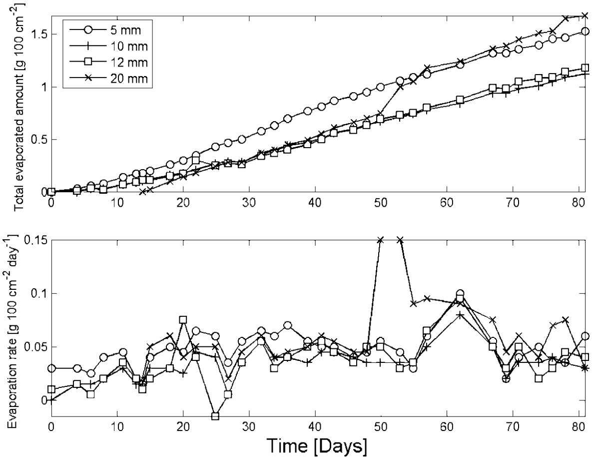

FIG. 1—*Evaporation of water through a floating lid of hexadecane of four different thicknesses. The experiment with a 20 mm layer thickness was started on Day 13, the others on Day 1. A few drops of hexadecane were accidentally spilled from the 20 mm container on Day 49. The temperature in the room was not entirely stable, which explains the fluctuations around Days 22–29 and 55–69.*

method tends to give slightly higher moisture contents than the volume method, about 1–2 %. The figures also indicate that the standard deviation between runs for the balance method is about twice that for the volume method.

The systematic difference between the two methods likely arises because the volume method tends to underestimate and the balance method tends to overestimate the moisture content. For the volume method, the measured equilibrium weight of the samples at these high relative humidity levels can only be too low, never too high, as the samples will start losing moisture as soon as the pressure is released. A test was carried out using a green sandstone sample where the sample was removed from the extractor, weighed, exposed to the laboratory climate for 10 min and weighed again. The evaporation from the sample resulted

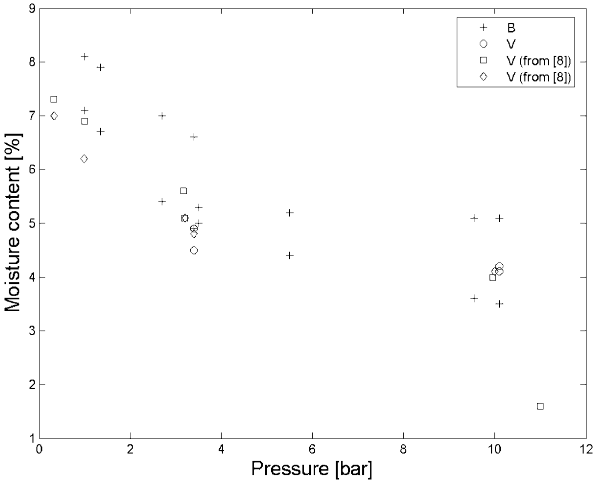

FIG. 2—*Moisture content for pressure levels below 12 bar for green sandstone samples. Results are shown both for the volume method (V) and the balance method (B).*

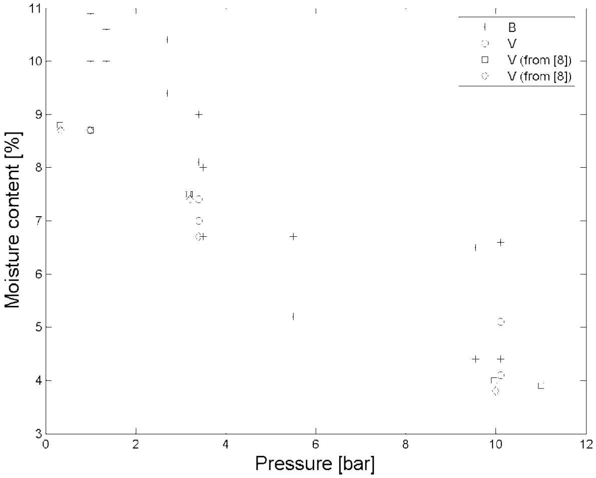

FIG. 3—*Moisture content for pressure levels below 12 bar for white sandstone samples. Results are shown both for the volume method (V) and the balance method (B).*

in a 0.2 % decrease in the calculated moisture content. Obviously, this loss may be reduced by wrapping the sample in plastic. The loss of moisture from the samples during the release of pressure is, however, unknown and may not be prevented. For the balance method, the measured weight of the expelled water can only be too low, never too high, leading to overestimation of the moisture content. The water, not registered as expelled, is assumed to be inside the extractor with a certain part of that water expected to be contained within the samples.

That the reproducibility from run to run is poorer for the balance method than for the volume method is most likely a result of the uncertainty of the estimate of the equilibrium moisture content of the disks. It is possible that even more rigorous standardization of the procedure could reduce this uncertainty somewhat.

Results obtained indicate that for sandstone the balance method appears to be about as accurate as the volume method, but unfortunately less precise.

Remaining Problems

The suction technique may sometimes give problems that are not mentioned in the Nordtest method [7]. For example occasionally the 48 h criterion is not enough time to ensure equilibrium [10]. Samples, both wood and sandstone, may appear to be in equilibrium, and may then start to lose moisture again. In one case it was calculated that the error resulting from stopping the experiment too early corresponded to a difference in the equilibrium moisture content of up to 0.3 % [10].

A problem which limits the applicability of the water balance method is the uncertainty in estimating the moisture content of the disk/membrane. This uncertainty implies that only samples above approximately a few hundred grams may be studied using this method. The reason is that the moisture content in the sample(s) is determined from the difference between the total amount of water inside the extractor and the amount present in the disk/membrane. For example, the dry weight of a ceramic disk including kaolin and cloth is typically around 1000 g during a run. Therefore, an uncertainty of 0.5 % moisture corresponds to 5 g of water, which only corresponds to 1 % for a sample with a dry weight of 500 g, but 10 % to a sample with a dry weight of 50 g. This uncertainty is the main drawback of the balance method.

Pressure Regulation of a 100 Bar Extractor

It is important that suction measurements are carried out under well-defined and stable temperature conditions. This is achieved by placing the extractor in a room with a constant temperature. It is also important

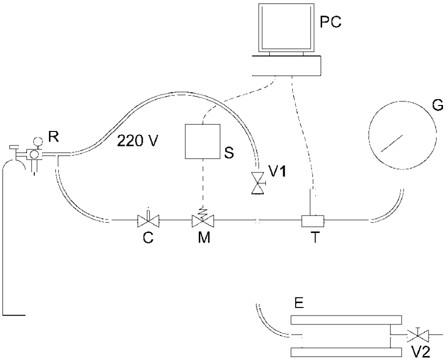

FIG. 4—*Schematic drawing of the pressure regulation system for the 100 bar extractor.*

that the pressure within the extractor does not fluctuate. In the earlier version of the 100 bar system in question, the pressure decreased by approximately one bar per day caused when the regulator did not respond to nitrogen escaping through fittings and diffusing through the cellulose membrane.

The new system described here keeps the pressure within a narrow range for several weeks. The system consists of a pressure transmitter to measure the pressure and send the value to a PC running an in-house Labview program. If the pressure is below the set point, the regulation software sends a signal to a solenoid valve, which opens for a short while and lets in a small amount of nitrogen gas in order to re-establish the pressure level.

The system is shown in Fig. 4. The procedure for establishing a pressure of, for example, 20 bar is as follows: Valve V2 on the extractor is closed and V1 is opened. By opening the regulator R the pressure throughout the system is manually adjusted to approximately 19.8 bar. Valve V1 is then closed. The default position of the solenoid valve M is closed so when the pressure is now increased to 25 bar by adjusting R, the regions between R and V1 and R and M are affected. The control valve C is slightly open. The pressure transmitter T signals the PC that the pressure is too low. The response of the Labview program is to signal the solid state relay S so that the solenoid valve may open for a short, predefined time (0.5 s). Henceforth, the pressure is measured once a minute and regulated as needed. The precision test gage G was used for calibrating the pressure transmitter, but is now only used for manual inspection.

Figure 5 shows that the pressure regulation keeps the pressure constant for more than a month. The normally used cellulose membrane was not used during this test, a 0.15 mm polyethylene foil was used instead. Figure 5 shows that even with a tight polyethylene foil in the extractor the pressure decreases due to leakage in the system. Without regulation the pressure would decrease by approximately 0.15 bar per day. The figure shows that when the decreasing pressure has reached the set point, which in this case is 20.00 bar, the pressure regulation system opens the solenoid valve for a short time increasing the pressure by 0.025 bar. From this level the pressure decreases again. In this way the pressure oscillates ±0.015 bar around a pressure of 20.01 bar with a cycle time of about two hours. By exchanging the polyethylene foil with the normally used cellulose membrane, the cycle time is expected to be less than two hours due to diffusion of nitrogen gas through the cellulose membrane.

Conclusions

Two different improvements to the suction method were developed. A procedure was tested that avoids possible hysteresis effects on the sample and is less time consuming than the standard method. The method was found to be about as accurate as the standard method, but less precise. It was also found that the new method gives unreliable results for samples with a dry weight less than a few hundred grams. The other improvement developed was a pressure regulation system. The new system ensures a constant pressure level during suction experiments.

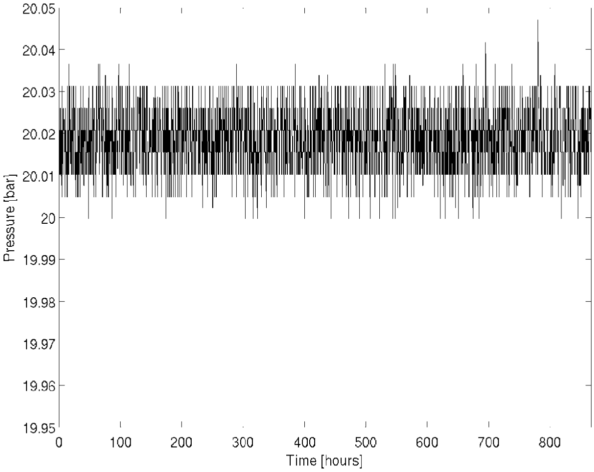

FIG. 5—*The pressure regulation system keeps the pressure constant (±0.015 bar) within the 100 bar extractor for more than a month.*

Acknowledgments

A grant from the Danish Research Council for Technology and Production Sciences is gratefully acknowledged (project no. 26-02-0100). The authors thank Bjarke Dahl Madsen and Ulla Gjøl Jakobsen for technical assistance.

References

[1] ASTM, Standard D 2325, "Standard Test Method for Capillary-Moisture Relationships for Coarse- and Medium-Textured Soils by Porous-Plate Apparatus" *Annual Book of ASTM Standards*, Vol. 4.08, ASTM International, West Conshohocken, PA, 1968, 184–190.

[2] ASTM, Standard D 3152, "Standard Test Method for Capillary-Moisture Relationships for Fine-Textured Soils by Pressure-Membrane Apparatus" *Annual Book of ASTM Standards*, Vol. 4.08, ASTM International, West Conshohocken, PA, 1972, pp. 301–306.

[3] Krus, M., "Moisture Transport and Storage Coefficients of Porous Mineral Building Materials: Theoretical Principles and New Test Methods," (in German), Der Fakultät Bauingenieur- und Vermessungswesen der Universität Stuttgart, Stuttgart, Germany, 1995.

[4] Janz, M., "Moisture Transport and Fixation in Porous Materials at High Moisture Levels," Doctoral thesis, Report TVBM 1018, Division of Building Materials, Lund Institute of Technology, Lund, Sweden, 2000.

[5] Johansson, P., "Water Absorption in Two-layer Masonry Systems. Properties, Profiles and Predictions," Doctoral Thesis, Report TVBM 1024, Division of Building Materials, Lund Institute of Technology, Lund, Sweden, 2005.

[6] Cloutier, A., and Fortin, Y., "Moisture Content—Water Potential Relationship of Wood from Saturated to Dry Conditions," *Wood Sci. Technol.*, Vol. 25, 1991, pp. 263–280.

[7] Nordtest Method, "Building Materials: Retention Curve and Pore Size Distribution," NT BUILD 481, 1997.

[8] Strømdahl, K., "Moisture Content in Building Materials—With Focus on Moisture Fixation in the Superhygroscopic Range," (in Danish), M.Sc. Thesis, Department of Structural Engineering and Materials, Technical University of Denmark, Lyngby, Denmark, 1997.

[9] Hansen, M. H., Houvenagehl, G., Janz, M., Krus, M., and Strømdahl, K., "Interlaboratory Comparison of the Measurement of Retention Curves," *Journal of Thermal Envelope and Building Science*, Vol. 22, 1999, pp. 334–348.

[10] Christensen, K. and Strømdahl, K., "Experimental Determination of Suction Curves for Lime Silica Brick by Use of Pressure Plate Extractor," (in Danish), Report, Department of Structural Engineering and Materials, Technical University of Denmark, Lyngby, Denmark, 1996.

Journal of ASTM International, Vol. 4, No. 8
Paper ID JAI100621
Available online at www.astm.org

Phalguni Mukhopadhyaya,[1] *Kumar Kumaran,*[1] *John Lackey,*[1] *and David van Reenen*[1]

Water Vapor Transmission Measurement and Significance of Corrections

ABSTRACT: Water vapor transmission properties of building materials play an important role in the overall moisture management and durability of the exterior building envelopes. The cup method, as described in the ASTM Standard Test Methods for Water Vapor Transmission of Materials (E 96), is widely used in North America and other parts of the world for this purpose. Recently the latest ASTM standard (E 96/E 96M–05) has started taking into account various corrections (e.g., buoyancy correction, correction for resistance due to still air and specimen surface, edge mask correction, etc.) while analyzing the results obtained from the cup methods. This paper presents the results obtained from the laboratory tests carried out on more than 50 building materials. These results have been used to demonstrate the significance of various corrections on the measured water vapor permeability or permeance of various commonly used building materials or components. The results presented in this paper were discussed in the ASTM technical task group to underline the importance of various corrections for the calculation of water vapor transmission properties of various building materials.

KEYWORDS: water vapor transmission, permeability, permeance, building materials, corrections

Introduction

Water vapor transmission characteristic of a building material is the most significant moisture transport property that is looked upon for the assessment of moisture management capability of the building envelope systems. Simply put, a building envelope designer or engineer would not recommend or use a construction material without knowing the implications of its water vapor transmission characteristics on the overall moisture response of the building envelope. On many instances, one material is preferred over another based on its water vapor transmission properties [1]. In particular, for membrane and coating materials (e.g., vapor barrier, sheathing paper, latex coating, etc.) the water vapor transmission characteristic is the single most important property that determines its utility and effectiveness from the moisture management point of view [2]. Hence, one cannot overemphasize the need to evaluate the water vapor transmission characteristics of building materials accurately by a standard test procedure.

Research Background

There are three terminologies that are commonly used to describe the water vapor transmission properties of building materials. These terminologies are: (1) water vapor transmission rate, (2) water vapor permeability, and (3) water vapor permeance (defined as the reciprocal of the water vapor resistance). As per the standard definitions described in ASTM C 168, Standard Terminology Relating to Thermal Insulation, these terminologies are described in the following paragraphs:

Water Vapor Transmission Rate

The water vapor transmission rate is the steady water vapor flow in unit time through unit area of a body, normal to specific parallel surfaces, under specific conditions of temperature and humidity at each surface.

Manuscript received May 9, 2006; accepted for publication July 24, 2007; published online August 2007. Presented at ASTM Symposium on Heat-Air-Moisture Transport: Measurements on Building Materials on 23 April 2006 in Toronto, Canada; P. Mukhopadhyaya and M. Kumaran, Guest Editors.

[1] Research Officer, Principal Research Officer, and Technical Officers, respectively, Institute for Research in Construction, NRC Canada, Ottawa, Ontario, Canada

TABLE 1—*Metric units and conversion factors.*[a,b]

Multiply	By	To Obtain (for the same test condition)
	WVT	
$g/(h \cdot m^2)$	1.43	$grains/(h \cdot ft^2)$
$grains/(h \cdot ft^2)$	0.697	$g/(h \cdot m^2)$
	Permeance	
$g/(Pa \cdot s \cdot m^2)$	1.75×10^7	1 Perm (in.-lb)
1 Perm (in.-lb)	5.72×10^{-8}	$g/(Pa \cdot s \cdot m^2)$
	Permeability	
$g/(Pa \cdot s \cdot m)$	6.88×10^8	1 Perm in.
1 Perm in.	1.45×10^{-9}	$g/(Pa \cdot s \cdot m)$

[a]These units are used in the construction trade. Other units may be used in other standards.

[b]For all calculations 1 mm of Hg=133.3 Pa.

$$\text{Rate of Water Vapor Transmission (WVT)} = \frac{G}{tA} = \frac{(G/t)}{A} \tag{1}$$

where G=amount of water vapor flow, kg, t=time, s, G/t=slope of the straight line, g/s, and A=test area (cup mouth area), m^2.

Water Vapor Permeance

The water vapor permeance is the time rate of water vapor transmission through unit area of flat material or construction induced by unit vapor pressure difference between two specific surfaces, under specified temperature and humidity conditions.

$$\text{Water Vapor Permeance } (WVP) = \frac{WVT}{\Delta p} = \frac{WVT}{S(R_1 - R_2)} \tag{2}$$

where Δp=vapor pressure difference, mm Hg (1.333×10^2 Pa), S=saturation vapor pressure at test temperature, mm Hg (1.333×10^2 Pa), R_1=relative humidity at the source expressed as a fraction (the test chamber for desiccant method; in the dish for water method), and R_2=relative humidity at the vapor sink expressed as a fraction.

Water vapor resistance (Z) is the reciprocal of the water vapor permeance, (i.e., $Z = 1/WVP$).

Water Vapor Permeability

The water vapor permeability is the time rate of water vapor transmission through unit area of flat material of unit thickness induced by unit vapor pressure difference between two specific surfaces, under specified temperature and humidity conditions.

It is to be mentioned here that water vapor permeability is a property of a material and water vapor permeance is a performance evaluation indicator/property of a component and not a property of a material. Mathematically, permeability is the arithmetic product of permeance and thickness.

$$\text{Water Vapor Permeability} = \text{Water Vapor Permeance} \times \text{Thickness} \tag{3}$$

The units used to express the water vapor transmission properties of building materials depend on the trade and location. The conversion factors for commonly used units are given in Table 1.

The water vapor permeability is a function of relative humidity (RH) and temperature (T). The relationship between water vapor permeability and relative humidity is very well established [3–5]. For nonhygroscopic materials, water vapor permeability values show little or no change with the variation of relative humidity. However, for hygroscopic materials, the water vapor permeability of materials increases with the increase of relative humidity [6,7].

On the other hand, temperature dependency of water vapor permeability (WVP) has been of interest to researchers for quite some time [3,4,8–10]. However, the extent of this influence of temperature on the water vapor permeability is not well known for most building materials. Though in general it is found that

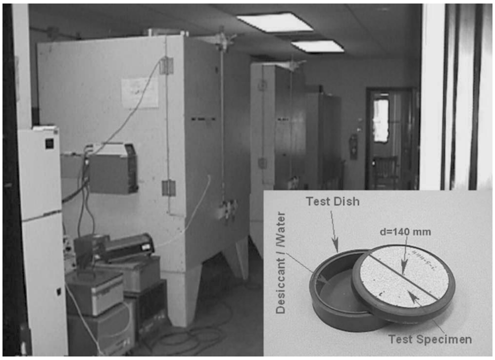

FIG. 1—*Test chamber (controlled atmosphere) and test assembly.*

the temperature effect on water vapor permeability is negligible [11] but there are research findings [12] that indicate an increase of water vapor permeability by 3 % per °C change (+ve) in temperature. Further investigation would be required to confirm these findings.

Test Procedure

The water vapor transmission measurements are usually done under isothermal conditions. A test specimen of known area and thickness separates two environments that differ in relative humidity (RH). Then the rate of water vapor flow across the specimen, under steady-state conditions (with known RHs as constant boundary conditions), is gravimetrically determined.

In the Desiccant or Dry Cup Method the test specimen is sealed to the open mouth of a test dish containing a desiccant, and the assembly placed in a controlled atmosphere (Fig. 1). Periodic weighings determine the rate of water vapor movement through the specimen into the desiccant.

In the Water or Wet Cup Method, the dish contains distilled water, and the weighings determine the rate of water vapor movement through the specimen from the water to the controlled atmosphere. The water vapor pressure difference is nominally the same in both methods except in the variation with extremes of humidity on opposite sides.

ASTM Standard E 96, Test Methods for Water Vapor Transmission of Materials, prescribes two specific cases of this procedure—a dry cup (desiccant) method that gives the permeance or permeability at a mean RH of 25 % and a wet cup (water) method that gives the permeance or permeability at a mean RH of 75 %. Various technical aspects, limitations of the test method, and procedures for analyses of the test data are available in published literatures [6,13–15].

Corrections and Why?

Corrections are important because they reduce the uncertainty of the test results and generate more realistic/accurate water vapor transmission properties that would positively influence the design process for moisture management. It is important that all applicable corrections are made appropriately. The procedures for making various corrections, as summarized below, are found in the literature [14,16–18].

Buoyancy Correction

The duration for one set of measurements can be many days or weeks. The atmospheric pressure may significantly change during such periods. If the test specimen is highly water vapor resistant, the changes in mass due to water vapor transport may be overshadowed by the apparent gravimetric changes observed. In such cases, all gravimetric data should be corrected to vacuum or any base line pressure (e.g., pressure at first weighing). The following equation can be used for buoyancy correction [16]

TABLE 2—*Materials in the database.*

1. Wood (pine, cedar, spruce, etc.)	2. Stone (lime, sand, granite, etc.)	3. Fiber cement board	4. Wall paper
5. Gypsum board (interior and exterior)	6. Polyurethane foam	7. Oriented strand board	8. Plywood
9. Brick (cementicious, clay, etc.)	10. Cellulose fiber insulation	11. Mortar	12.Polyisocyanurate foam insulation
13. Glass fiber insulation	14. Vapour barrier	15. Portland cement stucco	16. Acrylic stucco
17. Wood siding	18. Vinyl siding	19. Sheathing membrane or building paper	20. Calcium silicate insulation

$$\frac{m_2}{m_1} = 1 + \frac{\rho_a(\rho_1 - \rho_2)}{\rho_1(\rho_2 - \rho_a)} \tag{4}$$

where m_1= mass recorded by balance, kg, m_2= mass after buoyancy correction, kg, ρ_a= density of air, kg m^{-3}, ρ_1= density of material of balance weights, kg m^{-3}, and ρ_2= bulk density of test assembly, kg m^{-3}.

The density of air can be calculated using the ideal gas law for the measured atmospheric pressure and ambient temperature. The buoyancy correction is important when measured mass changes are in the range of 0 to 100 mg [15].

Corrections for Resistance Due to Still Air and Specimen Surface

In general, if the material is highly permeable, these corrections are more significant. With known thickness of the still air layer in the cup, the corresponding water vapor resistance can be calculated using the following equation for permeability [17]

$$\delta_a = \frac{2.306 \times 10^{-5} P_o}{R_v T P}\left(\frac{T}{273.15}\right)^{1.81} \tag{5}$$

where δ_a=permeability of still air, $\mathrm{kg \cdot m^{-1} \cdot s^{-1} \cdot Pa^{-1}}$, T=temperature, K, P=ambient pressure, Pa, P_o=standard atmospheric pressure, i.e., 101325 Pa, and, R_v=ideal gas constant for water, i.e., 461.5 $\mathrm{J \cdot K^{-1} \cdot kg^{-1}}$.

In the absence of any measured data, the surface resistances (i.e., inside and outside surfaces of the specimen) may be approximated using Lewis' relation [18]. For cup methods that follow this standard, the total surface resistance [14] should be $\approx 4 \times 10^7$ $\mathrm{Pa \cdot s \cdot m^2 \cdot kg^{-1}}$.

Edge Mask Correction

The following equation is to be used to correct the excess water vapor transmission (WVT) effect due to edge masking [9]:

$$\text{Percent excess WVT} = \frac{400t}{\pi S_1} \log_e\left(\frac{2}{1 + e^{-(2\pi b/h)}}\right) \tag{6}$$

where h=specimen thickness, m, b=width of masked edge, m, and S_1=four times the test area divided by the perimeter, m. If the cup assembly includes any edge masking this correction shall be made.

Effects of Various Corrections

Over a period of the past ten years or more, authors have measured water vapor transmission properties of numerous building materials commonly used in North America [19–21]. These materials included almost all the contemporary building materials used for the construction of exterior building envelopes (Table 2).

The minimum thickness of the material specimen was 0.141 mm and the maximum thickness was not over 32 mm, as required by the ASTM E 96 standard, except highly porous glass fiber (88 mm) and cellulose fiber insulation (64.5 mm) materials. The water vapor transmission properties were determined according to the wet and dry cup methods at 23±1 °C temperature. The dry cup tests with desiccant method test setup but with variable chamber RH levels were carried out at three nominal chamber RH levels: 50 ±1 %, 70±1 % and 90±1 %, and wet cup measurements with water method test setup but with

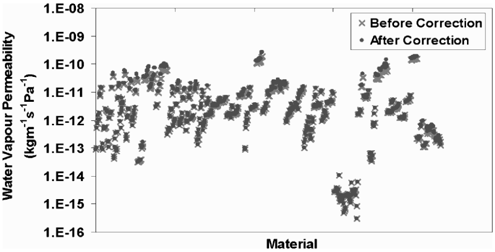

FIG. 2—*Water vapor permeability: before and after corrections.*

variable chamber RH were carried out at two nominal chamber RH levels: 70±1 % and 90±1 %. These tests were necessary to derive the functional relationship between RH and water vapor permeability. A detailed discussion on the principle and test data analysis techniques can be found in the relevant publication authored by Kumaran [6]. Results from these tests were analyzed at first with the conventional method using Eqs. 1 to 3, and then they were corrected appropriately using the steps outlined in Eqs. 4 to 6.A sample calculation on the test data is shown in the Appendix to this paper.

It should be mentioned here that the water vapor transmission properties presented in this paper were measured, using high precision equipments, by the trained technical staffs. But this does not mean that the physical quantities measured are known within a few fractions of 1 %. In addition, the basic inhomogeneity of all building products introduces uncertainties in the derived water vapor transmission properties that are far greater than the uncertainties in the measurements of the basic physical quantities. The magnitude of these uncertainties depends on the building products under investigation. A rigorous laboratory test data analysis indicates that water vapor transmission property for one test specimen can be determined well within a percent [22]. But when all measurements on all test specimens used are combined to designate the water vapor permeability or permeance of the product, the uncertainty may be as large as 30 % [22].

The general effects of corrections on all water vapor permeability and permeance values are shown in Figs. 2 and 3. These figures clearly quantify the differences between the permeance and permeability values after and before corrections. These corrections are always positive (i.e., higher values after corrections are applied) and the differences varied between 0.003 and 84 %. The upper limit of these variations is certainly a significantly large number to adequately justify the importance of various corrections. In order to look further into the effects of various corrections, the following paragraphs present the results obtained for two of the most common types of building materials: wood or wood-based materials (i.e., wood, plywood, oriented strand board, etc.), and membranes (i.e., sheathing membranes, building papers, vapor barrier, wall papers, etc.). The water vapor permeance of the wood or wood-based components normally stays within the relative range of high to moderate and the same for the membrane is considered to be in the lower range.

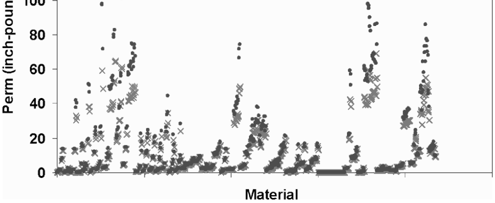

FIG. 3—*Water vapor permeance: before and after corrections.*

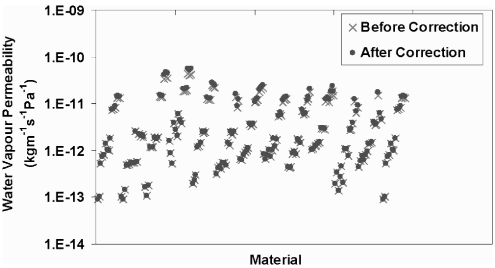

FIG. 4—*Water vapor permeability (wood and wood-based materials): before and after corrections.*

Correction Effects on Wood or Wood-based Materials

The water vapor permeability or permeance characteristic of wood or wood-based materials is a very important parameter for the determination of its moisture management capability in a particular application. The water vapor permeance and permeability values of various woods (pine, cedar, spruce, etc.) and wood-based building materials (OSB, plywood, etc.) are shown in Figs. 4 and 5. The thickness of the materials under consideration varies between 9 and 20 mm. These plots clearly indicate that water vapor permeability and permeance values of the wood or wood-based materials and components vary over a wide range. The permeance values varied between 0.08 and 38 perm (in.-lb) before correction and 0.08 and 51 perm (in.-lb) after correction. The maximum overall percentage change of the water vapor permeance values due to applied corrections is 34 %. It also appears that the effect of corrections is larger, in terms of percentage difference, for higher water vapor permeability or permeance values.

Correction Effects on Membranes

As far as the moisture management is concerned, the water vapor permeability or permeance characteristic of the membranes is the most important criterion that determines its suitability for a particular application. The membranes under consideration here include paper-based building papers, polymeric sheets, vinyl wall paper, felt paper, self adhering and torch applied membranes, etc. The thickness of the membranes varies within the range 0.14 and 2.44 mm. The water vapor permeability values of these membranes vary considerably (Fig. 6) and it can be clearly seen in Figs. 6 and 7 that many of these membranes are highly impermeable (water vapor permeance less than 0.1 perm (in.-lb)). The overall water vapor permeance values vary between 0.004 and 55 perm (in.-lb) before correction, and 0.004 and 86 perm (in.-lb) after correction. The maximum effect of correction on the water vapor permeance value is found to be about 57 % and the minimum is 0.003 %. Very much like wood or wood-based materials or components, in this case also the percentage correction values are higher for the membranes with higher water vapor permeability or permeance values.

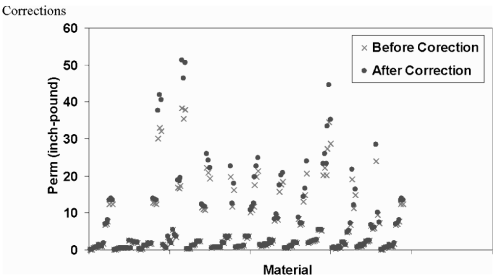

FIG. 5—*Water vapor permeance (wood and wood-based materials): before and after corrections.*

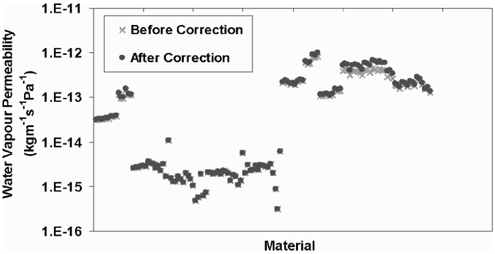

FIG. 6—*Water vapor permeability (membranes): before and after corrections.*

Water Vapor Permeance and Corrections

It has been shown so far that corrections due to buoyancy, still air resistance, specimen surface, and edge mask can significantly change the results of the water vapor transmission tests done according to the test method prescribed in the ASTM Standard Test Methods for Water Vapor Transmission of Materials (E 96-00e1). In this paper, close to 900 test points/results have been analyzed to establish this phenomenon. In general, it has also been observed that the effect of corrections is higher for relatively more permeable materials. Figures 8 and 9 show the relationship between the water vapor permeance and correction effect (% difference) for all the 900 test points obtained from 58 building materials. These plots make it very clear that the effects of corrections are more significant for material components that have higher water vapor permeance values. As mentioned earlier and quite naturally the effect of corrections is always positive (i.e., corrected water vapor permeance values are higher than the values before correction). It is also interesting to note that the effect of correction (% difference) is functionally related with the measured permeance value before correction (Fig. 9). In fact, the measured data indicate that it is possible to predict the corrected permeance values using a simple polynomial function (Fig. 9) without even doing the detailed calculation on the correction factors. However, it should be mentioned here that this is a simplistic

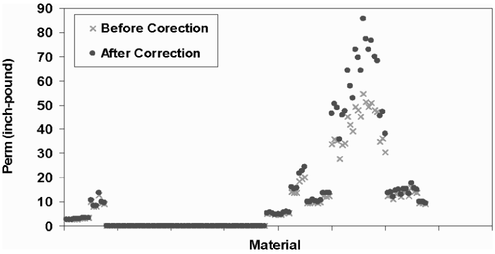

FIG. 7—*Water vapor permeance (membranes): before and after corrections.*

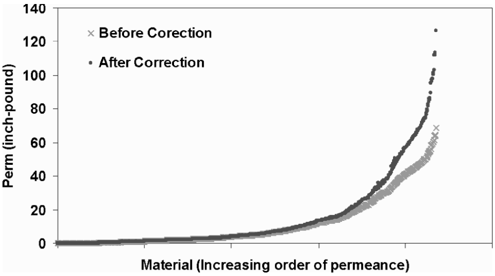

FIG. 8—*Water vapor permeance before and after corrections, and percentage differences.*

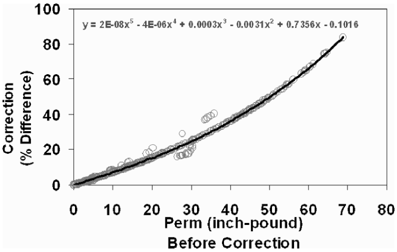

FIG. 9—*Relationship between water vapor permeance and corrections.*

attempt to estimate the correction effects and this polynomial function is valid only for the values generated at the IRC using the existing test setup. It is very likely that the polynomial shown in Fig. 9 will depend on the laboratory and the test setup being used.

Based on the observations presented in the above paragraphs, the experts and the members of the ASTM C16.33 E 96 task group have decided recently that it is important that all applicable corrections be made to all measurements that result in water vapor permeance value more than 2-perm (in.-lb). For permeance values of 2-perm (in.-lb) or less, the effect correction is a negligible 2 percent or lower. These observations or decisions have been implemented in the latest revision of the ASTM Standard Test Methods for Water Vapor Transmission of Materials (E 96/E 96M - 05).

Conclusions

Close to 900 water vapor transmission properties measurement test data obtained from 58 building materials are presented in this paper with the objective to demonstrate the effect of various corrections on the measured water vapor transmission properties. The critical observations and discussion on these results have been used as the basis for changes in the latest revision of the ASTM Standard Test Methods for Water Vapor Transmission of Materials (E 96/E 96M - 05). The observations and discussion presented in this paper clearly demonstrate:

1. Corrections applied to the water vapor transmission properties measurement can be significant for many building materials.
2. Resulting corrected water vapor transmission properties are higher than the same before correction.
3. The effect of corrections is relatively higher for material components that have lower resistance to water vapor transmission.
4. Based on these observations ASTM C16.33 - E 96 task group has recommended that all applicable corrections be made to all measurements that result in water vapor permeance value more than 2-perm (in.-lb).

Appendix

In a desiccant test on a sample of medium density glass fiber insulation the following results were recorded (see Table A1).

Thickness of the specimen =25.81 mm
Test area =0.01642 m^2
Mass of the test specimen =20.44 g
Mass of the desiccant =554.8 g
Initial mass of the test assembly =1.257810 kg
Thickness of air layer in the cup =15 mm

TABLE A1—*Recorded test data.*

Elapsed Time (h)	Mass of the Test Assembly (g)	Change in Mass (g)	Chamber Temperature (°C)	Chamber RH (%)	Barometric Pressure mm Hg (kPa)
0.000	1257.810	0.000	22.83	52.60	744.7 (99.27)
6.067	1259.469	1.659	22.84	52.6	741.11 (98.79)
26.633	1264.609	6.799	22.78	52.2	744.41 (99.23)
53.150	1271.062	13.252	22.82	52.1	743.21 (99.07)
143.767	1290.773	32.963	22.74	52.2	757.69 (101.00)
168.283	1296.389	38.579	22.78	52.1	749.81 (99.95)
192.883	1301.953	44.143	22.78	52.1	758.44 (101.10)

Buoyancy Correction

The buoyancy effect will be insignificant for this set of readings as recorded changes of mass are all above 100 mg. However, for example, the corrected mass of the test assembly weight 1257.810 g (1st reading) can be calculated using Eq. 4.

m_1=mass recorded by balance, kg=1257.810×10^{-3} kg
P=barometric pressure, Pa=99.27×10^{3} Pa
R=gas constant for dry air =287.055 J/(kg.K)
T=chamber temperature =22.83+273.15=295.98 K
ρ_a=density of air, kg m^{-3}=1.1684 kg m^{-3} ρ_1=density of material of balance weights, kg m^{-3}=8000 kg m^{-3}
h_1=height of the test assembly, m=44.7×10^{-3} m
d_1=diameter of the test assembly, m=168.0×10^{-3} m
ρ_2=bulk density of test assembly, kg m^{-3}= =$4\times m_1/\pi\times d_1^2\times h_1$=1269.4 kg m^{-3}
m_2=mass after buoyancy correction =1258.78×10^{-3} kg.

A graphic analysis of the data gives the following (Fig. A-1):

A linear least-squares analysis of the data gives the slope of the straight line as 0.225±0.002 g·h^{-1}, with a linear regression coefficient >0.998.

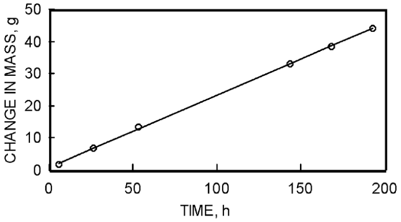

FIG. A-1—*Graphic analysis of the test data.*

WVT=0.225 $\text{g.h}^{-1}/0.01642\ \text{m}^2$
$=19.595\ \text{grains.h}^{-1}.\text{ft}^{-2}$ ($\approx 3.81\times 10^{-6}\ \text{kg}\cdot\text{m}^{-2}\cdot\text{s}^{-1}$)
$S=2775.6$ Pa
$R_1=0.523$
$R_2=0$
Permeance$=3.81\times 10^{-6}\ \text{kg}\cdot\text{m}^{-2}\cdot\text{s}^{-1}/(2775.6\ \text{Pa}\times 0.523)$
$=2.63\times 10^{-9}\ \text{kg}\cdot\text{m}^{-2}\cdot\text{s}^{-1}\cdot\text{Pa}^{-1}$

Corrections for Resistance due to Still Air and Specimen Surface

Permeability of still air layer (equation 5) =
$\delta_a = 2.306\times 10^{-5}\times 101325\big/461.5\times(22.79+273.15)\times 99860\left(22.79+273.15/273.15\right)^{1.81}$
$=1.98062\times 10^{-10}\ \text{kg}\cdot\text{m}^{-1}\cdot\text{s}^{-1}\cdot\text{Pa}^{-1}$
Permeance of 15-mm still air layer $=(1.98062\times 10^{-10})/(0.015)\text{kg}\cdot\text{m}^{-2}\cdot\text{s}^{-1}\cdot\text{Pa}^{-1}$
$=1.32041\times 10^{-08}\ \text{kg}\cdot\text{m}^{-2}\cdot\text{s}^{-1}\cdot\text{Pa}^{-1}$
Hence, the 15-mm air layer offers a vapor resistance $=1/(1.32041\times 10^{-08})\text{m}^2\cdot\text{s}\cdot\text{Pa}\cdot\text{kg}^{-1}$
$\approx 7.6\times 10^{7}\ \text{m}^2\cdot\text{s}\cdot\text{Pa}\cdot\text{kg}^{-1}$
Surface resistances $\approx 4.0\times 10^{7}\ \text{m}^2\cdot\text{s}\cdot\text{Pa}\cdot\text{kg}^{-1}$
Total corrections for resistance due to still air and specimen surface
$=(7.6\times 10^{7}+4.0\times 10^{7})\text{m}^2\cdot\text{s}\cdot\text{Pa}\cdot\text{kg}^{-1}$

Edge Mask Correction

The test assembly used does not include any edge masking. However, for example, if it includes an edge mask of width 5 mm then the following correction is to be made.

h=specimen thickness, m$=25.81\times 10^{-3}$ m
b=width of masked edge, m$=5\times 10^{-3}$ m
Test area$=0.01642\ \text{m}^2$
Perimeter=0.4541 m
S_1=four times the test area divided by the perimeter$=4\times 0.01642/0.4541=0.1446$ m
Percent excess WVT$=400\times 25.81\times 10^{-3}\big/\pi\times 0.1446\ \log_e\left(2\big/1+e^{-(2\pi\times 5\times 10^{-3})/(25.81\times 10^{-3})}\right)=9.86\ \%$
The applicable corrections required for the analysis of the test results in this case are due to resistance of still air and specimen surface.
Water vapor resistance of the test specimen+corrections$=1/\text{Permeance}=(1/2.63\times 10^{-9})\text{m}^2\cdot\text{s}\cdot\text{Pa}\cdot\text{kg}^{-1}=3.80\times 10^{8}\text{m}^2\cdot\text{s}\cdot\text{Pa}\cdot\text{kg}^{-1}$
The watervapor resistance of the test specimen
$=(3.80\times 10^{8}-(7.6\times 10^{7}+4.0\times 10^{7}))\text{m}^2\cdot\text{s}\cdot\text{Pa}\cdot\text{kg}^{-1}=2.64\times 10^{8}\text{m}^2\cdot\text{s}\cdot\text{Pa}\cdot\text{kg}^{-1}$
Permeance of the test specimen $=1/(2.64\times 10^{8}\ \text{m}^2\cdot\text{s}\cdot\text{Pa}\cdot\text{kg}^{-1})$
$=3.79\times 10^{-9}\text{kg}\cdot\text{m}^{-2}\cdot\text{s}^{-1}\cdot\text{Pa}^{-1}$
$=3790\ \text{ng}\cdot\text{m}^{-2}\cdot\text{s}^{-1}\cdot\text{Pa}^{-1}$
Permeability$=3.79\times 10^{-9}\ \text{kg}\cdot\text{m}^{-2}\cdot\text{s}^{-1}\cdot\text{Pa}^{-1}\times 0.02581$ m
$=9.78\times 10^{-11}\ \text{kg}\cdot\text{m}^{-1}\cdot\text{s}^{-1}\cdot\text{Pa}^{-1}$
$=97.8\ \text{ng}\cdot\text{m}^{-1}\cdot\text{s}^{-1}\cdot\text{Pa}^{-1}$
% difference in water vapor permeance/permeability due to corrections$=((2630-3790)/(2630))\times 100=44.1$ %.

References

[1] Mukhopadhyaya, P., Kumaran, M. K., Tariku, F., and van Reenen, D., "Final Report from Task 7 of MEWS Project at the Institute for Research in Construction: Long-Term Performance: Predict the Moisture Management Performance of Wall Systems as a Function of Climate, Material Properties, etc., Through Mathematical Modeling," Research Report, Institute for Research in Construction, National Research Council Canada, Vol. 132, p. 384, February 1, 2003, (IRC-RR-132), URL: http://irc.nrc-cnrc.gc.ca/fulltext/rr132/.

[2] Mukhopadhyaya, P., Goudreau, P., Kumaran, M. K., and van Reenen, D., "Influence of Material Properties on the Hygrothermal Response of an Ideal Stucco Wall—Results from Hygrothermal Simulations," *6th Nordic Building Physics Symposium*, Trondheim, Norway, 2002, pp. 611–618.

[3] Tveit, A., "Measurements of Moisture Sorption and Moisture Permeability of Porous Materials," Norwegian Building Research Institute, Report 45, Oslo, 1966, p. 39.

[4] Chang, S. C. and Hutcheon, N. B., "Dependence of Water Vapour Permeability on Temperature and Humidity," *American Society of Heating, Refrigerating, and Air-Conditioning Engineers (ASHRAE) Transactions*, Vol. 62, No. 1581, 1956, pp. 437–449.

[5] Burch, D. M., Thomas, W. C., and Fanney, A. H., "Water Vapour Permeability Measurements of Common Building Materials," *American Society of Heating, Refrigerating, and Air-Conditioning Engineers (ASHRAE) Transactions*, Vol. 98, Part 2, 1992, pp. 486–494.

[6] Kumaran, M. K., "Alternative Procedure for the Analysis of Data from the Cup Method Measurements for Determination of Water Vapor Transmission Properties," *J. Test. Eval.*, Vol. 26, No. (6), pp. 575–581.

[7] Kumaran, M. K., "Hygrothermal Properties of Building Materials," *ASTM Manual on Moisture in Buildings*, September 1, 2001, pp. 29–65.

[8] Barrer, R. M., *Diffusion In and Through Solids*, Cambridge University Press, London, UK, 1951.

[9] Joy, F. A. and Wilson, H. G., "Standardization of the Dish Method for Measuring Water Vapor Transmissions," National Research Council of Canada, Research Paper 279, January 1966, p. 263.

[10] Galbraith, G. H., Guo, J. S., and McLean, R. C., "The Effect of Temperature on the Moisture Permeability of Building Materials," *Build. Res. Inf.*, Vol. 28, No. 4, 2000, pp. 245–259.

[11] Mukhopadhyaya, P., Kumaran, M. K., and Lackey, J., "Use of the 'Modified Cup Method' to Determine Temperature Dependency of Water Vapor Transmission Properties of Building Materials," *J. Test. Eval.*, September 2005.

[12] Hedenblad, G., "Materialdata för fukttransportberäkningar," T19:1996. ISBN 91-540-5766-3. Byggforskningsrådet, Stockholm, Sweden.

[13] Hedenblad, G., "Moisture Permeability of Some Porous Building Materials," *Proceedings of the 4th Symposium, Building Physics in the Nordic Countries*, Espoo, Vol. 2, 1996, pp. 747–754.

[14] Hansen, K. K. and Lund, H. B., "Cup Method for Determination of Water Vapor Transmission Properties of Building Materials. Sources of Uncertainty in the Methods," *Proceedings of the 2nd Symposium, Building Physics in the Nordic Countries*, Trondheim, 1990, pp. 291–298.

[15] Lackey, J. C., Marchand, R. G., and Kumaran, M. K., "A Logical Extension of the ASTM Standard E 96 to Determine the Dependence of Water Vapor Transmission on Relative Humidity," *Insulation Materials: Testing and Applications; 3rd Volume, ASTM STP 1320*, R. S. Graves and R. R. Zarr, Eds., ASTM International, West Conshohocken, PA, 1997, pp. 456–470.

[16] McGlashan, M. L., "Physico-Chemical Quantities and Units," *Royal Institute of Chemistry Monographs for Teachers*, No. 15, 1971, p. 8.

[17] Schirmer, R., ZVDI, Beiheft Verfahrenstechnik, Nr. 6, S170, 1938.

[18] Pedersen, C. R., Ph.D. thesis, Thermal Insulation Laboratory, The Technical University of Denmark, 1990, p. 10.

[19] Kumaran, K., Lackey, J., Normandin, N., van Reenen, D., and Tariku, F., "Summary Report from Task 3 of MEWS Project," Institute for Research in Construction, National Research Council, Ottawa, Canada, (NRCC-45369), 2002, pp. 1–68.

[20] Kumaran, K., Lackey, J., Normandin, N., Tariku, F., and van Reenen, D., "A Thermal and Moisture Transport Property Database for Common Building and Insulating Materials," Final Report from ASHRAE Research Project 1018-RP, 2004, pp. 1–229.

[21] Mukhopadhyaya, P., Lackey, J., Normandin, N., Tariku, F., and van Reenen, D., "Hygrothermal Performance of Building Envelope Retrofit Options: Task 1—A Thermal and Moisture Transport Property Database," IRC/NRC, National Research Council Canada, Ottawa, Client Final Report, 2004, pp. 1–37, (B-1137.5).

[22] Kumaran, M. K., "A Thermal and Moisture Property Database for Common Building and Insulation Materials," *American Society of Heating, Refrigerating, and Air-Conditioning Engineers (ASHRAE) Transactions*, Vol. 112, Part 2, 2006, pp. 485–497.

Journal of ASTM International, Vol. 4, No. 5
Paper ID JAI100369
Available online at www.astm.org

Carsten Rode,[1] *Ruut Peuhkuri,*[2] *Berit Time,*[3] *Kaisa Svennberg,*[4] *and Tuomo Ojanen*[2]

Moisture Buffer Value of Building Materials

ABSTRACT: When building materials are in contact with indoor air they have some capacity to moderate the variations of indoor humidity in occupied buildings. But, so far, there has been a lack of a standardized quantity to characterize the moisture buffering capability of materials. It has been the objective of a recent Nordic project to define such a quantity, and to declare it in the form of a NORDTEST method. The Moisture Buffer Value is the figure that has been developed in the project as a way to appraise the moisture buffer effect of materials, and the value is described in the paper. Also explained is a test protocol which expresses how materials should be tested for determination of their Moisture Buffer Value. Finally, the paper presents some of the results of a round robin test on various typical building materials that has been carried out in the project.

KEYWORDS: building materials, moisture transport, humidity, buffer effect, indoor climate, material properties

Nomenclature

Symbol = *Explanation Unit*
A = Area m^2
b_m = Moisture effusivity kg/(m^2·Pa·s$^{1/2}$)
Bi_m = Moisture Biot number -
d_p = Penetration depth m
g = Moisture flux kg/(m^2·s)
G = Moisture uptake kg/m^2
$\dot{G}$ = Moisture release rate g/h
m = Mass kg
MBV = Moisture Buffer Value kg/(m^2· % RH)
n = Air change rate h^{-1}
p = Water vapor pressure Pa
p_s = Saturation vapor pressure Pa
RH = Relative humidity %
t = Time s
t_p = Period s
u = Moisture content kg/kg
V = Volume m^3
Z_p = Vapor diffusion resistance Pa·m^2·s/kg
β_p = Moisture transfer coefficient kg/(Pa·m^2·s)
δ_p = Water vapor permeability kg/(m·s·Pa)
φ = Relative humidity -
ν = Water vapor concentration kg/m^3
ρ = Density kg/m^3

Manuscript received February 5, 2006; accepted for publication May 2, 2007; published online May 2007. Presented at ASTM Symposium on Heat-Air-Moisture Transport: Measurements on Building Materials on 23 April 2006 in Toronto, Canada; P. Mukhopadhyaya and M. Kumaran, Guest Editors.

[1] Assoc. Prof., Technical University of Denmark, DK-2800 Kgs. Lyngby, Denmark.

[2] Research Scientist and Senior Research Scientist, respectively, VTT Technical Research Centre of Finland, FIN-02044VTT, Finland.

[3] Research Director, SINTEF Building and Infrastructure, N-7491Trondheim, Norway.

[4] Researcher, Lund Institute of Technology, SE-221 00Lund, Sweden.

Introduction

Indoor humidity is an important parameter to determine the occupants' perception of indoor air quality [1], and is also an important parameter as a cause of processes which are harmful to the health of occupants [2]. Thus, it is known that humidity has an impact on both the working efficiency and health of occupants. But due to the varying loads, the indoor humidity exhibits significant daily or seasonal variation. Materials that absorb and release moisture can be used positively to reduce the extreme values of humidity levels in indoor climates. Consequently, there is an interest when making performance analysis of buildings to consider the moisture buffering properties of absorbent, porous building materials.

The interest in moisture buffering is not new. Experimental results from climatic chambers were published along with some analytical considerations by Künzel in 1960 [3]. Other climatic chamber tests and field studies were carried out in Sweden in the beginning of the 1980s [4]. These and other early investigations are presented in a recent overview paper [5].

A method to characterize the moisture buffer effect has been proposed already in Ref [6]. An example is given in Ref [7] of the way in which moisture transfer between wood-based structures and indoor air significantly reduces the peak indoor humidity (by as much as 35 % RH) and increases the minimum indoor humidity (up to 15 % RH). A method to calculate the moisture penetration depth has been described in Ref [8].

In Ref [9] a range of different porous building materials was investigated to find their moisture buffer capacity on the indoor air humidity. A specially constructed climate chamber (volume about 0.5 m^3) was used to measure the moisture buffering when there was a periodically varying vapor flux. End grain wood panels showed the best buffering capacity due to the rapid diffusion and the great moisture capacity of wood. On the other hand, cellular concrete covered by a thin gypsum plaster turned out to be the best buffering commercial construction.

In Ref [10] a room size test cell was used to investigate the moisture buffer capacity of plasterboard, chipboard, cellular concrete, plywood, wood panels, and painted plasterboard. The relative humidity of the test cell was a result of given rates of moisture release and removal to/from the cell air and the moisture exchanged with the materials. The highest buffer capacity was measured for wood panels and cellular concrete. The same setup was used in investigations where the layers of a lightweight interior wall were added successively and walls of aerated cellular concrete were tested with and without surface treatment [11]. The results indicated a significant reduction of the moisture buffer effect even when rather permeable surface treatments and layers were applied.

An approach to develop a test method and device to test the effective moisture capacity of structures or material layers is described in Ref [12]. The results showed that pine with moisture transport along the grain has the highest moisture buffer capacity while painted gypsum board has the lowest. These small-scale tests were supplemented by a full-scale experiment together with numerical investigations. The inner surfaces of two identical test rooms were covered by either unpainted or painted gypsum boards, unpainted wood, or aluminum foil. Also, these results pointed out the significance of surface treatments on the moisture buffering.

In Ref [13] the hygroscopic inertia of some covering materials was studied numerically and experimentally which proposed the use of inertia classes for characterization of materials. The tests were performed with 12/12 h cyclic steps between 65 and 85 %RH.

The role of interior furnishings on the total moisture buffer capacity of a room was studied experimentally and numerically in Ref [14]. Pieces of furniture were added step-by-step in the test room with a given moisture production/removal rate. The results showed that it is necessary to include the moisture buffering effect of furniture when studying whole buildings.

An attempt to derive the moisture buffer capacity of various insulation materials by using different dynamic experiments was done in Ref [15]. Both isothermal and nonisothermal tests were used. The results indicated a high sensibility of the resulting moisture buffer capacity on whether one is using parameters from steady-state measurements or one of several types of dynamic measurements.

More results were presented and discussed during a NORDTEST Seminar on Moisture Buffer Capacity in August 2003 [16]. The workshop concluded that there was a need for a definition of the term, which should be technically appropriate, yet comprehensible and indisputable for the industry and users that will apply it. The workshop and the information about recent or ongoing activities on the subject was the background for starting this NORDTEST project, which is comprised of the following activities:

- To establish a robust definition of the moisture buffer ability of materials and material systems used in the indoor environment.
- To define and present a test method to measure the moisture buffer ability according to the definition.
- To carry out a round robin test in order to ensure that testing laboratories are able to handle the test methods, and to establish the first reference measurements on a limited number of representative materials and material systems and to obtain an indication of the expected accuracy level in such measurements.

The primary objective of the project has been the development of a NORDTEST method with a test protocol on how materials and systems should be tested for their moisture buffer ability. It is proposed to call this desired property the Moisture Buffer Value.

The project has now been completed and reported in Ref [17]. This paper will report on some of the main results from the project.

Partners in the NORDTEST project have been the Technical University of Denmark (DTU) (as project leader), VTT, Finland, Byggforsk, Norway (NBI), and Lund University, Sweden (LTH). In addition, the project was followed by an international reference group with participants from six other research institutions.

Definition of Moisture Buffer Value

Different Levels of Moisture Buffering

The moisture buffer performance of a room is the ability of the materials within the room to moderate variations in the relative humidity. These variations can be seasonal or diurnal. Most attention is paid to the moisture buffering of diurnal variations. The moisture buffer phenomena of a room can be described with the scheme of Fig. 1.

The moisture buffer performance depends on the moisture buffer capacities of each material combination and furniture in the room together with the moisture production and air change rate and the ratio between the material surface area and the air volume. The simplest material combination is a homogenous material with a thin layer of stagnant air. The thickness of the boundary air layer will be determined by the air velocity in the room.

On the next level, the system level, the moisture buffer value, which is the subject of this test proposal, depends on the air velocity, area, and thickness of the sample.

In order to have both a theoretical, physics-based definition, and a simple and easily understandable method for categorization, a two-fold description of the moisture buffer capacity has been chosen: A theoretical and a practical one.

Moisture Effusivity: b_m

The theoretical description of moisture buffer capacity on the material level is based on the heat-mass transfer analogy. Well known from heat transport theory is the thermal effusivity which expresses the rate of heat transfer over the surface of a material when the surface temperature changes. The thermal effusivity is defined as the square root of the product of material density, specific heat capacity, and thermal conductivity. By introducing the moisture effusivity, b_m [kg/(m^2 Pa·s$^{1/2}$)], see Eq 1, in a similar way to the definition of thermal effusivity, we can describe the ability of a material to absorb or release moisture.

$$b_m = \sqrt{\frac{\delta_p \cdot \rho_0 \cdot \dfrac{\partial u}{\partial \varphi}}{p_s}} \tag{1}$$

where δ_p [kg/(m·s·Pa)] is the water vapor permeability, ρ_0 [kg/m^3] dry density of the material, u [kg/kg] moisture content, φ [−] relative humidity, and p_s [Pa] saturation vapor pressure. Apart from p_s, which is given by the test conditions, the other parameters in the definition of b_m are all standard material properties.

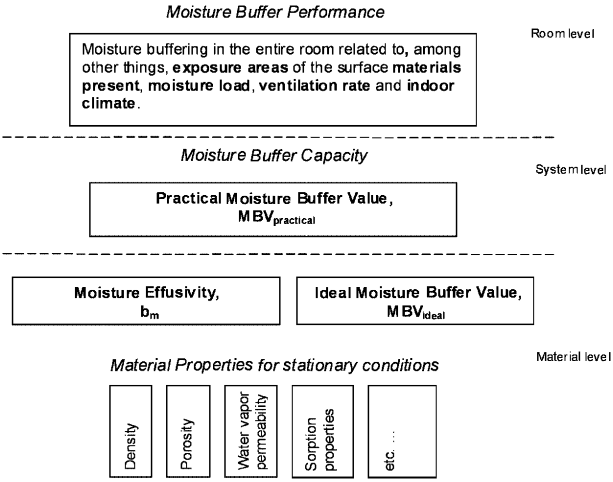

FIG. 1—*Definition scheme for the moisture buffer phenomena in the indoor environment divided into three descriptive levels—material level, system level, and room level. On the material level the quantities are determined with negligible influence from the surrounding climate, e.g., boundary air layers. The system level includes material combinations where the simplest form of a material combination is a homogeneous material with the convective boundary air layer normally present in indoor environments. Systems may also comprise composite products. The room level includes the building and furnishing materials exposed to the indoor air as well as moisture loads, ventilation rate, indoor climate, and other factors influencing the moisture buffering in the room.*

The moisture effusivity constitutes one theoretical possibility to express the rate of moisture absorbed by a particular material (i.e., as a material property) when it is subjected to a sudden increase in surface humidity. The use of this quantity could be extended to cases where the humidity increase takes place in the surrounding air, if the convective mass transfer coefficient tends to infinity.

Ideal Moisture Buffer Value

From the heat transport theory it is known how to handle surface transport phenomena in cases not only when the surface temperature suddenly jumps from one level to another, but also when it varies according to a sine function (harmonic variations). Furthermore, by using Fourier analysis, these results can be transformed into cases with other functional forms of the time variation of the surface conditions.

One such functional form is the signal function, which is a steadily repeating function with a high level of the surface condition for one duration of time, and a low surface condition for another period of time. Of interest for this project is a signal function of humidity where the high humidity is maintained for eight hours, and the low humidity lasts for sixteen hours. Fourier analysis makes it possible to predict the surface moisture flux versus time, $g(t)$, for such an exposure. The accumulated moisture uptake $G(t)$ [kg/m^2], respectively, moisture release, that both happen within the time period t_p are found by integrating the moisture flux over the surface $g(t)$ as in Eq 2:

$$G(t) = \int_0^t g(t)dt = b_m \cdot \Delta p \cdot h(\alpha)\sqrt{\frac{t_p}{\pi}} \tag{2}$$

where

$$h(\alpha) = \frac{2}{\pi}\sum_{n=1}^{\infty} \frac{\sin^2(n\pi\alpha)}{n^{3/2}} \approx 2.252[\alpha(1-\alpha)]^{0.535} \tag{3}$$

α [−] is the fraction of the time period where the humidity level is high. For the 8/16 h scheme, $\alpha = 1/3$, which makes $h(\alpha) = 1.007$ and the accumulated moisture uptake can be expressed in a simpler form:

$$G(t) \approx 0.568 \cdot b_m \cdot \Delta p \sqrt{t_p} \tag{4}$$

The moisture uptake within eight hours corresponds to the moisture release during sixteen hours.

We define a Moisture Buffer Value as a characteristic of the material based on this moisture uptake/release. The Moisture Buffer Value is expressed based on the moisture exchange from Eq 4 normalized with the change in surface relative humidity, ΔRH, and we abbreviate it as MBV. The MBV is proportional to the moisture effusivity b_m times the square root of the time period, $t_p^{1/2}$ [$s^{1/2}$]. The thus defined theoretical, or *ideal*, value of MBV is given by Eq 5, which is derived from Eq 4.

$$MBV_{ideal} \approx \frac{G(t)}{\Delta RH} = 0.00568 \cdot p_s \cdot b_m \cdot \sqrt{t_p} \tag{5}$$

The moisture effusivity is theoretically based on material properties which are usually determined under steady-state and equilibrium conditions. However, the buffer property represents a dynamic characteristic. There *may* be some discrepancy between the basic material properties depending on whether they have been determined under steady-state or dynamic conditions, and this may have some influence on the determination of the moisture buffer value.

Since the ideal experimental conditions rarely exist, and therefore Eq 5 is only an approximation, a calculation tool has been developed that simulates numerically the same type of experiment as used for determination of Moisture Buffer Value using the same stationary material properties as for the calculation of moisture effusivity. Further information on the background and theoretical approach to the calculation tool is given in Ref [17].

The ideal moisture buffer capacity is based on the assumption that the materials studied have a thickness that exceeds the penetration depth of that material or a material combination.

Practical Moisture Buffer Value

For practical categorization of materials the Moisture Buffer Value based on an experimental method can be used. The determination of a practical Moisture Buffer Value should involve a run time which corresponds to that of typical exposure in practice—typically a daily variation. Likewise, it should be useful for the material thickness, surface mass transfer conditions, and surface coatings normally used in practice.

The practical Moisture Buffer Value ($MBV_{practical}$) indicates the amount of water that is transported in or out of a material per open surface area, during a certain period of time, when it is subjected to variations in relative humidity of the surrounding air. When the moisture exchange during the period is reported per open surface area and per % RH variation, the result is the $MBV_{practical}$. The unit for $MBV_{practical}$ is $kg/(m^2 \cdot \%RH)$.

The concept of the practical Moisture Buffer Value can easily be appreciated and understood from an experimental point of view, and likewise, it is relatively straightforward to measure.

The practical Moisture Buffer Value is determined in an experimental setup where the sample is exposed to cyclic step changes in RH between high and low values for eight and sixteen hours, respectively. For example the normal case will be a periodic exposure of 8 h at 75 % RH and 16 h at 33 %, the size of the RH interval will then be 42 % RH. This kind of measurement sequence is shown later in Fig.3.

The value is a direct measure of the amount of moisture transported to and from a material when the exposure is given. The value should ideally be a property of the material, but it may turn out that it is somewhat influenced by the experimental and geometrical conditions. For instance, the practical and the ideal moisture buffer value will only be similar if the material is homogenous and its thickness exceeds the depth to which the periodic signal from the surface will penetrate.

Sample Thickness

The penetration depth, d_p, at which the excitation of the moisture variation is only 1 % of the amplitude at the surface, is:

$$d_{p,1\,\%} = 4.61\sqrt{\frac{\delta_p p_s t_p}{\rho_0 \dfrac{\partial u}{\partial \varphi}\pi}} \tag{6}$$

Samples should be thicker than $d_{p,1\,\%}$.

Surface Coefficient

In the determination of penetration depth, the periodic changes are supposed to take place on the material surface. But in reality, the variations occur in the ambient air, and a surface resistance to moisture transfer exists which slows down the moisture exchange. The correlation between the theoretical moisture effusivity and $\mathrm{MBV}_{\mathrm{practical}}$ can be found only in the limit when the convective mass transfer coefficient tends to infinity—the ideal situation.

When water vapor is transmitted from within a material to the ambient air, the primary resistance to this flow is quite often within the material itself, $Z_{p,m}$. However, there is also a relatively small resistance, $Z_{p,s}$, related to the convective moisture flow over the surfaces of the material. The convective surface coefficient for moisture transfer can be expected to be around $\beta_p = 2.0 \cdot 10^{-8}$ kg·m^2·s/Pa. This corresponds to a convective surface resistance for moisture transfer of $Z_{s,p} = 5.0 \cdot 10^7$ Pa/(kg·m^2·s). These are normal values for environments with an ambient air velocity around 0.1 m/s.

A Biot-number could be defined to express the ratio between the resistance to moisture flow internally in the material and the resistance to surface moisture transfer. If the moisture penetration depth from Eq 6 is used to give a measure of the internal surface resistance, the moisture Biot-number, Bi_m, could be written as:

$$Bi_m = \frac{d_{p,1\,\%}}{\delta_p Z_{p,s}} \tag{7}$$

It may be suggested that Bi_m should have a value of at least 50 to ensure an acceptably low influence of the surface moisture resistance.

Duration of Cycle

The MBV has its validity only for a certain declared period length, which for the NORDTEST method is chosen to be 24 h (8+16 h).

In Ref [18] some further analysis of the Moisture Buffer Value's sensitivity to material thickness is given, but also to the influence of the surface mass transfer coefficient, and duration of the periodic exposure.

Finally, it is worth noting that determination of the Moisture Buffer Value involves processes which are nonlinear, since both vapor permeability and sorption depend on the moisture content; it involves sorption processes which exhibit some hysteretic effects; and the processes are also somewhat temperature dependent.

Test Protocol

The NORDTEST project defines a test protocol for experimental determination of the moisture buffer value. The principle is based on climatic chamber tests, where a specimen is subjected to environmental changes that come as a square wave in diurnal cycles.

The test protocol proposes to use climatic exposures which vary in 8 h+16 h cycles: 8 h of high humidity followed intermittently by 16 h of low humidity. The reason for the asymmetry in this time scheme is two-fold: (1) it replicates the daily cycle seen in many rooms, e.g., offices or bedrooms, where the load comes in approximately 8 h, and (2) for practical reasons during testing if the climatic chamber conditions are changed manually, it is a scheme which is easier to keep than a 12 h+12 h shift.

The low humidity is proposed to be 33 % RH, while the high should be 75 % RH. During the tests, it is important that the equipment is able to make rapid RH changes. Testing should always be carried out at 23°C as a reference.

TABLE 1—*Materials tested in the round robin test, and institutions performing the tests.*

Material/Product	DTU	VTT	LTH	NBI
Spruce Plywood (pretest)	x	XX	x	x
Spruce boards	x	XX		x
Precast concrete	XX		x	x
Drywall (paper-faced gypsum)		x	XX	x
Laminated wood	XX	x		x
Lightweight aggregate concrete	XX		x	x
Cellular concrete	XX	x	x	
Brick	XX	x	x	
Birch wood panels		x	x	XX

XX=Country responsible for supplying the material.

Specimens will normally be sealed on all but one or two surfaces so the minimum exposed surface area should be 0.01 m^2. The thickness of the specimen should be at least the moisture penetration depth for daily humidity variations. At least three specimens should be used.

Using an accurate scale, the specimens should be weighed continuously or intermittently during the test. At least five weight measurements should be carried out during the 8 h high humidity part of the last cycle. A minimum of three cycles have to be carried out, and the weight amplitude must not vary by more than 5 % from day to day. This is defined as the three stable cycles. The stable cycles are also characterized by the fact that the daily amounts of moisture uptake and release are approaching each other as shown later in Fig. 4. The mass change should be plotted and normalized as mass change ($m_{8\ hours}-m_0$) per m^2 and per ΔRH to give the MBV.

Round Robin Test and Results

A round robin test has been carried out within the NORDTEST project to try the testing paradigm and to obtain some initial results for typical building materials. In addition, and to guide the formulation of the test protocol, a preliminary test was carried out on some spruce plywood boards that were distributed to all project partners. The materials tested and the institutions doing the tests are listed in Table 1. Each material is tested by three partners.

The institutions did not have quite the same experimental equipment available, and some of the operational routines were also dissimilar, although in accordance with the common test protocol. For example, some institutes did manual weighing of the specimen, while for others it took place by automated logging of a scale. Thus, it has been part of the round robin test to see if it was possible to obtain similar and agreeable results by all institutions.

Figure 2 shows a drawing and photograph of one of the climatic chambers used at DTU. The humidity control of the chamber works by supplying it with either humid or dry air in an intermittent mode, such that the desired humidity in the chamber is achieved.

Figure 3 shows the measured weight change response of one of the specimens when it was subjected to cycles that varied the ambient humidity between 33 and 75 % RH for 16 and 8 h, respectively. The choice of stable cycles and the moisture uptake is marked in the figure.

Figure 4 shows for three different specimens of the same type of material how the moisture uptake and moisture release varied from cycle to cycle until the three stable cycles were attained. Thus the results of measurements of one type of material give the following background for statistical analysis: three specimens with results from three cycles of both moisture uptake and release—altogether $3\times3\times2=18$ bids for the MBV result. The results should be represented at least with their mean value and standard deviation together with information about the number of tested specimens and stable cycles (if different from 3 $\times$3).

Figure 5 shows the MBV for the materials tested by the participating institutions. The bar diagrams indicate for each material and testing laboratory the average of the MBV value and its standard deviation. However, it seems that the order of magnitude for the tested materials is around 1 $g/(m^2\cdot\%\ RH)$, and there may be approximately a factor three of a difference between the materials with the highest and lowest MBV among those tested.

The overall conclusion on the results of the round robin was encouraging: the determination of the

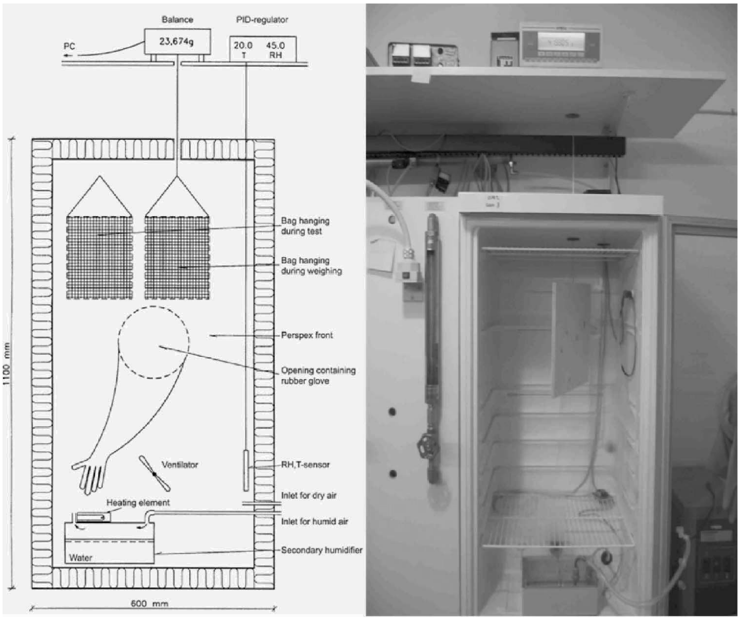

FIG. 2—*Drawing and picture of one of the climatic chambers used at DTU.*

practical Moisture Buffer Value with four very different laboratory equipments gave results that are comparable with each other. Also, consistent differences were found between the ability of different materials to buffer variations in RH of the ambient air: materials like untreated spruce and birch boards and cellular concrete performed as best buffers while materials like brick and concrete were able to buffer under the half of the best buffers (Fig. 5). Further discussion of the results can be found in Ref [17].

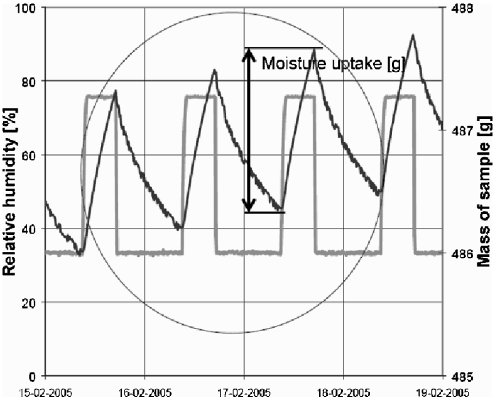

FIG. 3—*Determination of* $MBV_{practical}$ *from dynamic measurements. Definition of quasisteady-state (the three cycles inside the ellipse) and the moisture uptake and release. Also RH for the cyclic steps is given. The rising tendency of the mass is due to the initial conditions that have been lower than the average of the quasisteady-state conditions that will arise after some cycles.*

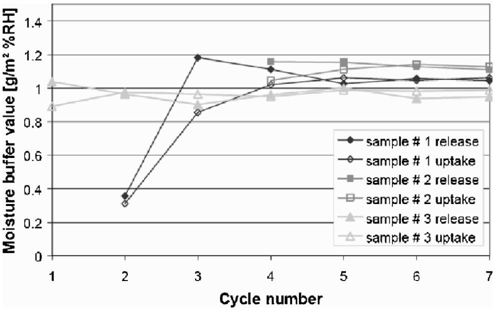

FIG. 4—*MBV of spruce boards as a function of cycle number and uptake versus release. The last three cycles are the stable cycles (=quasisteady).*

Practical Application of the Moisture Buffer Value

The Moisture Buffer Value is primarily meant as a number that can be used to appraise a material's ability to absorb and release moisture from an adjacent space. For practical application it can also be useful as a number for estimation of the moisture balance of rooms, as indicated by the following example.

Example

A room has dimensions 4 by 5 by 2.5 m, and thus a volume of $V=50\ \mathrm{m}^3$. The occupancy and activity in the room releases $\dot{G}=100$ g of moisture per hour. The room is clad with $A=45\ \mathrm{m}^2$ wall panels of spruce board with MBV=1.2 $\mathrm{g/(m^2 \cdot \Delta RH)}$. Initially the room is assumed unventilated, and the storage capacity of the room air is neglected. By how much will the indoor humidity increase during a working day (eight hours)?

All the released moisture is absorbed by the spruce board, and thus, the increase in indoor relative humidity can be calculated from the amount of absorbed moisture, and the moisture buffer value of the wood:

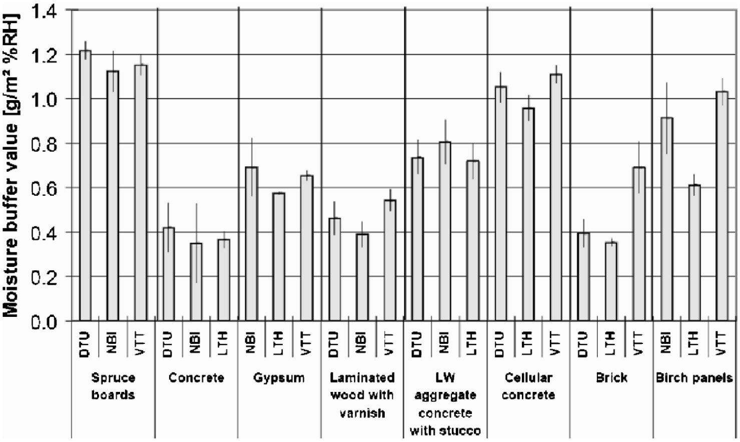

FIG. 5—*Moisture Buffer Values found by different institutions for the different materials. Each bar indicates the average of three specimens over three stable cycles. The thin vertical line bars indicate standard deviations.*

TABLE 2—*Ranges for practical moisture buffer value classes.*

$MBV_{practical}$ Class	Minimum MBV Level	Maximum MBV Level
	[g/(m^2 %RH) @ 8/16 h]	
Negligible	0	0.2
Limited	0.2	0.5
Moderate	0.5	1.0
Good	1.0	2.0
Excellent	2.0	…

$$\Delta RH = \frac{\dot{G} \cdot \Delta t}{\mathrm{MBV} \cdot A} = \frac{100\ \mathrm{g/h} \cdot 8\ \mathrm{h}}{1.2\ \mathrm{g/(m^2 \cdot\ \%\,RH)} \cdot 45\ \mathrm{m^2}} = 15\ \ \%\,\mathrm{RH}$$

In comparison the RH would increase in principle by about 90 % RH (or condensation would occur before then) if there were no ventilation or absorbing materials—this is evaluated at 20°C.

Finally, if the room were ventilated at an air change rate of $n = 0.5\ \mathrm{h^{-1}}$, the indoor humidity would in an equilibrium situation have an indoor vapor concentration, ν, which is higher than the outdoors by:

$$\Delta \nu = \frac{\dot{G}}{n \cdot V} = \frac{100\ \mathrm{g/h}}{0.5\ \mathrm{h^{-1}} \cdot 50\ \mathrm{m^3}} = 4\ \mathrm{g/m^3}$$

At 20°C this would correspond to 23 % higher indoor relative humidity compared to the same room without moisture release.

These calculations are too simplistic to fully represent the real dynamic conditions of a room which is influenced by both ventilation and buffering of room air and materials. However, they indicate some orders of magnitude and render some possibility to reflect over which parameters are important to govern indoor humidity variation in an indoor space with occupancy and cladding with various materials.

Classification of Materials Using Practical Moisture Buffer Values

When moisture buffering of building materials causes the same magnitude of average moisture flow rate as what the minimum required air change causes, the buffering effect can be considered to be quite significant for the moisture performance of a room space. It is obvious that the optimum moisture buffering response should be as high and fast as possible, but it has to be compared to the determined $MBV_{practical}$ values for different building materials in order to evaluate the realistic ranges. Most of the round robin test materials (measured without surface coating) had moisture buffering capacity in the range of 0.5–1.2 g/(m^2 %RH) @ 8/16 h. Thus the $MBV_{practical}$ level 2 g/(m^2 %RH) @ 8/16 h represents a very high efficiency moisture buffering material. On the other hand, if the $MBV_{practical}$ value corresponds to less than 10 % of the effect of the ventilation, it has a (close to) negligible effect on the whole building performance aspect. Based on these approximations, the $MBV_{practical}$ values can be classified using five different categories. Table 2 and Fig. 6 present the selected limits for the moisture buffering capacity values. These are the first approximations for classification of the moisture buffer performance of building materials and products and they can be adjusted and updated for different applications and with new research results.

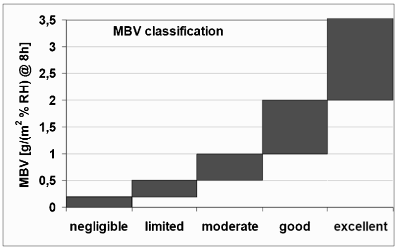

FIG. 6—*Graphic presentation of practical moisture buffer value classes.*

Discussion and Conclusion

The described work has produced a definition of a quantity, the Moisture Buffer Value (MBV), which can be used to describe the ability of building materials and systems of materials to exchange moisture with the indoor environment. The moisture buffer value indicates how much moisture is absorbed or released by a material when the humidity of air changes in the environment that surrounds the material. The property is dedicated for this purpose, and therefore constitutes a better choice as a parameter to express the moisture buffer property of building products than other standard hygrothermal properties, such as the sorption curve and sorption capacity, water vapor permeability, and penetration depth. Although the standard properties have a relation with the MBV, they do not precisely stipulate the flow of moisture being exchanged between a material and the surrounding air—and different relative rankings of materials result from the other parameters simply because they express some different properties. It is proposed therefore to use the Moisture Buffer Value concept when assessing the ability of materials and systems to moderate humidity variations in the environment that surrounds them.

The Moisture Buffer Value can be seen either as a pure material property or a practical performance property. The pure material property is valid only for a homogenous material layer, and it can be measured only under ideal surface transfer conditions. Under these ideal conditions the convective moisture transfer process at the material surface presents no resistance to the flow of moisture in or out of the material. This MBV_{ideal} has a close relationship with the so-called moisture effusivity, which is a parameter that can be derived purely from standard hygrothermal material properties.

However, in practice there is some degree of a convective resistance at surfaces—both in normal indoor environments and in climate chambers where the properties are tested. In addition, many building products are not homogenous and may have particular surface treatments. The project therefore has introduced the $MBV_{practical}$ definition. For $MBV_{practical}$ is assumed a surface resistance corresponding to normal air flow conditions seen in indoor environments (air velocity between 0.05 and 0.15 m/s), and an exposure with daily variations with eight hours of high air humidity (75 % RH) and sixteen hours with low humidity (33 % RH). Due to this $MBV_{practical}$ definition, the value can be determined also for other multilayer building components than just materials with surface coatings. In this case the result should be clearly separated from the pure material property. For example, the thickness of the material layer may have a significant effect on the practical performance value.

A test protocol has been developed to determine the practical Moisture Buffer Value. The test protocol constitutes the project's proposal for a NORDTEST method.

A round robin test has been carried out as part of the project where eight different building materials and material systems were tested for their moisture buffer performance. Each material was tested by three different institutes, and the objective was to see that even if the equipment was not the same, it was possible to obtain reasonably similar results. The round robin has given some first results of $MBV_{practical}$ for those materials and systems which were involved in the test.

A side product from the project has been the development of a computer program which can be used to convert between standard moisture transport properties for building materials and the MBV value, and to display a comparison between measured results and the theoretical moisture uptake/release by a material.

One objective of this standardization project was to define a practical performance value that is easy to comprehend and possible to compare with the moisture loads and effects of ventilation. The other objective was to represent a practical and easy to use method to determine this value. This practical approach was aimed to serve the needs of industry in their product development, for performance comparison, application assessment, and for marketing. Connection of the Moisture Buffering Value to theory and standardized material property values is clear, but the presented method has a practical performance approach.

The MBV can be applied in design practices by comparing the moisture buffering properties of different materials and products used as indoor siding or furnishing purposes. Practical design tools can be developed to quantify the needed or possible MBV levels in different applications. One prospect could be to have an accepted and known MBV classification of materials and products that could be used in marketing and to inform consumers about this performance property. The property and the classification could also serve as a help to obtain understanding and focus in the building industry about the rather comprehensive topic of moisture performance in buildings.

Acknowledgments

This work was supported by the Nordic Innovation Centre, by manufacturers of the tested materials, and by the participant's institutions. The support is gratefully acknowledged.

References

[1] Fang, L., Clausen, G., and Fanger, P. O., "Temperature and Humidity: Important Factors for Perception of Air Quality and For Ventilation Requirements," *ASHRAE Trans.*, Vol. 106, No. 2, 2000, pp. 503–510.

[2] Bornehag, C. G., Sundell, J., and Hägerhed, L., "DBH Study Group, 2003, Dampness in Dwellings and Sick Building Symptoms Among Adults: A Cross-sectional Study on 8918 Swedish Homes," *Proceedings of Healthy Buildings*, 2004, p. 582.

[3] Künzel, H., "Die "klimaregelnde Wirkung" von Innenputzen," *Gesund.-Ing.*, Vol. 81, No. 7, 1960, pp. 196–201.

[4] Harderup, L.-E., *Luftfuktighet i bostäder*, The Department of Building Physics, Lund Institute of Technology, Sweden, 1983, TVBH-3009.

[5] Svennberg, K., Lengsfeld, K., Harderup, L.-E., and Holm, A., "Previous Experimental Studies and Measurements on Moisture Buffering by Indoor Surface Materials," *Journal of Building Physics*, Vol. 30, No. 3, 2007, pp. 261–274.

[6] Time, B., "Hygroscopic Moisture Transport in Wood," Norwegian University of Science and Technology, Dr. Ing. Thesis, 1998.

[7] Simonson, C., Salonvaara, M., and Ojanen, T., "Humidity, Comfort and Air Quality in a Bedroom with Hygroscopic Wooden Structures," *Proceedings of the 6th Symposium on Building Physics in the Nordic Countries*, Trondheim, 2002.

[8] Arfvidsson, J., "Moisture Penetration for Periodically Varying Relative Humidity at the Boundary," *Nordic Journal of Building Physics (Acta Physica Aedificiorum)*, Vol. 2, 1999.

[9] Padfield, T., "The Role of Absorbent Building Materials in Moderating Changes of Relative Humidity," Ph.D. Thesis, Dept. of Structural Engineering and Materials, Technical University of Denmark, Series R No. 54, 1999.

[10] Mitamura, T., Rode, C., and Schultz, J., "Full Scale Testing of Indoor Humidity and Moisture Buffering in Building Materials," *ASHRAE Conference, IAQ 2001—Moisture, Microbes and Health Effects: Indoor Air Quality and Moisture in Buildings*, San Francisco, 2001.

[11] Mortensen, L. H., Peuhkuri, R., and Rode, C., "Full Scale Tests of Moisture Buffer Capacity of Wall Materials," *Proceedings of 7th Nordic Symposium on Building Physics*, Reykjavík, 2005, pp. 662–669.

[12] Salonvaara, M., Ojanen, T., Holm, A., Künzel, H. M., and Karagiozis, A. N., "Moisture Buffering Effects on Indoor Air Quality—Experimental and Simulation Results," *Proceedings of Buildings IX*, Clearwater, FL, 2004.

[13] Ramos, N. and de Freitas, V. P., "Hygroscopic Inertia as a Function of Transient Behavior of Covering Materials," *Proceedings of Buildings IX*, Clearwater, FL, 2004.

[14] Svennberg, K., Hedegaard, L., and Rode, C., "Moisture Buffer Performance of a Fully Furnished Room," *Proceedings of Buildings IX*, Clearwater, FL, 2004.

[15] Peuhkuri, R., Rode, C., and Hansen, K. K., "Moisture Buffer Capacity of Different Insulation Materials," *Proceedings of Buildings IX*, Clearwater, FL, 2004.

[16] *Workshop on Moisture Buffer Capacity—Summary Report*, Dept. of Civil Engineering, Technical University of Denmark, R-067, C. Rode, Ed., 2003.

[17] *Moisture Buffering of Building Materials*, Dept. of Civil Engineering, Technical University of Denmark, Report R-126, C. Rode, Ed., 2005.

[18] Roels, S. and Janssen, H., "A Comparison of the Nordtest and Japanese Test Methods for the Moisture Buffering Performance of Building Materials," *Journal of Building Physics*, Vol. 30, No. 2, 2006, pp. 137–161.

Journal of ASTM International, Vol. 4, No. 8
Paper ID JAI100459
Available online at www.astm.org

Kenneth E. Wilkes,[1] *Jerry A. Atchley,*[1] *Phillip W. Childs,*[1] *and Andre Desjarlais*[1]

Effects of Drying Conditions, Phase Transformations, and Carbonation Reactions on Measurements of Sorption Isotherms of Building Materials

---

ABSTRACT: The sorption isotherm is one of the basic material properties used in hygrothermal modeling of building envelope performance. Measurement of this property is deceptively simple. Specimens are first dried and then exposed to a series of higher relative humidities to develop a curve of moisture content versus relative humidity at constant temperature. This paper discusses some confounding effects that we have observed while performing measurements on a number of common building materials. Materials studied included gypsum products, wood and wood products, and cementitious materials.

KEYWORDS: sorption isotherm, gypsum, wood, wood products, cement, hygrothermal properties

Introduction

The sorption isotherm is a curve of moisture content (MC) versus relative humidity (RH) at a fixed temperature and is one of the basic material properties used in hygrothermal modeling of building envelope performance. Measurement of this property is deceptively simple. Specimens are first dried to remove hygroscopically bound water and then exposed to a series of constant relative humidity conditions until equilibrium mass has been reached at each condition. Moisture content at a given RH may be expressed variously as a percentage of dry mass, fraction of dry mass, volume of moisture divided by volume of dry material, or mass of moisture divided by volume of dry material. For this paper, the moisture content is expressed as a percentage of the dry mass. Measurements of sorption isotherms are covered by ASTM Test Method for Hygroscopic Sorption Isotherms of Building Materials (C 1498-01 and C 1498-04a), and by ISO 12571:2000 (E) [1]. While the method seems straightforward, we have observed a number of effects that confound the results. In particular, we have observed that the drying conditions can have a large effect on the measured isotherms for some building materials.

ASTM C 1498-01 specified drying temperatures as: "(a) for materials which do not change either structure or dimensions at 105°C (221°F), for example, some mineral materials, use 105±4°C (221±8 °F); (b) for materials in which structural or dimensional changes occur between 70°C (158 °F) and 105°C (221 °F), for example, for some cellular plastics, use 70±2°C (158±4 °F); (c) for materials in which elevated temperatures bring about chemical or physical changes, for example, crystalline water in gypsum or blowing agent solubility in some cellular plastics, use 40±2°C (104±4 °F)." ISO 12571:2000 (E) references ISO 12570:2000 (E) [2] for drying conditions, which are the same as for ASTM C 1498-01. ASTM C 1498-01 did not address the RH conditions for drying, while ISO 12570:2000 (E) specifies an RH of less than 10 %.

Measurements on gypsum materials showed that a wide range of sorption isotherms could be obtained under differing drying conditions [3]. Partly in response to these results, the ASTM standard was modified in ASTM C 1498-04a to include provision for a fourth drying condition as: "(d) when drying at the specified aforementioned temperatures adversely affects the building material, dry specimen to moisture free weight (that is, dry weight, see 7.2) in a desiccator at room temperature or inside an airtight chamber flushed with dry air having a dew point less than −40°C (−40 °F)." ASTM C 1498-04a also added a

---

Manuscript received February 13, 2006; accepted for publication August 13, 2007; published online September 2007. Presented at ASTM Symposium on Heat-Air-Moisture Transport: Measurements on Building Materials on 23 April 2006 in Toronto, Canada; P. Mukhopadhyaya and M. Kumaran, Guest Editors.

[1] Distinguished R&D Staff Member, Research Technician, Staff Engineer, and Group Leader, respectively, Oak Ridge National Laboratory, P.O. Box 2008, Oak Ridge, Tennessee 37831-6075.

specification that the relative humidity in the drying oven must be less than 10 %.

In addition to the drying conditions, some materials have other peculiarities that influence the measured isotherms, such as phase transformations and chemical reactions. This paper discusses some confounding effects that we have observed while performing measurements on a number of common building materials. Materials studied include gypsum products, wood and wood products, and cementitious materials.

Experimental Procedures

Two ovens were used to dry the specimens. One oven was ventilated with openings to the ambient air. It is expected that the dew point within this oven would be nearly the same as in the ambient air and thus the RH within the oven would be a function of the oven temperature and the temperature and RH of the air surrounding the oven. The other oven was tightly sealed and was continuously flushed with compressed air piped in from the laboratory's power plant. The air was dried at the power plant to a dew point that varied between −40°C (−40 °F) and −51°C (−60 °F), depending upon the condition of the drying columns. ASTM C 1498 considers drying to be complete when three successive daily weighings produce mass changes of less than 0.1 % of the specimen mass.

After drying, the specimens were placed in air-tight desiccators containing saturated salt solutions that maintained RHs between 11.3 and 97.4 % at a temperature of 23°C (see ASTM C 1498 and ASTM Standard Practice for Maintaining Constant Relative Humidity by Means of Aqueous Solutions (E 104-02)). The desiccators were placed inside controlled temperature/humidity cabinets where the temperature was controlled at 23.0±0.1°C (73.4±0.2 °F). Measurements were started at the lowest RH, and after equilibrium was reached, the specimens were transferred to the next higher RH until measurements had been made over the range of RHs. ASTM C 1498 considers equilibrium to be achieved when five successive daily weighings produce mass changes of less than 0.1 % of the specimen mass.

The specimens consisted of about 10 to 15 g (0.02 to 0.03 lb) of material, usually cut into roughly 12.7 mm $\left(\frac{1}{2}\text{ in.}\right)$ cubes. The specimens were contained in 60 mL (2 fluid oz) flint glass jars with tightly-fitting polypropylene lids from which the cardboard liners had been removed. The lids were placed on the jars for weighings on a balance that had a capacity of 5 kg (11 lb) and a resolution of 1 mg (2×10^{-6} lb). Each data point is the average of three replicates, as specified by ASTM C 1498.

Results and Discussion

Gypsum Materials

Wilkes et al. studied the effects of drying conditions on measurement of sorption isotherms of gypsum building materials [3]. Materials studied were regular gypsum wallboard, regular treated core gypsum sheathing board, and glass mat gypsum substrate, all nominally 12.7-mm $\left(\frac{1}{2}\text{-in.}\right)$ thick. Tests were also performed on regular gypsum wallboard with the paper facings removed. Figure 1 shows a comparison of isotherms obtained with three drying methods with data from the literature [4–7]. This shows that the wide variations in the literature are probably due to differences in drying procedures. In particular, it was found that drying at 40°C (104 °F) at ~0.2 % RH in the oven flushed with dry air was sufficiently adverse to result in complete loss of the water of hydration in gypsum (or dihydrate, $CaSO_4 \cdot 2H_2O$) such that it was converted to anhydrite ($CaSO_4$). The resulting isotherm has large moisture contents that are due to rehydration to form hemihydrate ($CaSO_4 \cdot \frac{1}{2}H_2O$) at about 11 % RH and then dihydrate at 84–94 % RH. Drying in the oven flushed with dry air at temperatures as low as 30°C (86 °F) was found to cause loss of the water of hydration. On the other hand, drying at 40°C (104 °F) at 11–12 % RH in the vented oven was insufficient to remove all of the hygroscopically bound water. However, elevating the temperature in the vented oven to 65°C (149 °F) caused loss of part of the water of hydration to form hemihydrate, and raising the temperature to 103°C (217 °F) caused complete loss of the water of hydration. Based on these results it was recommended that specimens be dried at 23°C (73 °F) and ~0.5 % RH.

Recent measurements on a family of gypsum building products have shown that some as-manufactured materials may contain a significant amount of hemihydrate (a metastable phase) in addition to dihydrate. Figure 2 shows sorption isotherms for two types of gypsum sheathing material made by the

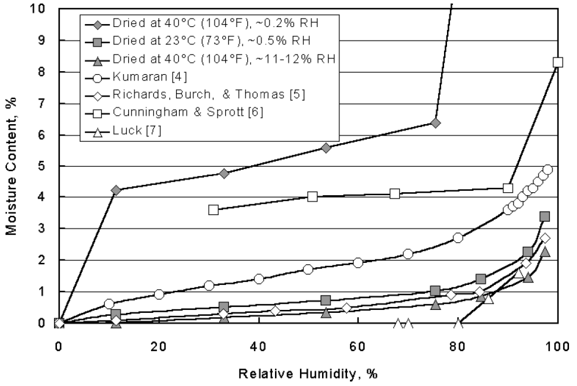

FIG. 1—*Comparison of sorption isotherms for gypsum wallboard with data from literature.*

same manufacturer. Material A was paper-faced and contained 95 % gypsum, 5 % paper, and 1 % starch, while Material B contained 85 % flue-gas-desulfurization gypsum, 10 % cellulose, and 1 % starch, and did not have paper facers. The isotherms were nearly identical up to about 85 % RH, but above this level, the MC for Material B was much greater than for Material A. Upon desorption from 97.4 % RH, the isotherm for Material B remained much higher than for Material A. After redrying, the residual MC for Material A was 0.4 %, while that for Material B was 2.3 %. The sorption and desorption curves between 0 and about 85 % RH are nearly parallel and are offset by approximately the amount of the residual MC. Conversion of pure hemihydrate to pure dihydrate results in a weight gain of 18.6 %. Assuming the residual MCs to be due to the mass change in conversion from hemihydrate to dihydrate, as-received Materials A and B, respectively, would contain 2.2 and 12.4 % by weight of hemihydrate.

Figure 3 shows the change in moisture content versus time as the two gypsum sheathing materials were transitioning from the 84.6 % RH level to 94.0 % RH. While equilibria at lower RHs were achieved in one or two weeks, Material A took about two months to reach equilibrium at 94.0 % RH and Material B took about six months. The sluggish transition for Material B is similar to that observed by Wilkes et al. [3] for the specimens that had been dried so as to remove the water of hydration, and is a further indication of the presence of hemihydrate in the as-received materials, especially for Material B.

Measurement of sorption isotherms requires that the specimens come to equilibrium conditions, but the practical applicability of sorption isotherms that require six months for one step along the RH curve may certainly be questioned. Further work is needed to define what data are needed for these types of materials for building envelope performance analysis purposes.

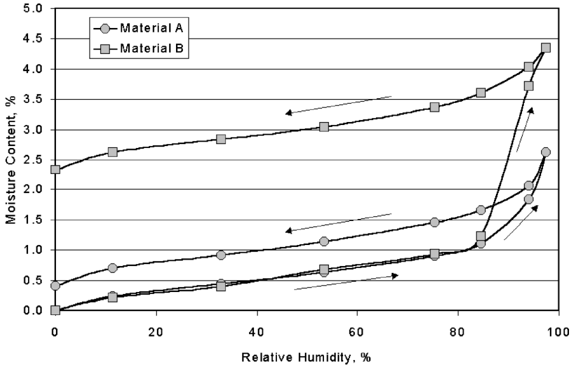

FIG. 2—*Sorption/desorption isotherms for two types of gypsum sheathing.*

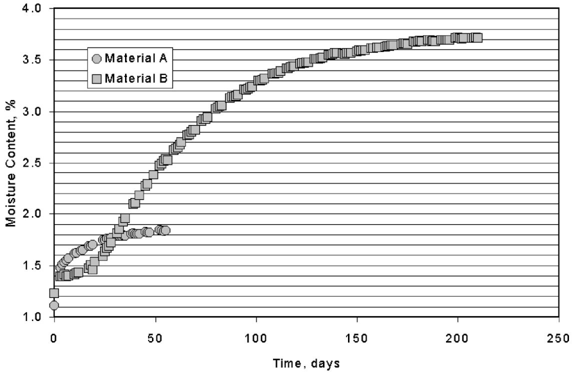

FIG. 3—*Moisture content of gypsum sheathing materials during measurements between 84.6 and 94.0 % RH (the first 24 days were at 90 % RH for Material B).*

Wood-based Materials

ASTM Test Methods for Direct Moisture Content Measurement of Wood and Wood-based Materials (D 4442-92) gives test methods for determining the moisture content of wood and wood products. One of these methods is oven-drying, in which specimens are dried in a vented oven at 103±2°C (217±4 °F). This method utilizes three-hour intervals between weighings rather than daily weighings as used in ASTM C 1498. ASTM D 4442 notes that the moisture content is a misleading term for wood-based materials because of varying amounts of volatile compounds which are evaporated during the drying process. In addition, ASTM D 4442 notes that wood-based materials thermally degrade during oven-drying and this causes the final moisture-free mass to decrease from small but continuous losses.

The effect of drying conditions on the sorption isotherms was studied for four wood-based materials: 11-mm thick (7/16-in. thick) oriented strand board (OSB), 12.7-mm thick ($\frac{1}{2}$-in. thick) plywood, and framing lumber from nominal 2 by 4 and 2 by 6 studs. The specimens were preconditioned to constant mass at 23°C and 32.9 % RH prior to drying. One set of specimens was dried at 103°C (217 °F), as specified in ASTM D 4442, but with daily weighings, as specified in ASTM C 1498. The other set of specimens was dried at room temperature in the oven flushed with dry air such that the RH was less than about 0.5 %.

Table 1 shows the mass losses due to the two drying conditions. After the first day of drying at 103°C (217 °F), the specimens lost mass at a nearly constant rate that ranged from 0.013 % per day to 0.039 % per day. These loss rates agree with a rate of about 0.015 % per day reported by Stamm [8] for dry coniferous wood. Stamm attributes this continuous mass loss as loss of water of constitution, i.e., loss of hydroxyls and hydrogen atoms from the molecular cellulosic structure. The lower final mass losses for OSB and plywood may be because of the lower fraction of wood in these materials due to the glues.

Other specimens were dried at ~23°C (73 °F) and ~0.5 % RH for 69 to 97 days, although most of the mass loss was accomplished within the first 30 days. As Table 1 shows, the final mass loss from drying at this low temperature was about 0.3 to 0.5 percentage points less than drying at 103°C (217 °F).

TABLE 1—*Drying of wood-based materials.*

	Drying at 103°C, <1 %RH			Drying at ~23°C, ~0.5 %RH	
Material	Days	Final Mass Loss, %	Mass Loss Rate, %/day[a]	Days	Final Mass Loss, %
OSB	4	5.1	0.039	69	4.6
Plywood	4	6.0	0.019	97	5.5
2 by 4 Framing	7	7.5	0.013	91	7.2
2 by 6 Framing	7	7.4	0.024	91	7.1

[a] After the first day of drying.

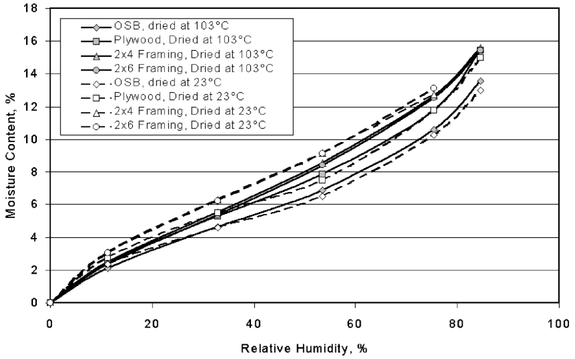

FIG. 4—*Sorption isotherms for wood and wood products.*

Sorption isotherms measured on these materials are shown in Fig. 4, while Fig. 5 shows the difference between the sorption isotherms obtained with the two drying conditions. For framing lumber, the moisture content after drying at 23°C (73 °F) and 0.5 % RH was higher than after drying at 103°C (217 °F). This is the opposite of what would be expected based only on the mass losses during drying. Drying at low temperature gave lower mass losses. If this were due to insufficient drying, then the measured sorption moisture content would also be expected to be lower. This trend is well known in the wood science literature. According to Stamm, "heating wood to the point where there is a loss in the dry weight, causes a significant loss in hygroscopicity of the wood." Stamm further states that this "is believed to be largely due to decomposition of the hemicellulose forming insoluble resinous products prior to further decomposition to form volatile products."

The moisture contents of OSB and plywood were lower than those for framing lumber. The effect of drying conditions was also less for these products than for framing lumber. These effects are partly due to the glue content which is less hygroscopic than wood, and also partly due to the higher temperatures at which OSB and plywood are processed, which would make them less hygroscopic [9].

Based on these results, it appears that drying of wood and wood products at room temperature under desiccated conditions is to be preferred over high temperature oven-drying. The downside is that drying at room temperature takes a much longer time. Richards et al. also advocated desiccant drying at room temperature, especially for wood-based materials [5]. It is likely that drying at some intermediate temperature, e.g., 70°C (158 °F), under desiccated conditions would avoid the loss in hygroscopicity while allowing for a shorter drying time.

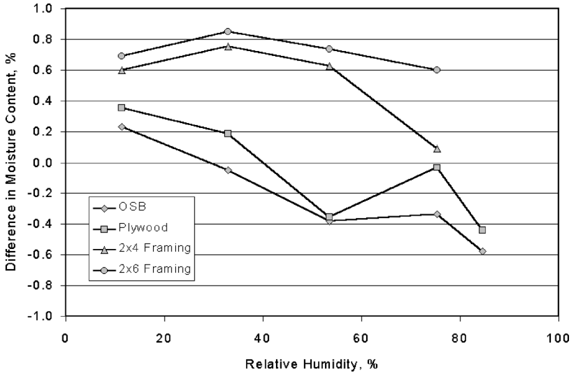

FIG. 5—*Effect of drying conditions on sorption isotherm of wood and wood products. MC for 23°C drying minus MC for 103°C drying.*

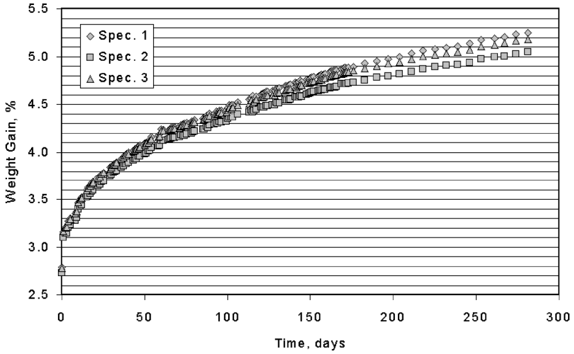

FIG. 6—*Weight gain of cement board specimens during sorption measurements between 53.5 and 75.4 % RH.*

Cementitious Materials

Cementitious materials are complex both physically and chemically. Water can be distributed variously as free water, capillary water, gel water, and water combined in hydrated cement compounds, with no distinct boundaries between the various types. Numerous chemical compounds exist in set cement, the primary ones being calcium hydroxide, calcium silicate hydrates, calcium aluminate hydrates, and calcium sulfoaluminate hydrates.

Two effects (at least) can cause confusion with measurements of sorption isotherms of cementitious materials. One is that drying specimens at too high a temperature can result in loss of water of hydration as well as hygroscopic water. For example, drying at 105 °C can cause calcium sulfoaluminate and calcium aluminate hydrates to lose part of their water of hydration [10]. A second, more subtle effect is carbonation, which is a reaction of carbon dioxide from the atmosphere with chemical compounds in the cement to form carbonates with the release of water. The reaction relies on the presence of liquid water into which the atmospheric CO_2 is dissolved to form carbonic acid, and into which the solid compounds partially dissolve. One such net reaction is $Ca(OH)_2 + CO_2 \rightarrow CaCO_3 + H_2O$, with the $CaCO_3$ precipitating out as solid. The water that is formed by the reaction should come into equilibrium with the specimens and surrounding humid air, but the net effect of the reaction is an extra mass gain since a molecule of carbon dioxide weighs more than one of water. During a sorption isotherm measurement, this extra mass gain will be confused with an increase in moisture content. Salmon and Tye have attributed irreversible mass changes in sorption measurements to this mechanism [11].

Figure 6 shows the weight gain during sorption isotherm measurements on a cement board after the RH was increased from 53.5 to 75.4 %. During the first 117 days other specimens were in the desiccator and these may have influenced the course of weight gain of the cement board specimens. However, after Day 117 no other specimens were present. The specimens were weighed daily (except for weekends) during the first 176 days and after that they were weighed weekly. Over this period of about nine months, the specimens continuously gained weight, and there was no evidence of an approach to equilibrium. These specimens had been dried at 105 °C and part of the weight gain might be rehydration. However, the continuous weight gains might also be due to carbonation.

Figure 7 shows a second example, this one for a stucco material during sorption measurements after the RH was increased from 32.9 to 53.5 %. The mass showed a rapid initial gain and then a peculiar sawtooth pattern with weight gains during the working days and then no gain or even a small loss over each weekend. Again there was no evidence of an approach to equilibrium over the two-month period. This time, the specimens had been dried at room temperature and ~0.5 % RH, so there should be no effect due to loss of hydrated water during drying and then rehydration during the sorption measurements. These weight gains are consistent with a relatively rapid carbonation reaction during the weekdays when the desiccator was opened daily, and slower carbonation along with evaporation of excess water over the weekend when the desiccator remained closed.

These two examples illustrate the difficulty in measuring the sorption isotherms of cementitious

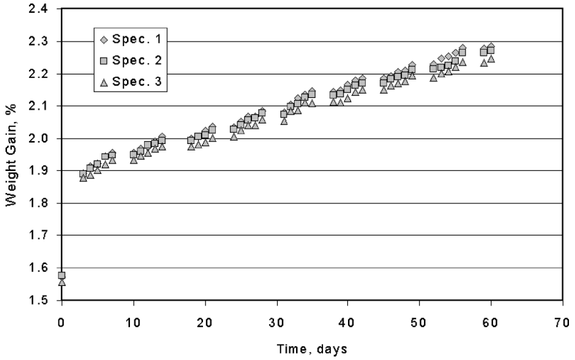

FIG. 7—*Weight gain of stucco specimens during sorption measurements between 32.9 and 53.5 % RH.*

materials. When a single set of specimens is taken through a sequence of increasing RHs, an unknown amount of excess mass gain may be accumulated at each step that would be attributed to moisture content. The final sorption isotherm curve would be subject to a large amount of uncertainty. One partial solution to this problem is to use separate specimens for each RH level.

The effects of carbonation were studied in more detail using specimens of a cement board that consisted of portland cement, fly ash, expanded clay or shale, and a fiberglass mesh. Figure 8 shows the weight gain as specimens were exposed to a sequence of RHs inside the temperature/humidity chambers where the supply of CO_2 should be nearly unlimited. The initial condition for the specimens was as-received, without any initial drying. After periods of time at 50, 70, and 90 % RH, the weight gain curves became nearly linear and had slopes of 0.012, 0.039, and 0.071 % per day, respectively. Again there was no evidence of an approach to equilibrium at any of these three RHs. After dropping back to 70 % RH, the specimens quickly lost a relatively small amount of weight and the weights were constant over two months at this condition. After a further drop to 50 % RH, another small amount of weight was quickly lost and the weight was then nearly constant over a period of 23 days. Figure 8 shows that there is a large irreversible change in MC between increasing and decreasing RHs, which may be attributable to carbonation.

Specimens of the same cement board were used to measure the sorption isotherm curve using separate specimens for each RH. Seven sets of triplicate specimens were prepared to correspond to the seven RH conditions. Three drying procedures were used in the following order: (1) vented oven at 46°C (115 °F), which was recommended by the manufacturer to avoid chemical changes that might occur at higher temperatures; (2) oven flushed with dry air at ~23°C (73 °F) such that the RH was less than about 0.5 %;

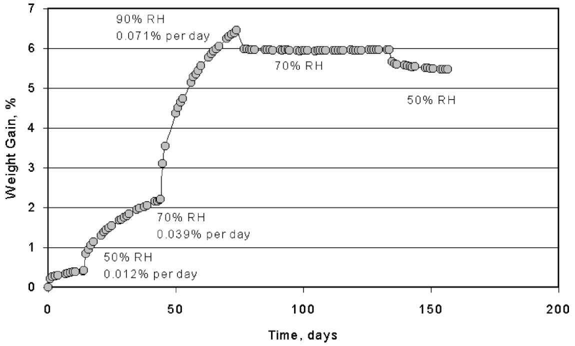

FIG. 8—*Weight gain of cement board in temperature/humidity chambers. The base condition was ≈23°C, ≈35 % RH.*

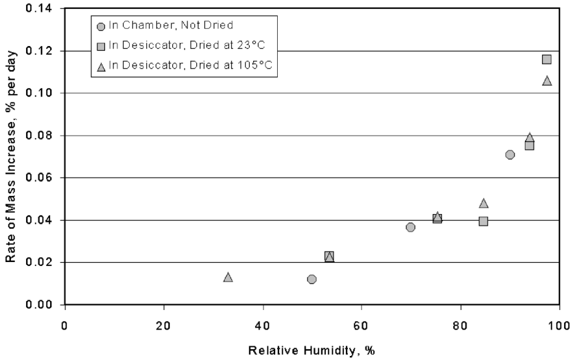

FIG. 9—*Linear mass increases during sorption isotherm measurements. The rates given in Fig. 8 are included for comparison.*

and (3) vented oven at 105 °C (221 °F), which is one of the drying conditions recommended by ASTM C 1498. After sorption measurements were completed following the first drying, the specimens were redried at the same conditions to observe any residual changes in mass. The same specimens were then used for the other two drying conditions in sequence. All three drying procedures were used for the three lowest RHs, but to avoid excessive accumulation of extra mass due to carbonation, only the last two procedures were used for the four highest RHs.

Sorption measurements were limited to times of ten days to two weeks to prevent excessive weight gains. The specimens at the lowest RHs reached equilibrium within this time period, but for higher RHs the mass increased rapidly for the first several days, and then increased nearly linearly. Figure 9 shows that the linear rate of mass increase was a strong function of relative humidity. At relative humidities above about 70 %, the rate of increase is greater than 0.025 % per day, so that the criterion of five successive daily weighings within 0.1 % could not be met. Figure 9 shows that the rate of increase was the same for drying at 23 and 105 °C, so that the increases were not due to rehydration following drying at too high a temperature. Also, the rates of mass increase were nearly the same for specimens contained within desiccators as for specimens contained in the temperature/humidity chambers, so that the increases were not limited by the supply of carbon dioxide.

The sorption isotherm curves obtained with the various drying procedures are compared in Fig. 10. The shaded symbols correspond to the MC measured at the end of ten days to two weeks exposure to the selected RH. The corrected values were obtained by subtracting off the residual MCs after redrying. Figure

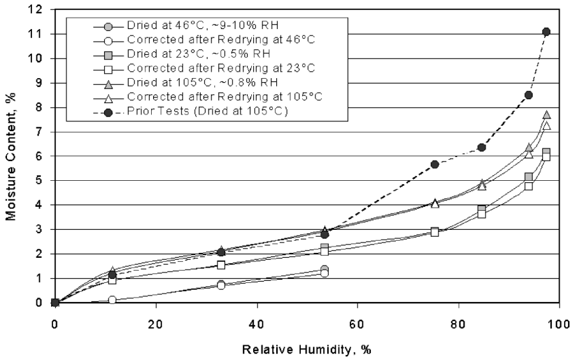

FIG. 10—*Sorption isotherms of cement board after various drying procedures.*

10 shows that small residual MCs were measured in all cases except at the lowest RHs, indicating small amounts of permanent weight gain that should be attributed to carbonation rather than to real moisture content.

The isotherms for drying at 46°C and ~23°C are nearly parallel and differ by ~1 %, which corresponds to the amount of extra moisture removed during drying at ~23°C and the very low RH. The difference is attributed to inadequate drying in the vented oven at 46°C (115 °F), where the RH inside the oven would have been about 9–10 % (based on equality of dewpoint with the 33–38 % RH in the laboratory air).

Drying at 105°C after the redrying step at ~23°C removed an additional mass of about 1.4 %, which may be due to loss of part of the water of hydration from calcium sulfoaluminate and calcium aluminate hydrates. The difference between this isotherm and that for drying at 23°C is 0.4 % at 11.3 % RH and increases to 1.3 % at 97.4 % RH. The divergence between these two isotherms may be due to partial to nearly total rehydration of the cement compounds depending upon the RH conditions. The rehydration must occur quickly since the linear increases at the latter portions of the sorption measurements shown in Fig. 9 do not depend upon the drying conditions.

Finally, Fig. 10 shows the sorption isotherm that was obtained with the earlier tests on cement board that correspond to the mass gain curves in Fig. 6. The curves for the two cement boards dried at 105°C are nearly identical up to 53.5 % RH. The bump for the earlier cement board test at 75.4 % RH is due to the mass increase shown in Fig. 6. This bump affects the remainder of the isotherm, making it much different from the curve obtained using separate specimens for each RH, limiting the amount of time available for carbonation to occur during sorption measurements, and redrying to correct for permanent weight gains.

Summary and Conclusions

Drying conditions can have a substantial effect on measured sorption isotherms. Isotherms for gypsum materials are susceptible to large errors due to loss of water of hydration when specimens are dried improperly. Drying conditions must be sufficient to remove hygroscopically bound water but not so severe as to remove chemically bound water. Drying at 40°C in a vented oven did not remove all of the hygroscopically bound water, especially for gypsum materials that include paper facings. Drying at higher temperatures in a vented oven runs the risk of removal of chemically bound water. Drying under desiccated conditions (such as a desiccator or an oven flushed with dry air) at slightly elevated temperatures will remove chemically bound water. Drying under desiccated conditions at room temperature (~23°C) did not remove chemically bound water and is the recommended procedure. The large variations in literature data on sorption isotherms of gypsum building materials appear to be related to the (often unreported) drying conditions. In addition, some gypsum materials contain significant amounts of metastable hemihydrate that can rehydrate over long periods of time (e.g., ~ six months) during sorption isotherm measurements, leading to large hysteresis upon desorption, and large uncertainty in applicability to hygrothermal modeling efforts.

Sorption isotherms for wood dried at high temperature (103°C) were lower than for similar specimens dried under desiccated conditions at room temperature (~23°C), even though the higher drying temperature resulted in higher mass loss. According to wood science literature, this effect is due to loss of hygroscopicity of wood by high temperature drying. Again, drying under desiccated conditions at room temperature (~23°C) appears to be preferable to the conventional method of drying in a vented oven at 103°C.

Sorption isotherm measurements for cementitious materials can be affected by at least two phenomena. One effect has been attributed to carbonation, which is a reaction of carbon dioxide from the atmosphere with cement chemical compounds such as calcium hydroxide to produce compounds such as calcium carbonate. This can lead to a continuous increase in mass that could erroneously be attributed to an increase in moisture content. When a single specimen is measured through the entire range of RHs, extra mass gains at each RH can accumulate to produce a highly erroneous sorption isotherm. The other phenomenon that can affect the sorption isotherm is again improper drying before the sorption measurements. Drying in a vented oven at too low a temperature can be inadequate to remove hygroscopic moisture, while drying at too high a temperature (e.g., 105°C) can cause loss of water of hydration (similar to that observed with gypsum materials) and subsequent rehydration during sorption measurements.

For all three types of materials studied here, it appears that drying near room temperature under desiccated conditions is preferable to higher temperatures. The peculiar effects attributed to carbonation reactions in cementitious materials can potentially be handled by using separate specimens for each RH, limiting the time available for the reaction to occur, and by redrying to correct for the permanent weight gain. Further study is required to determine how best to deal with materials that undergo slow phase transformations during sorption isotherm measurements, such as observed with some gypsum materials that appear to contain a significant amount of metastable hemihydrate.

While the sorption isotherm curve is a fundamental material property, the quantity that is often used in hygrothermal modeling is the derivative of this curve. In some cases, different drying conditions produce relatively parallel sorption isotherm curves and the derivatives of the curves may be less sensitive to drying conditions than are the moisture contents. Further work is needed to define the impact of drying conditions for building envelope performance analysis purposes.

Acknowledgments

Funding for this project was provided by the U.S. Department of Energy, Office of Building Technology, State, and Community Programs under contract number DE-AC05-00OR22725 with the Oak Ridge National Laboratory, managed by UT-Battelle, LLC.

References

[1] ISO, ISO-12571:2000(E), "Hygrothermal Performance of Building Materials and Products—Determination of Hygroscopic Sorption Properties," Geneva, Switzerland: International Standards Organization, 2000.

[2] ISO, ISO-12570:2000(E), "Hygrothermal Performance of Building Materials and Products—Determination of Moisture Content by Drying at Elevated Temperature," Geneva, Switzerland: International Standards Organization, 2000.

[3] Wilkes, K. E., Atchley, J. A., and Childs, P. W., "Effect of Drying Protocols on Measurement of Sorption Isotherms of Gypsum Building Materials," *Proceedings of the International Conference on Performance of Exterior Envelopes of Whole Buildings IX*, 2004.

[4] Kumaran, M. K., "Hygrothermal Properties of Building Materials," *Moisture Analysis and Condensation Control in Building Envelopes*, H. R. Trechsel, Ed., ASTM International, West Conshohocken, PA, 2001, pp. 29–65.

[5] Richards, R. F., Burch, D. M., and Thomas, W. C., "Water Vapor Sorption Measurements of Common Building Materials," *ASHRAE Transactions*, Vol. 98, Pt. 2, Atlanta: American Society of Heating, Refrigerating, and Air-Conditioning Engineers, 1992.

[6] Cunningham, M. J., and Sprott, T. J., "Sorption Properties of New Zealand Building Materials," Research Report R43, Building Research Association of New Zealand. (as reported by Richards et al., [5]), 1984.

[7] Luck, W., "Feuchtigkeit," Grundlagen, Messen, Regeln. Munich, Vienna: R. Oldenburn (as reported by Richards et al. [5]), 1964.

[8] Stamm, A. J., *Wood and Cellulose Science*, Ronald Press, New York, 1964, pp. 304–310.

[9] Haygreen, J. G., and Bowyer, J. L., *Forest Products and Wood Science, An Introduction*, 3rd ed., Iowa State University Press, Ames, 1996, p. 166.

[10] Lea, F. M., *The Chemistry of Cement and Concrete*, 3rd ed., Edward Arnold Publishers Ltd., 1970, p. 270.

[11] Salmon, D. R., and Tye, R. P., "Measurements of Thermal and Moisture Properties of Moist Masonry Materials: Issues and Problem Areas," *Thermal Conductivity 27/Thermal Expansion 15*, H. Wang and W. Porter, Eds., DEStech Publications, Inc., Lancaster, PA, 2005, pp. 207–219.

Journal of ASTM International, Vol. 4, No. 2
Paper ID JAI100498
Available online at www.astm.org

Gregor Scheffler,[1] *John Grunewald,*[2] *and Rudolf Plagge*[1]

Evaluation of Functional Approaches to Describe the Moisture Diffusivity of Building Materials

---

ABSTRACT: With a set of material parameters and a material model called *engineering model of hygrothermal material characteristics*, both proposed in (Scheffler, 2004), the material functions used for input to hygrothermal building component simulation programs can be adjusted. Using inverse identification of functional parameters by simulation of laboratory experiments, the model is calibrated to reproduce measured water uptake and drying curves. The developed material functions contain an approach to describe the liquid water conductivity of building materials. In addition, moisture storage data approximated by a GAUSSian functional approach, showing sufficient flexibility in the whole moisture range, is available. There with the derivative of the moisture retention curve is known at high precision and the liquid water diffusivity can be derived, too. There exists a wide interest in applicable material functions based on literature data. But literature reviews of hygrothermal material parameters often yield incomplete datasets and experimentally determined curves are lacking or are available at lower accuracy only. Different authors introduced several diffusivity approaches requiring less input parameters for description of liquid water transport in building materials. These models are evaluated by means of diffusivity data derived from the calibrated liquid water conductivity function of the engineering model. A selection of four accurately measured materials is used for this investigation. The investigation is based on controlled laboratory data of high resolution. With the knowledge gained from this study, the uncertainties in interpretation of incomplete datasets frequently encountered in literature reviews shall be reduced.

KEYWORDS: diffusivity, hygrothermal material characteristics, moisture storage, moisture retention curve, liquid water conductivity, liquid water diffusivity, material functions, functional approach

Introduction

The usage of building simulation programs is steadily increasing, in research projects as well as in engineering applications. Part of the *whole building simulation* or *integrated building simulation* is the *building component simulation*. The building component simulation accounts for the hygrothermal behavior of the building envelope and the microclimate near to the wall surfaces. Therefore, apart from an adequate description of the material configuration (layering, dimensions, etc.), the quality of simulation results depends mainly on properly known hygrothermal material parameters and well defined climatic boundary conditions.

The authors developed a material model to ensure high quality in description of hygrothermal material properties, called engineering model of hygrothermal material characteristics [1,2]. The material model is based on thermodynamic potentials to describe coupled heat and moisture flow properly in the whole moisture range. The calibration procedure requires detailed approximation of the moisture storage function and involves simulation of laboratory experiments to ensure the measured water uptake and drying curves can be reproduced by simulation.

Literature data, on the other hand, usually lacks an adequate general material identification (e.g., producer, charge, investigator, sampling method, and date) and datasets are often found to be incomplete. Measured values for water uptake curves and drying behavior are usually not documented. The generation of material functions on the basis of incomplete data is not possible without knowing additional informa-

---

Manuscript received February 17, 2006; accepted for publication January 19, 2007; published online March 2007. Presented at ASTM Symposium on Heat-Air-Moisture Transport: Measurements on Building Materials on 23 April 2006 in Toronto, Canada; P. Mukhopadhyaya and M. Kumaran, Guest Editors.

[1] Ph.D. Student and Head of Laboratory, respectively Institute of Building Climatology, Dresden University of Technology, 01062 Dresden, Germany

[2] Adjunct Associated Professor, Department of Mechanical and Aerospace Engineering, Syracuse University, Syracuse, NY 13244-1240, USA

tion about the material. To interpret such data, the material should be identified by its basic parameters in order to assign it to a respective material group. This procedure is proposed to complement incomplete material information by means of "typical" suitable material functions to be determined for the material group as whole. In a first step, the investigation focused on the evaluation of different liquid water diffusivity approaches of building materials. The aim of this study is to identify suitable diffusivity function types for description of the liquid moisture transport.

After a short introduction of the whole set of material functions determined by application of the engineering model, the model is used to characterize a selection of accurately measured materials and to determine their liquid water diffusivities. Then, the derived diffusivity data are approximated by different function types known from literature [3–9]. This allows to differentiate the functional approaches according to their ability to represent the respective material property.

Classification of Material Parameters and Experiments

Hygrothermal material parameters and laboratory experiments can be classified in different ways. The authors consider in their classification the relation to input data of simulation programs to be the most important criterion. Following this argument, one can introduce three classes: *standard (basic) parameters, extended parameters*, and *transient tests.*

Standard Experiments and Basic Parameters

The basic parameters are determined by standard experiments which are commonly known in the research and testing community. These tests are usually regulated by standards which describe the experiments to be carried out in more or less detail. However, recent research showed that even in this field a considerable uncertainty exists due to individual decisions of the laboratory personnel [10]. The comparison of measurements of internationally renowned building physical laboratories (see also [3,10,11]) showed that the actual level of standardization is not sufficient to ensure measurements on a high quality level.

The basic parameters and related European standards are in detail:

- Determination of the bulk density, e.g., according to DIN ISO 11272;
- Determination of the matrix density and the porosity;
- Thermal conductivity, e.g., according to DIN EN ISO 12664;
- Sorption and retention measurements according to DIN EN ISO 12571 and DIN ISO 11274;
- Water uptake coefficient according to DIN EN ISO 15148; and
- Vapor diffusion resistance factor according to DIN EN ISO 12572.

Extended Parameters and Measurements

The set of basic parameters is introduced as a minimum of information required for hygrothermal material characterization. Additional measurements increase the quality of the material functions and will thus allow more precise simulation results. This can be achieved by:

- Additional measurement points of the moisture storage function in the high and low moisture range;
- Permeability measurements in the saturated and unsaturated moisture range;
- Vapor diffusion measurements in the wet cup range;
- Determination of the water uptake course; and
- Determination of the drying course, especially in the second drying period.

The engineering model is calibrated using water uptake and drying curves. For that purpose, automatic water uptake and drying apparatuses have been designed and built at the IBK-Lab (Building Physical Laboratory of the Institute of Building Climatology at the Dresden University of Technology, see Figs. 1 and 2).

The automatic water uptake measurement delivers the increase of water content versus time of a one-dimensional suction experiment. The water uptake coefficient can be derived from the data as well as the integral water content at capillary saturation. The automated measurement allows to obtain the whole experimental course, which is important if the material behavior diverges from a linear mass increase over the square root of time.

The drying apparatus was designed to measure the drying behavior of building materials under defined

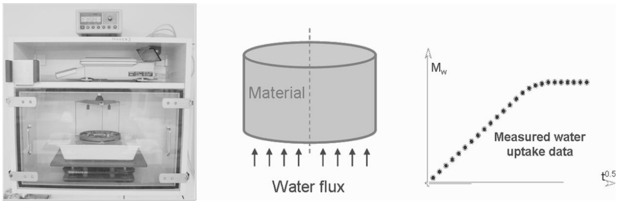

FIG. 1—*Automated water uptake apparatus designed at the IBK-Lab [12].*

boundary conditions. The drying process is not only influenced by the material properties, but also by the boundary temperature and humidity as well as the air flow conditions. Thus it is important to measure all these conditions to be able to evaluate the experiment in a proper way.

Transient Tests

For the analyses of moisture flow and the determination of the moisture diffusivity in porous building materials several advanced nondestructive techniques have been developed to measure the evolution of moisture content profiles in time. The NMR-technique [9], the γ-ray attenuation technique, and the X-ray projection method [3] are known measurement methods to determine moisture profiles during free uptake experiments. The measured profiles require the application of the Boltzmann transformation. If the Boltzmann-conditions of no gravitation and constant and isothermal boundary conditions at a semi-infinite homogeneous medium are fulfilled, all measured moisture profiles fall on a single λ-profile. The results presented in Fig. 3 indicate deviations between different experimental methods.

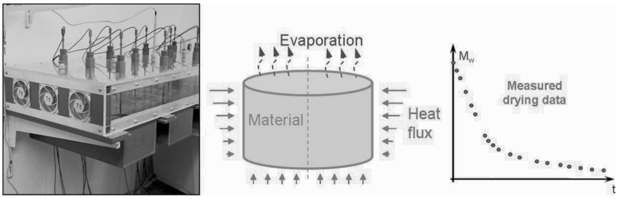

FIG. 2—*Automated drying apparatus designed at the IBK-Lab for twelve samples. The air velocity is controlled by fans and measured by anemometers [13].*

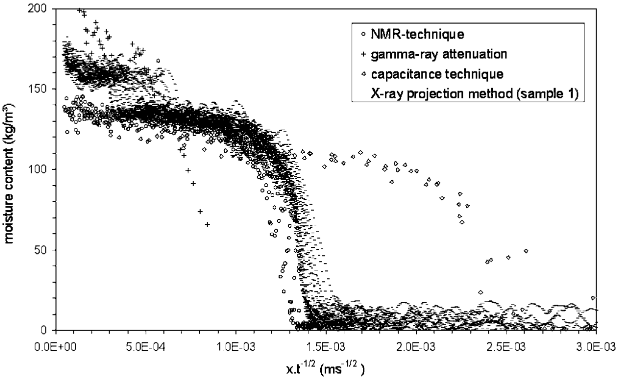

FIG. 3—*Experimental data obtained by different techniques for samples of fired clay brick plotted as moisture content versus* $\lambda (\lambda = x/\sqrt{t})$ *[11].*

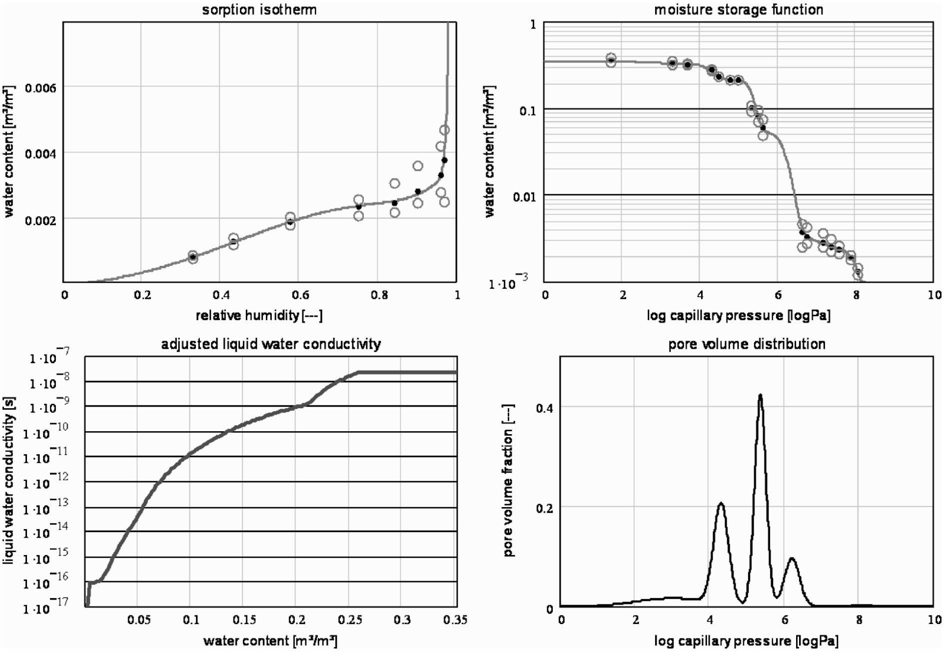

FIG. 4—*Adjusted material functions according to the engineering model of a ceramic brick.*

The λ-profile data can be used to derive the moisture diffusivity as a function of water content. The material variation additionally causes remarkable deviations of the λ-profiles making a clear determination of a unique λ-profile and derivation of a moisture diffusivity difficult. Because of the nonuniqueness of the water retention characteristics during transient tests [14,15] and the lack of validity of the diffusivity equation [16], there is a need for alternative methods to determine transient moisture transport profiles.

Alternative transient tests, as the TDR-technique [4], can be used for simultaneous determination of moisture content and capillary pressure/relative humidity (see [17,18]). In general, transient tests are not applicable to routine measurements of larger numbers of materials (special sample preparation, expensive laboratory facilities, experienced personnel needed) but they have the potential to validate hygrothermal material models and to support further research in the field of moisture transport phenomena.

Introduction to the Engineering Model of Material Characteristics

Input to the engineering model of hygrothermal material characteristics are the standard and extended parameters as shown above. The determination of extended parameters is necessary for two reasons:

- the model can be calibrated using water uptake and drying curves; and
- the moisture storage function is known at higher precision, its derivative function can be used to transform the liquid conductivity into diffusivity and vice versa.

One important prerequisite in development of a material model is the selection of suitable material functions with sufficient flexibility in description of the nonlinear dependencies of the material properties. To generate those material functions, one has to make model assumptions, i.e., use a pore model to calculate fluxes in a pore system. The models, in turn, introduce new parameters which have to be determined by simulation of laboratory experiments and comparison of measured and simulated values. This step is called the *calibration* of the material model [2]. The calibration result of the material model is demonstrated by means of a ceramic brick (Fig. 4) that has been measured in the IBK-Lab. The pore structure is approximated by a weighted sum of GAUSSian distribution functions. Their cumulative frequency curve represents the moisture storage function, where its parameters are adjusted to the mea-

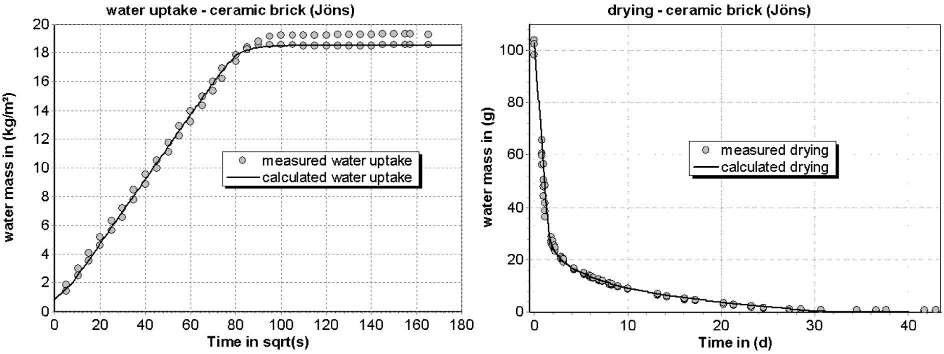

FIG. 5—*Comparison of measured and calculated water uptake and drying data of ceramic brick.*

sured data from sorption and retention measurements. A pore model is applied to the moisture retention curve in order to determine an estimated liquid water conductivity function. In the saturated moisture range, the liquid water conductivity is adjusted to its measured value at full (effective) saturation. In the hygroscopic range, the dry cup vapor diffusion resistance factor is employed for adjustment of the vapor diffusivity. Despite these adjustments, the liquid water conductivity and the vapor diffusivity are still regarded as estimations which have to be calibrated by using numerical simulation to determine the internal modeling parameters.

The liquid water conductivity is calibrated in the overhygroscopic moisture range by simulation of the water uptake experiment. The liquid water conductivity and the vapor diffusivity in the transition range between hygroscopic and overhygroscopic range are calibrated by the drying experiment. The measured and simulated water uptake curves of the ceramic brick are shown in Fig. 5.

Introduction to the Diffusivity Approaches

In literature, there exist various approaches to describe the liquid water diffusivity function depending on a different amount of adjustable parameters. All approaches have in common the fact that they are derived under isothermal conditions from moisture profiles of the water uptake experiment [3,9]. The differential diffusion equation for moisture mass can be written as

$$\frac{\partial\theta_l}{\partial t}=\frac{\partial}{\partial x}\left[D_l(\theta_l)\frac{\partial\theta_l}{\partial x}\right] \tag{1}$$

Using the Boltzmann transformation $\lambda=x/\sqrt{t}$, determining both derivatives and applying it to Eq 1, the diffusion equation can be written as follows, depending only on one variable.

$$2\frac{d}{d\lambda}\left[D_l(\theta_l)\frac{d\theta_l}{d\lambda}\right]=-\lambda\frac{d\theta_l}{d\lambda} \tag{2}$$

Equation 2 can be transformed into Eq 3, where the diffusivity can be directly calculated from measured moisture profiles:

$$D_l(\theta_l)=-\frac{1}{2}\frac{d\lambda}{d\theta_l}\int_{\theta_0}^{\theta_l}\lambda d\theta_l \tag{3}$$

Generally, this derivation is valid only under isothermal conditions and within a moisture content range in which the diffusivity function can be defined. Basically, the lower integration boundary is set to $\theta_0=0$, while the upper integration boundary is introduced as capillary saturation water content θ_{cap}. However, the water diffusivity function can be calculated from measured moisture content profiles according to Eq 3 or from measured integral water uptake curves using certain approaches for the moisture profile shape/the diffusivity function. Then, the lower integration boundary is set to a value $\theta_0>0$ and θ_{cap} is determined either as maximum moisture content reached inside the specimen (inside the boundary layer of the imbibition surface) or, as a simplification, as the mean water content of the specimen when the water uptake curve deviates from a linear function versus square root of time (first knick point of the curve).

For some materials as, e.g., aerated concrete, this can lead to a large deviation between mean and maximum values of capillary saturation and thus, using different θ_{cap}-values, would yield a different parameter identification. The denotation θ_{cap} for the mean value is maintained here, since it is already widely used in this manner. When the maximum capillary saturation is used instead, it will be clearly indicated in the text.

Different authors found different approaches to describe the shape of moisture profiles to be used in Eq 3. For this research, the approaches of Pel [9], Häupl et al. [5], and Häupl and Fechner [6], Holm [7], and Krus, Holm [8], and Carmeliet et al. [3] were selected. They are described as follows.

Diffusivity Approach According to Pel [9]

Pel uses an exponential function containing two adjustable parameters to describe the liquid water diffusivity, given in its normalized form:

$$D_{l,Pel}(\theta_l) = D_0 \exp\left[\beta \cdot \theta_{cap} \cdot \frac{\theta_l}{\theta_{cap}}\right] \tag{4}$$

The parameter D_0 is the minimum diffusivity at θ_0. The parameter β delivers the slope of the function. In Ref. [9], values for a couple of materials are given for the parameters. The advantage of this approach is its flexibility and adjustability. Disadvantages are the fixed exponential slope and the need of moisture profile measurements to adjust the parameters correctly.

Diffusivity Approaches According to Häupl et al. [5] and Häupl and Fechner [6]

Häupl specifies two different rational approaches for the diffusivity function. The first approach 5 reported in Ref. [5] contains only one adjustable parameter k_1. The other parameters are the water uptake coefficient A_w and the water content at capillary saturation θ_{cap}, both known from the water uptake experiment. The parameter k_1 can either be adjusted at measured moisture profiles or by simulating the water uptake experiment.

$$D_{l,Häupl\_1}(\theta_l) = D_{cap}\left[(k_1+1)\left[\frac{\theta_l}{\theta_{cap}}\right]^{1/k_1} - k_1\left[\frac{\theta_l}{\theta_{cap}}\right]^{2/k_1}\right] \quad \text{with} \quad D_{cap} = \left(\frac{A_w}{\rho_w \cdot \theta_{cap}}\right)^2 \cdot \frac{k_1+1}{2k_1} \tag{5}$$

The second approach 6 reported in Ref. [6] requires a fixed water content $\theta_l(\varphi_0)$ at which liquid water transport inside the material begins. It has been introduced as the sorption moisture content of φ_0 taking values between 35 and 80 % relative humidity. Häupl does not fix φ_0, why it has to be adjusted, too. Further parameters are the water content at capillary saturation θ_{cap}, the water uptake coefficient A_w and the parameter k_2. In Ref. [6] a relation for k_2 is given, depending on the water penetration coefficient $B = x_E/\sqrt{t}$. But as the influence is rather small and the penetration depth of the water front x_E also requires to measure moisture profiles, Häupl proposes therefore to set k_2 fixed to $k_2=3$.

$$D_{l,Häupl\_2}(\theta_l) = D_{cap}\left[\left[1 - \frac{\theta_l - \theta_l(\varphi_0)}{\theta_{cap} - \theta_l(\varphi_0)}\right]^{1/k_2 - 1} - \left[1 - \frac{\theta_l - \theta_l(\varphi_0)}{\theta_{cap} - \theta_l(\varphi_0)}\right]^{2/k_2}\right]$$

$$\text{with} \quad D_{cap} = \left(\frac{A_w}{\rho_w \cdot (\theta_{cap} - \theta_l(\varphi_0))}\right)^2 \cdot \frac{k_2+1}{2k_2^2} \tag{6}$$

The advantage of approach 5 is that all required parameters can be measured during a simple water uptake experiment. Only the parameter k_1 needs to be adjusted which can easily be done by simulating the experiment or by the aid of measured moisture profiles. Häupl specifies typical values of k_1 for a number of materials. Approach 6 generally holds higher diffusivity values, especially at lower water contents and contains two parameters. If, as proposed, k_2 is set to $k_2=3$, only the moisture content $\theta_l(\varphi_0)$ remains, that is of lower influence and can be set to a sorption value between 35 and 80 % relative humidity. Disadvantageous is the low flexibility of both approaches and the imprecision in the definition of $\theta_l(\varphi_0)$.

Diffusivity Approach According to Holm [7] and Krus and Holm [8], IBP Holzkirchen

Holm and Krus again use an exponential approach for the diffusivity function. They propose an implicit formulation as follows:

$$D_{l,Holm,Krus}(\theta_l) = D_0 \cdot \exp\left(\frac{\theta_l}{\theta_{cap}} \ln \frac{D_{cap}}{D_0}\right) \tag{7}$$

Basically, Eq 7 forms an exponential function between the two points $D_0(\theta_l=\theta_0)$ and $D_{cap}(\theta_l=\theta_{cap})$. According to the specifications of Holm and Krus, D_0 can be determined from the difference in moisture flux between dry cup and wet cup experiments assuming the contribution of the liquid flux in the dry cup experiment to be negligible. Generally D_0 is proposed to be set to $D_0=2\cdot 10^{-10}$. The other parameters can be calculated with the following relations.

$$D_{cap} = \frac{K \cdot \pi \cdot A_w^2 \cdot \ln(D_{cap}/D_0)}{4 \cdot \theta_{cap} \cdot (\theta_{cap} - \theta_l(\varphi = 0.8)) \cdot \rho_w^2} + D_0 \quad \text{with} \quad K = 0.025 \cdot 10^{(-0.4\cdot(\log(D_{cap}/D_0)-3))} + 0.61 \tag{7a}$$

The formulas of Eq 7a can be inserted into each other leaving the term 7b with all known material parameters at the right-hand side and the unknown parameter D_{cap} at the left-hand side. D_{cap} can be determined either by iteration or by graphical evaluation given in Ref. [7]. The evaluation for this paper was done by iteration.

$$\frac{4 \cdot (D_{cap} - D_0)}{K \cdot \pi \cdot \ln(D_{cap}/D_0)} = \frac{A_w^2}{\theta_{cap} \cdot (\theta_{cap} - \theta_l(\varphi = 0.8)) \cdot \rho_w^2} \tag{7b}$$

Holm proposes two different diffusivity functions, one for capillary suction under water contact and one for liquid water transport without water contact (redistribution). As the water uptake experiment is the basis of all treated diffusivity approaches, this article focuses only on the diffusivity for capillary suction. The difference between both is only another value for D_{cap} which then is determined by numerical simulation of a drying experiment.

The advantage of this approach is that all required parameters can be determined from typically known basic material parameters and—except for the iteration—no further adjustment of parameters is needed. On the other hand, this leaves the disadvantage of less flexibility of the general functional approach as well as during the parameter identification.

Diffusivity approaches according to Carmeliet et al. [3]

Carmeliet et al. [3] introduce two different diffusivity approaches, one general exponential approach, which is comparable to the one given by Pel [9], and another as the sum of a decaying exponential function in the lower moisture range and an increasing one in the higher moisture range. The first, so-called general diffusivity approach is given with

$$D_{l,Carmeliet\_1}(\theta_l) = D_{cap} \exp\left[F \frac{\theta_l - \theta_{cap}}{\theta_{cap} - \theta_l}\right] \tag{8}$$

Both parameters, D_{cap} and F, have to be adjusted by the help of measured moisture profiles or by the help of numerical simulation. For normal building stones, F ranges between 5 and 10 [3]. While the approach of Pel [9] uses the diffusivity at the begin of liquid water transport and the slope as adjustable parameters, the approach documented by Carmeliet et al. [3] uses the slope and the diffusivity at capillary saturation. Advantages and disadvantages are the same.

The second and in the lower moisture range much more flexible approach is given in Ref. [3] with

$$\ln(D_{l,Carmeliet\_2}(\theta_l)) = \ln(D_{l,a}(\theta_l)) + \ln(D_{l,b}(\theta_l)) \tag{9}$$

$$\ln(D_{l,a}(\theta_l)) = \ln(D_{cap}) + [\ln(D_0) - \ln(D_{cap})]\exp(-c_a \cdot \theta_l) \tag{9a}$$

$$\ln(D_{l,b}(\theta_l)) = \ln(D_1) + c_{b1}(\theta_l - \theta_1) \quad \text{while} \quad \theta_l \leqslant \theta_1$$

$$\ln(D_{l,b}(\theta_l)) = \ln(D_1) + c_{b2}(\theta_l - \theta_1) \quad \text{while} \quad \theta_l \geqslant \theta_1 \tag{9b}$$

The approach Eq 9 contains all together seven parameters (θ_1, D_0, D_1, D_{cap}, c_a, c_{b1}, and c_{b2}) which have to be adjusted. This can be done using moisture profiles from water uptake experiments, using wet-cup vapor diffusion resistance measurements and numerical simulation of transport experiments. Carmeliet et al. in Ref. [3] neither specify the meaning of each parameter, nor are there any instructions given as to how to identify them.

Advantage of the approach is the higher flexibility in the lower water content range. Disadvantageous are the many parameters to be adjusted. It is difficult to have as much measured data as are required for a unique parameter identification. Unfortunately, example values for the parameters or an instruction how to adjust them are not given in Ref. [3].

Approximation of Data by Liquid Water Diffusivity Models

The parameters of the different diffusivity approaches 4–9 were adjusted in comparison to a water diffusivity $D_l(\theta_l)$ derived from the liquid water conductivity $K_l(\theta_l)$ of the engineering model. This diffusivity can be determined by the help of the reverse moisture storage function $p_c(\theta_l)$ according to Eq 10.

$$D_l(\theta_l) = \frac{K_l(\theta_l)}{\rho_w}\frac{d}{d\theta_l}(p_c(\theta_l)) \tag{10}$$

To determine the parameters of the functional approaches 4–9, the measured water uptake coefficient is used in all cases. For the remaining parameters, there are different options:

1. *Mean* or *maximum capillary saturation* can be used (see discussion under "introduction of diffusivity approaches" above).
2. *Adsorption* or *desorption* moisture retention can be used to convert a conductivity into a diffusivity.
3. *Recommended general values* for the remaining parameters proposed by the authors of the models are *taken into account* or are *neglected* because more flexibility and, thus, a better approximation of the diffusivity calculated by the engineering model could be achieved. An advantage of accepting recommended values would be that necessary input information is limited to the values that can be directly obtained from standard experiments or literature reviews, respectively.

The materials, the diffusivity approaches were evaluated for, are a ceramic brick (called Brick Jöns, a yellow brick from Northern Germany), a traditional lime-sand brick, an industrially manufactured aerated autoclaved concrete (AAC), and a capillary active insulation material, calcium silicate. The first option is only relevant for materials with a difference between mean and maximum capillary saturation, which is the AAC in this article. Therefore, two approximations were made for AAC.

The engineering model uses adsorption and desorption moisture retention curves for simulation of the water uptake and drying experiment, respectively. Consequently both functions were used for generation of the diffusivities after Eq 10, yielding adsorption and desorption diffusivities. Concerning the third option, it was tried to approximate the given function of the engineering model as close as possible, using all free parameters of the models.

Graphical comparison of adsorption diffusivity functions as well as values for all adjusted parameters are given in Figs. 6–9 and Table 1, respectively. While the shape of the function calculated from conductivity (bold black line in all graphs) is rather unsteady due to the mathematical conversion after Eq 10, it is considered to be a correct diffusivity function. The term of correctness means here the ability to reproduce the experimentally measured wetting and drying behavior. Proof is given below (chapter simulations) how good the different models can approximate the measured curves. Since the measured values are reproducible in the same quality by the conductivity and the diffusivity as well, the diffusivity from the engineering model is used as reference for the other approaches.

Ceramic Brick—In Fig. 6 the comparison of the different adsorption diffusivities for a ceramic brick is shown. If the peaks in the reference function are ignored, the principle shape of the function can be fairly approached by the models. The model Häupl 1 follows it best, the other models approach a mean linear (in logarithmic scale) function, which seems to fit quite well.

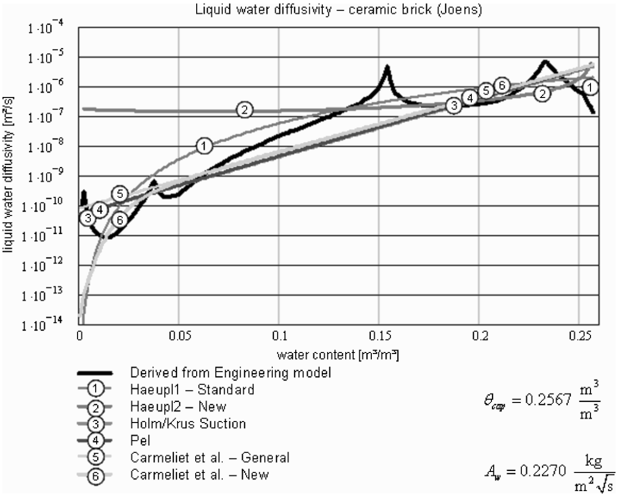

FIG. 6—*Adsorption liquid water diffusivities according to different approaches compared with the diffusivity function calculated from the engineering model for ceramic brick (Joens).*

Lime-sand Brick—Figure 7 shows the comparison of the different adsorption diffusivities for a lime-sand brick. The derived reference function from the engineering model again shows an unsteady shape. Over a wide moisture range, the exponential diffusivities approach that shape well. Only the two approaches by Häupl deviate from that.

Calcium Silicate—Figure 8 shows the comparison of the different adsorption diffusivities for the calcium silicate insulation material. The derived diffusivity from the engineering model shows an almost

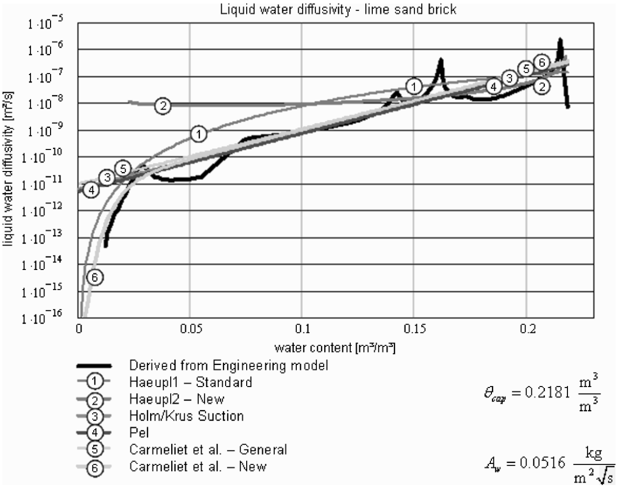

FIG. 7—*Adsorption liquid water diffusivities according to different approaches compared with the diffusivity function calculated from the engineering model for lime-sand brick.*

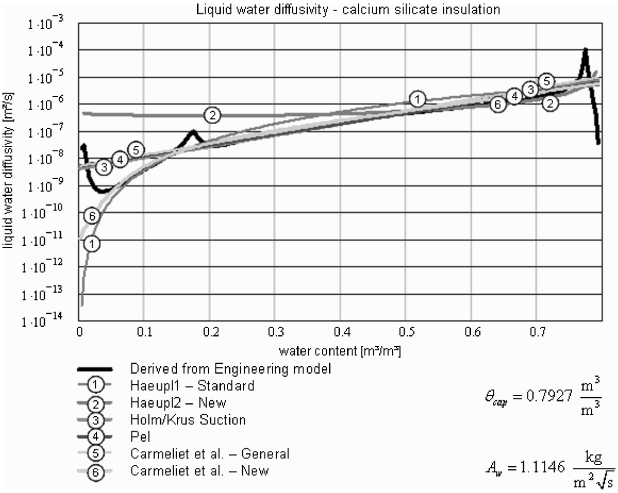

FIG. 8—*Adsorption liquid water diffusivities according to different approaches compared with the diffusivity function calculated from the engineering model for calcium silicate insulation.*

linear behavior (in logarithmic scale) over a wide water content range. Only in the low moisture range and close to capillary saturation the function behaves different. Thus the exponential diffusivities are able to approach that shape well, while the approach of Häupl 2 deviates from that.

Aerated Concrete—Figures 9 and 10 show the comparison of the different adsorption diffusivities for AAC with a mean value (Fig. 9) and a maximum value (Fig. 10) for capillary saturation. The θ_{cap}-values determined experimentally are 26 and 62 Vol %, respectively. The latter value can be found by simulating

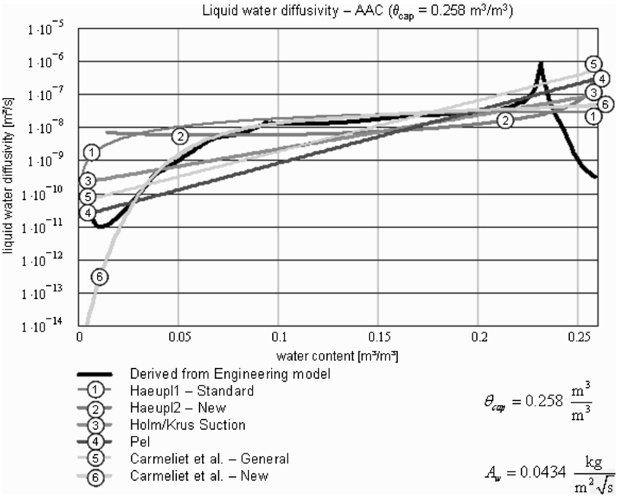

FIG. 9—*Adsorption liquid water diffusivities according to different approaches compared with the diffusivity function calculated from the engineering model for AAC; using mean* θ_{cap}.

TABLE 1—*List of adjusted adsorption diffusivity model parameters for the shown materials.*

Model	Parameter		Ceramic Brick (Jöns)	Lime-sand Brick	Calcium Silicate	AAC, Mean θ_{cap}	AAC, Max. θ_{cap}
Häupl 1 (Standard)	k_1	[–]	0.25	0.25	0.28	1	0.3
Häupl 2 (New)	k_2	[–]	3.0	4.0	3.0	3.0	3.0
	θ_0	$[m^3/m^3]$	0.0018	0.0225	0.0044	0.0132	0.0132
Holm, Krus (IBP Holzkirchen)	D_0	$[m^2/s]$	5.0e−11	6.0e−12	4.0e−09	2.0e−10	2.0e−10
	D_{cap}	$[m^2/s]$	4.7e−06	3.3e−07	7.4e−06	9.3e−08	1.1e−08
Pel	D_0	$[m^2/s]$	5.0e−11	5.0e−12	5.0e−09	2.0e−11	2.0e−10
	β	[–]	45	50	9	37	10
Carmeliet 1 (General)	D_{cap}	$[m^2/s]$	5.0e−06	3.0e−07	9.0e−06	5.0e−07	5.0e−07
	F	[–]	11	10	7.5	9	8
	θ_1	$[m^3/m^3]$	0.0012	0.008	0.0017	0.004	0.045
Carmeliet 2 (New)	D_0	$[m^2/s]$	2.0e−09	1.0e−13	1.0e−06	1.0e−10	1.0e−13
	D_1	$[m^2/s]$	9.0e−06	1.0e−05	1.0e−05	1.0e−05	2.0e+01
	D_{cap}	$[m^2/s]$	1.0e−05	1.0e−06	1.0e−03	1.0e−03	1.0e+02
	c_a	[–]	80	120	15	40	4.5
	c_{b1}	[–]	10	100	10	50	1
	C_{b2}	[–]	43	50	8	6	−70

the second stage of the water uptake process.

Figure 9—The shape of the function calculated from the engineering model can be hardly reproduced by any model except for Carmeliet 2. Nevertheless, an acceptable mean approximation by the other models is possible.

Figure 10—Due to the large pores and the high water content at the imbibition surface the derived diffusivity function has a significant maximum and decreases afterward to very low diffusivity values at capillary saturation. Only the model Carmeliet 2 is able to generally approach this functional shape. The other models fail.

All adjusted model parameters for the adsorption diffusivity models are listed in Table 1. For the model Carmeliet 2 the values of c_a, c_{b1}, and c_{b2} might have a different order of magnitude than those adjusted by other authors. Equation 9 is given in Ref. [3] for the gravimetric moisture content w in kg/m^3;

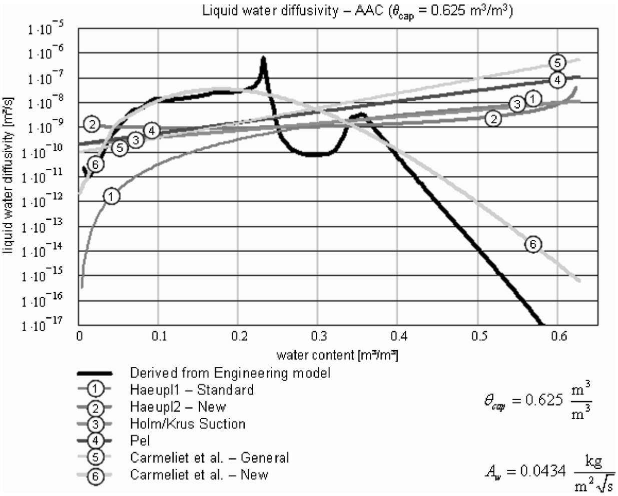

FIG. 10—*Adsorption liquid water diffusivities according to different approaches compared with the diffusivity function calculated from the engineering model for AAC; using max* θ_{cap}.

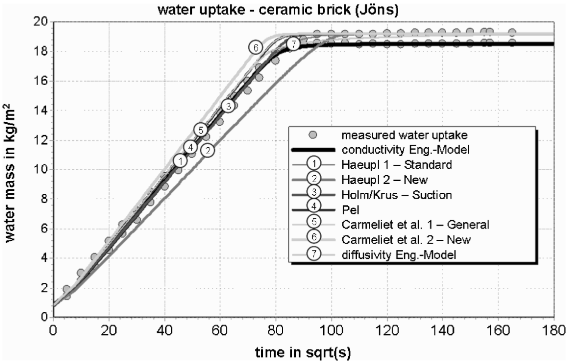

FIG. 11—*Comparison of measured and calculated water uptake behavior for ceramic brick.*

here, the volumetric moisture content θ_l in m^3/m^3 is used.

Comparing both versions of AAC, larger deviations of the parameters can be noticed. If higher water content of the boundary layer is used in simulation of the water experiment (the second set of parameters, AAC with maximum θ_{cap}) then the further water absorption after the knick point can be modeled (see section Simulations below).

Water Uptake and Drying Simulations

The water uptake experiments and the drying experiments were simulated using the numerical simulation program DELPHIN4, developed at the Institute of Building Climatology at the Dresden University of Technology. The simulation code allows description of material functions by data point interpolation. Thus, no restriction exists in usage of any mathematical function type.

The calculations were based on:

- the conductivity after the engineering model adjusted by the experiments,
- and the water diffusivity functions Eqs 4–9 that were fitted to the liquid water diffusivity after the engineering model, and
- the diffusivity after the engineering model derived from the conductivity and the derivation of the reverse moisture retention curve according to Eq 10.

The water uptake and drying experiments were simulated using different moisture retention curves for wetting and drying. In case of the conductivity model, *one* function could be used for both, wetting and drying. In case of the diffusivity models, *adsorption* and *desorption* diffusivities had to be used.

The questions were:

1. The conversion from conductivity to diffusivity after Eq 10 delivers mathematically identical expressions. Does this numerically hold, or in other words, is it possible to describe a wetting or a drying process by a "mathematically derived" diffusivity function when the conductivity does?
2. What are the differences in water uptake and drying curves caused by "limited" flexibility of the diffusivity functions 4–9?
3. What about the two questions above for materials like AAC?

The graphs in Figs. 11–16 show the comparison between the measurements and the numerical results achieved for the different approaches. The results will be discussed here briefly:

Figure 11—The graphs show the water uptake curves for ceramic brick. Despite of the different functional approaches, the results of all simulations are in well agreement with the measurements. Neither the rather unsteady shape of the engineering-diffusivity nor the deviations between the approaches have a noticeable influence on the integral curves. The little deviation in results indicates that the water uptake process is not profoundly influenced by the whole conductivity/diffusivity curve but rather by its course and value close to capillary saturation. The simulation results for lime sand brick and calcium silicate show the same trend.

Figure 12—The graphs show the water uptake curves for autoclaved concrete with functions adjusted

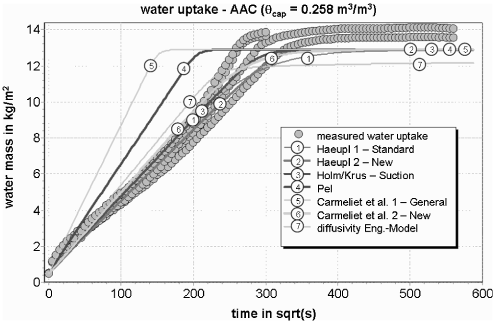

FIG. 12—*Comparison of measured and calculated water uptake behavior for aerated concrete.*

to the *mean* capillary saturation value. In principle, it can be stated the same as above. The first stage of water uptake can be well reproduced by all models. The little deviation of Pel and Carmeliet 1 is due to a different parameter adjustment. It can be further noticed that none of the models is able to describe a second stage of the water uptake process (not very pronounced here due to the short measurement time). However, preferential flow and redistribution processes can cause a remarkable deviation of the water uptake behavior from the "standard" curve.

Figure 13—The graphs show the water uptake curves for autoclaved concrete with functions adjusted to the *maximum* capillary saturation value. Adjustment to the maximum capillary saturation affects the other parameters of the models, too. These can be adjusted again to reproduce the first stage of water uptake. This was done for all models except for Pel and Carmeliet 1. Since both models are very similar

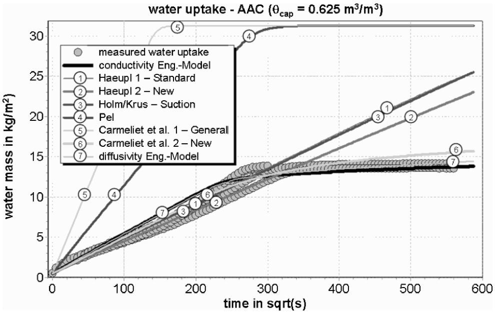

FIG. 13—*Comparison of measured and calculated water uptake behavior for aerated concrete.*

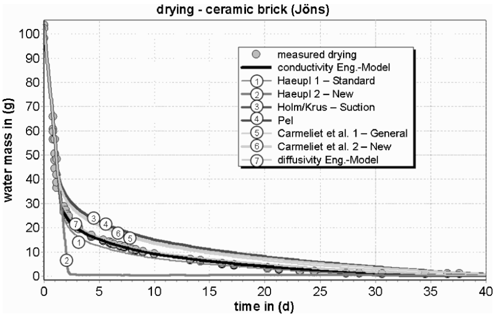

FIG. 14—*Comparison of measured and calculated drying behavior for ceramic brick.*

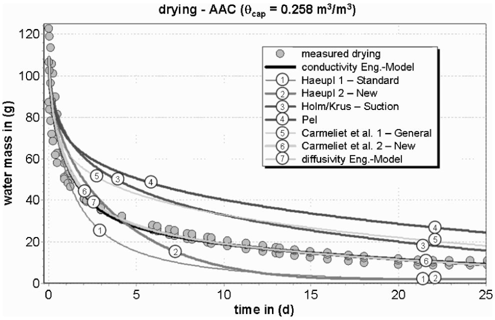

FIG. 15—*Comparison of measured and calculated drying behavior for aerated concrete.*

to that of Holm/Krus (linear in the logarithmic scale), they were left unchanged with the consequence of a faster water uptake.

While all curves except of the engineering-conductivity, engineering-diffusivity, and Carmeliet 2 overshoot the measured values drastically, these three models are able to describe a change of the process at first knick point with fast water uptake before and a continuous redistribution afterward.

Figure 14—The graphs show the drying curves for ceramic brick. The drying curves of the models show fairly good agreement with the measurements. The exception is the model Häupl 2 which leads to much faster drying due to its overestimation of the liquid flow in the lower moisture range. It is remarkable that the linear models Holm/Krus, Pel, and Carmeliet 1 slightly underestimate the drying rate while the Häupl-models overestimate it.

Figure 15—The graphs show the drying curves for autoclaved aerated concrete with functions adjusted to the *mean* capillary saturation value. The curves for AAC diverge more than those for ceramic brick. A systematic underestimation of the drying rate can be observed for the linear models Holm/Krus, Pel, and Carmeliet 1. Surprisingly, despite of different water uptake curves, their drying curves lay fairly close together. The Häupl models overestimate the drying rate. The engineering-diffusivity and the one after Carmeliet 2 follow the measurements very closely.

Figure 16—The graphs show the drying curves for autoclaved aerated concrete with functions adjusted to the *maximum* capillary saturation value. This causes a complete underestimation of the drying rate by all models except the engineering-diffusivity and the one after Carmeliet 2 that, again, follow very closely the measurements. An increase of the capillary saturation must be compensated by a lower liquid diffusivity to maintain the same water uptake rate (the Carmeliet 2 approach has enough other parameters to compensate this). This lowered liquid diffusivity is not able to describe the transport to the surface adequately. The consequence is a drastic underestimation of the drying rate.

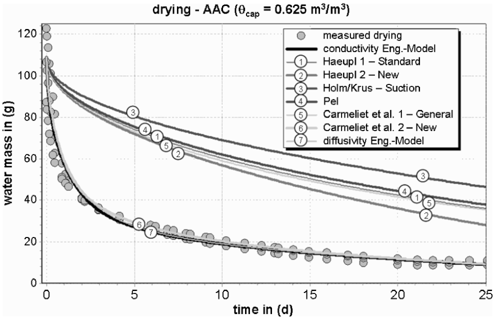

FIG. 16—*Comparison of measured and calculated drying behavior for aerated concrete.*

Conclusions

The material functions derived by the engineering model of hygrothermal material characteristics can be successfully applied in description of wetting and drying processes. For both processes, adsorption and desorption, only one liquid water conductivity function is sufficient but two liquid water diffusivities must be distinguished. The liquid water conductivity and the liquid water diffusivities derived after the engineering model yield identical results. This applies to materials showing redistribution processes and remarkable preferential flow during the second stage of the water uptake experiment, too. Materials with separate pore systems, e.g., autoclaved aerated concrete, show this behavior. For those materials, a maximum capillary saturation value should be taken into account in addition to its mean value.

Despite remarkable differences between diffusivity functions selected from a literature review, all models were able to reproduce the measured integral water uptake behavior in the first suction stage. Common parameters of the models have no consistent meaning and a unique parameter identification is hard to manage. Only one diffusivity approach succeeded to reproduce the behavior in the second stage of the suction process. This approach shows sufficient flexibility to describe a two-stage water uptake processes but involves a high number of parameters that is not maintainable.

Drying processes can be fairly described by the diffusivity approaches requiring a separate parameter adjustment for desorption processes. In case of materials with separate pore systems, again, only the one diffusivity approach succeeded to reproduce the drying curve.

The original aim of the work—to identify suitable functional approaches that limit input to standard parameters only—was partly achieved. For materials with a single water uptake behavior like ceramic brick, a linear diffusivity in the logarithmic scale can be recommended. This does not apply for materials with separate pore systems, e.g., autoclaved aerated concrete. No suitable simplified diffusivity approach could be found for this class of materials.

References

[1] Grunewald, J., and Häupl, P., "Gekoppelter Feuchte-, Luft-, Salz und Wärmetransport in porösen Baustoffen," *Bauphysik-Kalender 2003*, pp. 377–434.

[2] Scheffler, G., Grunewald, J., and Häupl, P., "Calibration of an Engineering Model of Hygrothermal Material Characteristics," contribution to CIB-W40 meeting in Glasgow, September 2004.

[3] Carmeliet, J., Hens, H., Roels, S., Adan, O., Brocken, H., Cerny, R., Pavlik, Z., Hall, C., Kumaran, K., and Pel, L., "Determination of Liquid Water Diffusivity from Transient Moisture Transfer Experiments," *Journal of Thermal Envelope & Building Science*, Vol. 27, No. 4, 2004.

[4] Hansen, M. H., and Hansen, E. J. de Place, "Determination of Liquid Diffusivity Using Single Point Moisture Content Measurements and Boltzmann Transformation," *Proceedings of 6th Symposium on Building Physics in Nordic Countries*, Trondheim 2002.

[5] Häupl, P., Fechner, H., Neue, J., and Stopp, H., "Bestimmung der Parameter der Kapillarwasserleitfähigkeit aus dem Wasseraufnahmekoeffizienten," *10th Symposium of Building Physics, Proceedings, Vol. 2*, Dresden University of Technology, 1999.

[6] Häupl, P., and Fechner, H., "Hygric Material Properties of Porous Building Materials," *Research in Building Physics, Proceedings of 2nd International Conference in Building Physics*, Leuven, 2003.

[7] Holm, A., "Ermittlung der Genauigkeit von instationären hygrothermischen Bauteilberechnungen mittels eines stochastischen Konzepts," Ph.D. thesis, University of Stuttgart, 2001.

[8] Krus, M., and Holm, A., "Approximationsverfahren für die Bestimmung feuchtetechnischer Materialkennwerte," *10th Symposium of Building Physics, Proceedings, Vol. 2*, Dresden University of Technology, 1999.

[9] Pel, L., "Moisture Transport in Building Materials," Ph.D. thesis, Technical University of Eindhoven, 1995.

[10] Roels, S., Carmeliet, J., Hens, H., Brocken, H., Hall, C., Plagge, R., Cerny, R., Pavlik, Z., and Kumaran, K., "Interlaboratory Comparison of the Measurement of Basic Hygric Properties of Porous Building Materials," *Journal of Thermal Envelope & Building Science*, Vol. 27, No. 4, 2004.

[11] Roels, S., Carmeliet, J., Hens, H., Brocken, H., Hall, C., Plagge, R., Cerny, R., Pavlik, Z., and Kumaran, K., "A Comparison of Different Techniques to Quantify Moisture Content Profiles in

Porous Building Materials," *Journal of Thermal Envelope & Building Science*, Vol. 27, No. 4, 2004.

[12] Plagge, R., and Scheffler, G., "Automatic Measurement of the Water Uptake Behaviour for Building Materials," *7th Conference of Building Physics in Northern Countries*, Reykjavik, 2005.

[13] Scheffler, G., and Plagge, R., "Defined Drying Behaviour of Building Materials," *7th Conference of Building Physics in Northern Countries*, Reykjavik, 2005.

[14] Hassanizadeh, S. M., and Gray, W. G., "Recent Advances in Theories of Two-phase Flow in Porous Media," contribution to "Fluid Transport in Porous Media" in *Advances in Fluid Mechanics*, Vol. 13, 1997.

[15] Mualem, Y., "Hysteretical Models for Prediction of the Hydraulic Conductivity of Unsaturated Porous Media," *Water Resour. Res.* Vol. 12, 1976, pp. 1248–1254.

[16] Rawlins, S. L., and Gardner, W. H., "A Test of the Validity of the Diffusion Equation for Unsaturated Flow of Soil Water," *Soil Science Society of America Proceedings*, Vol. 27, pp. 507–511.

[17] Plagge, R., Scheffler, G., and Grunewald, J., "Measurement of Water Retention and Moisture Conductivity at Transient Conditions," *3rd International Building Physics/Science Conference*, Montreal, 2006, accepted for publication.

[18] Scheffler, G., Plagge, R., Grunewald, J., and Häupl, P., "Evaluation of Instantaneous Profile Measurements Indicating Dependencies of Moisture Transport on Hysteresis and Dynamics," *3rd International Building Physics/Science Conference*, Montreal, 2006, accepted for publication.

[19] Worch, A. "The Behaviour of Vapour Transfer on Building Material Surfaces: The Vapour Transfer Resistance," *Journal of Thermal Envelope & Building Science*, Vol. 28, No. 2, 2004.

Journal of ASTM International, Vol. 3, No. 10
Paper ID JAI100265
Available online at www.astm.org

Mavinkal K Kumaran,[1] *Phalguni Mukhopadhyaya,*[2] *and Nicole Normandin*[3]

Determination of Equilibrium Moisture Content of Building Materials: Some Practical Difficulties

---

ABSTRACT: Though the definition of equilibrium moisture content of porous materials is straightforward from the point of view of equilibrium thermodynamics, experimental determination of this quantity may not always be easy. Many factors play roles from an experimentalist's point of view. Hysteresis, the reference dry state, the initial moisture content, the history of the test specimen, the size of the test specimen, the drying technique, and drying temperature—all influence the value that is arrived at by an experimentalist. This paper reports results from several series of measurements on gypsum board, eastern white pine, aerated concrete, and calcium silicate brick using the ASTM Standard C 1498 in the hygroscopic ranges and pressure plate techniques above the hygroscopic range of equilibrium moisture content. These results show the ambiguities that may surround the experimental definition of equilibrium moisture content. The results presented in the paper demand a few refinements in the existing ASTM Standard C 1498 as well as in the procedure that is used in the pressure plate method. The paper proposes a few refinements for both. The need for the development of an ASTM standard for the pressure plate technique is identified.

KEYWORDS: adsorption, desorption, equilibrium moisture content, hysteresis

Introduction

All porous building materials, when in contact with moist air, adsorb or desorb water molecules to attain an equilibrium moisture content [1]. This equilibrium moisture content depends very strongly on the partial pressure of the water vapor in the surrounding air and rather weakly on the air temperature [2–6] that are commonly experienced in buildings. The International Energy Agency Annex 24 Report on material properties [6] gives three definitions for "moisture content" in building materials. These are:

(i) mass of moisture per unit volume of the dry material,
(ii) mass of moisture per unit mass of the dry material, and
(iii) volume of condensed moisture per unit volume of the dry material.

In this paper, the second definition is invariably used.

If the moisture content of the material does not vary with time for a given combination of water vapor pressure and air temperature, it is then said that it has reached the equilibrium moisture content (EMC) of the material at that water vapor pressure and temperature. When left undisturbed, the natural end of any adsorption or desorption process is the attainment of EMC. This, though a natural process, is often very slow. Building materials may take several days or weeks to reach equilibrium.

When the water vapor pressure of the air approaches the saturation water vapor pressure at the temperature of the air, the EMC of building materials increases rapidly. At these stages, the process undergone by the building material is not only adsorption. Water vapor begins to condense within the pore structures of the building materials. Theoretically, if the building material is in contact with air that is 100 % saturated for a very long period, all pores of the material should be filled with the condensed moisture. The EMC that corresponds to that hypothetical state is called the saturation moisture content of the material. However, in practice, the rate of this process becomes infinitesimally small at an EMC that is known as the capillary saturation moisture content and which is often substantially less than the

---

Manuscript received January 6, 2006; revised July 19, 2006; accepted for publication August 1, 2006; published online November 2006. Presented at ASTM Symposium on Heat-Air-Moisture Transport: Measurements on Building Materials on 23 April 2006 in Toronto, Canada; P. Mukhopadhyaya and M. Kumaran, Guest Editors.

[1] Principal Research Officer, Building Envelope and Structure, Institute for Research in Construction, National Research Council Canada

[2] Research Officer, Building Envelope and Structure, Institute for Research in Construction, National Research Council Canada

[3] Technical Officer, Building Envelope and Structure, Institute for Research in Construction, National Research Council Canada

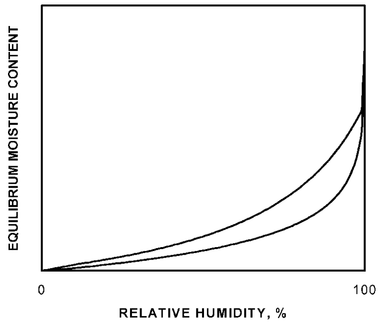

FIG. 1—*Sorption-desorption isotherm for porous building materials; the upper curve represents desorption and the lower sorption.*

saturation moisture content referred to above. In practice, in order to reach the saturation moisture content, a fully evacuated porous building material is kept immersed in de-aerated water for several days. For this reason, this EMC is often referred to as the vacuum saturation moisture content.

The EMC of a building material thus spans from an absolute dry state of zero moisture content to its vacuum saturation moisture content, as the partial pressure of water vapor varies from zero to full saturation value for a given temperature. However, the path that connects these two extremes is often not unique. This is due to a phenomenon called hysteresis. For example, in an investigation at the Institute, two specimens of identical dimensions of eastern white pine were prepared. Both were dried to a reference dry state at 105 °C. One of them was brought to capillary saturation while the other was kept in the dry state. Then both were exposed to air at 21 °C and 67 % relative humidity (RH) for several days. The specimen that underwent adsorption attained an EMC=0.082 $\mathrm{kg\,kg^{-1}}$ while the specimen that underwent desorption attained an EMC=0.120 $\mathrm{kg\,kg^{-1}}$. This is entirely due to hysteresis. Thus, for adsorption and desorption there are at least two separate sets of moisture contents for a building material that exhibits hysteresis. This generally results in an EMC diagram similar to the one shown in Fig. 1, for many common building materials. The two curves in such an EMC diagram are referred to as sorption-desorption isotherms.

The definition of EMC appears to be rather straightforward. However, the experimental determination of this quantity may not always be easy. Many factors play major roles in a reliable determination of EMC. Hysteresis obviously is a factor. In addition, the reference dry state, the initial moisture content, the history of the test specimen, the size of the test specimen, the drying technique, and drying temperature—all influence the EMC value that is arrived at by an experimentalist.

Internationally accepted procedures are available for the determination of sorption-desorption isotherms. ASTM Standard Test Method for Hygroscopic Sorption Isotherms of Building Materials (C 1498) [7] and the Pressure Plate Method [8] are generally used for this purpose. The principles of these two methods are given below.

ASTM Standard C 1498

For sorption measurements, the test specimen is dried at an appropriate drying temperature to constant weight. While maintaining a constant temperature, the dried specimen is placed consecutively in a series of test environments, with relative humidity increasing in stages, until equilibrium is reached in each environment. Equilibrium in each environment is confirmed by periodically weighing the specimen until constant weight is reached. From the measured weight changes, the EMC at each test condition can be calculated and the adsorption isotherm drawn.

The ideal starting point for the desorption measurements is from an equilibrium condition very near 100 % RH. While maintaining a constant temperature, the specimen is placed consecutively in a series of test environments, with relative humidity decreasing in stages, until equilibrium is reached in each environment. Equilibrium in each environment is confirmed by periodically weighing the specimen until constant weight is reached. Finally, the specimen is dried at the appropriate temperature to constant weight. From the measured weight changes, the equilibrium moisture content at each test condition can be calculated and the desorption isotherm drawn. ASTM Standard Test Method for Hygroscopic Sorption Isotherms of Building Materials (C 1498) gives further details of the procedure.

Equilibrium Moisture Content from Pressure Plate (Desorption) Measurements

The test specimens are saturated with water under vacuum. Those are then introduced in a pressure plate apparatus that can maintain pressures up to 100 bar for several days. The plates in perfect hygric contact with the specimens extract water out of the pore structure until an equilibrium state is established. The equilibrium values for moisture contents in the specimens and the corresponding pressures (measured as the excess over atmospheric pressure; the negative of this value is referred to as the pore pressure, while the absolute value is the suction) are recorded. The equilibrium pressure p_h can be converted to a relative humidity φ using the following equation:

$$\ln \varphi = -\frac{M}{\rho R T} p_h \tag{1}$$

where,

M = the molar mass of water,
R = the ideal gas constant,
T = the thermodynamic temperature, and
ρ = the density of water.

The Nordtest Technical Report [8] briefly describes a procedure for pressure plate measurements for building materials and reports the results from an interlaboratory comparison. The “nordtest” method, NT BUILD 481 [9] also describes the procedure. ASTM International Standards D 2325, Standard Test Method for Capillary-Moisture Relationships for Coarse- and Medium-Textured Soils by Porous-Plate Apparatus [10] and D 3152, Standard Test Method for Capillary-Moisture Relationships for Fine-Textured Soils by Pressure-Membrane Apparatus [11] present test procedures to determine equilibrium moisture contents for soils. No standard is yet developed for building materials.

This paper reports many sets of adsorption, desorption and suction measurements on test specimens of aerated concrete (density 460±15 kg m^{-3}), eastern white pine (density 460±60 kg m^{-3}), interior gypsum board (density either 625±7 kg m^{-3} referred to as “A” or 720±10 kg m^{-3} referred to as “B”) and calcium silicate brick (density 2000±80 kg m^{-3}) and examines various practical difficulties that one may encounter during the implementation of the two test methods that are mentioned above.

The Dry “Reference” Weight

As mentioned above, the EMC at any given condition is calculated in terms of a weight change with reference to a dry state. But what is meant by a dry state? Theoretically, the dry state corresponds to an equilibrium state that is attained by a test specimen when exposed to absolutely dry air or 0 % RH. How does one practically attain a dry state? The most common method is to dry the test specimen to a constant weight in an oven that is maintained at a temperature that is much higher than the standard laboratory temperature. Here is the practical difficulty. The drying ovens that are used for this purpose are integral parts of laboratories. Then, the air inside the oven is supplied from the laboratory air that is not dry. Even if the temperature inside the oven is 100°C, if it is in contact with the laboratory air that is at 20°C at 50 % RH, the air inside the oven is just above 1 % RH. At lower oven temperature the effect is much higher; say at 50°C the air inside the oven will be near 10 % RH! For various reasons, such as softening of the test specimen in the case of expanded polystyrene insulation specimen, or loss of water of crystallization as in the case of interior gypsum board test specimens cannot be dried at much above 50°C. Obviously, such test specimens never reach the theoretical dry state if dried in an oven that is in contact with the laboratory air. An alternative procedure is to dry the test specimens using desiccants. However, this also needs much attention, as is illustrated below.

A set of test specimens of interior gypsum board B were dried at 50°C, then equilibrated in air at

TABLE 1—*Weights of test specimens of interior gypsum board B as dried using two different procedures.*

Specimen no.	Weight after drying at 50°C, g	Weight after exposure to 23°C and 33 % RH, g	Weight after drying with the desiccant, g
1	32.315	32.415	32.295
2	32.948	33.053	32.927
3	32.063	32.165	32.045
4	32.396	32.500	32.391
5	32.747	32.851	32.731
6	32.261	32.364	32.240
7	32.742	32.846	32.731
8	33.195	33.304	33.180
9	32.370	32.478	32.352

23°C and 33 % RH and once again dried, this time using anhydrous calcium chloride as a desiccant. The results are listed in Table 1.

It can be seen that for all the nine specimens that are listed in Table 1, the dry mass obtained by oven drying is slightly higher than that obtained using the desiccant. The former yields an EMC equal to $(3.20\times10^{-3}\pm7\times10^{-5})$ kg kg^{-1} and the latter $(3.7\times10^{-3}\pm2\times10^{-4})$ kg kg^{-1}. Does this then mean that the procedure that uses the desiccant gives the right dry weight? There is no straightforward answer to this question either, as illustrated below.

In a second series of measurements, test specimens of interior gypsum board B were first oven dried at 50°C, equilibrated at 23°C and 80 % RH, and then dried using the desiccant. The results are listed in Table 2.

In this case, the weight obtained after oven drying is consistently lower than that obtained using the desiccant. The former yields an EMC $(9.6\times10^{-3}\pm1.2\times10^{-3})$ kg kg^{-1} and the latter $(8.8\times10^{-3}\pm1.2\times10^{-3})$ kg kg^{-1}. This means that drying with the desiccant in this case resulted in unacceptable dry weight. The reason for this discrepancy is not clear.

This problem may be very specific to the interior gypsum board. Nevertheless, when the ASTM Standard C 1498 is applied to this material, very specific instructions are to be given to assign the dry weight for the material. By consensus, it can be the mass that corresponds to oven drying at 50°C. It could equally be from a specified procedure that uses the desiccant as the drying material. Then, indeed, the starting point of the drying process also need to be specified.

Specification of the drying temperature and procedure is important for each type of building material, as is illustrated with a series of measurements on test specimens of eastern white pine. The results from this series are listed in Table 3.

It can be seen that there are appreciable and consistent differences in the dry weights of all six test specimens for the five different progressive drying conditions used. If the EMC for eastern white pine is calculated with reference to the dry weight obtained at 50°C after a four-day-drying period, from the measurements that followed at 95 % RH and 22.3°C, the result would have been (0.20 ± 0.01) kg kg^{-1} instead of (0.215 ± 0.005) kg kg^{-1}. Here the error is not very large, but at a lower RH the error can be substantial. For example, for a set of measurements at 70 % RH and 22.7°C for the dry weights obtained at 50°C the EMC is (0.076 ± 0.002) kg kg^{-1} instead of (0.101 ± 0.001) kg kg^{-1}, the EMC with reference to the final dry weight at 105°C. For wood, 105°C appears to be the appropriate drying temperature.

TABLE 2—*Weights of test specimens of interior gypsum board B as dried using two different procedures.*

Specimen no.	Weight after drying at 50°C, g	Weight after exposure to 23°C and 80 % RH, g	Weight after drying with the desiccant, g
1	31.751	32.038	31.778
2	32.174	32.462	32.205
3	32.651	32.931	32.671
4	32.271	32. 566	32.289
5	32.962	33.266	32.983
6	32.085	32.494	32.106
7	32.237	32.537	32.258
8	32.789	33.093	32.812
9	32.218	32.515	32.240

TABLE 3—*Weights of test specimens of eastern white pine as dried progressively at five different conditions.*

	Weight of the specimen, g				
Specimen No.	Four days at 50°C	Constant weight at 50°C	Constant weight at 70°C	Constant weight at 95°C	At 105°C for 2 h
1	4.519	4.485	4.439	4.408	4.404
2	4.679	4.643	4.600	4.566	4.562
3	4.628	4.598	4.554	4.520	4.516
4	4.515	4.491	4.445	4.414	4.408
5	4.475	4.454	4.409	4.379	4.372
6	4.593	4.578	4.530	4.498	4.493

However, to avoid charring of the specimens, it is advisable to dry them first at 95°C to constant mass and then keep at 105°C for a short period of 2 h. Likewise, for each class of building materials an appropriate drying temperature and procedure shall be specified in the Standard. For practical purposes, the intent of any such specification need not be the attainment of an absolute dry state as the reference, but a reproducible one, such that results from different sources on the same material allow inter-comparisons. For building applications one does not have to know the absolute moisture content of a material. The increment from a practically reproducible reference state will be sufficient for any building design considerations.

The Size of the Test Specimen

The time that a test specimen takes to attain equilibrium as prescribed by Standard C 1498 depends on the nature of the building material as well as the size of the specimen. It may vary between several days to several weeks. A 5 cm × 5 cm test specimen of interior gypsum board (1/2-in. nominal thickness) attains equilibrium at 75 % RH near standard laboratory temperature within a week. A similar eastern white pine specimen may take several weeks to reach equilibrium in a similar environment. For a stucco specimen it can be even longer. Therefore, in order to reduce the duration of the exposure at each test condition, authors in the past have used powdered specimens, shavings, very thin specimens, etc. However, how does such sizing down of test specimen affect the EMC? In an attempt to address this a series of measurements was done with pine, aerated concrete, and calcium silicate brick. The results from that series are presented below.

Several test specimens of the three building materials were prepared in three categories as follows.

Pine: Twelve specimens, 5 mm × 5 mm and 20 mm thick, twelve specimens, 5 mm × 5 mm and 10 mm thick, and six specimens of saw dust (approximately 90 g). All 30 specimens were dried to constant weight in a ventilated oven that was maintained at 100°C.

Aerated Concrete: Twelve specimens, 5 mm × 5 mm and 25 mm thick, twelve specimens, 5 mm × 5 mm and 13 mm thick, and six specimens of fine dust after crushing (approximately 50 g). All 30 specimens were dried to constant weight in a ventilated oven that was maintained at 80°C.

Calcium Silicate Brick: Twelve specimens, 5 mm × 5 mm and 20 mm thick, twelve specimens, 5 mm × 5 mm and 8 mm thick, and six specimens of fine dust after crushing (sizes varied between 35 g and 75 g). All 30 specimens were dried to constant weight in a ventilated oven that was maintained at 60°C.

The test specimens in each category for each material were grouped into three batches and then one batch each of all three materials was equilibrated at 22.5°C and 50.1 % RH, the second batch at 22.5°C and 70.9 % RH, and the third at 22.5°C and 88.7 % RH. The results are summarized in Table 4.

From the data given in Table 4, it is not possible to generalize the influence of specimen size on the EMC obtained. If one looks at the data for pine alone, it appears that the saw dust gave consistently lower values for the EMC. The reason for this can be only speculated at this stage as an increase in the reference dry weight due to some unknown reasons. The EMCs for the 20-mm-thick and 10-mm-thick specimens are the same within the limits of the experimental uncertainties. It is noted that the time taken by the saw dust to equilibrate was not significantly different from the other two sets of specimens, for all three conditions. Therefore, it is advisable not to use saw dust for the determination of the EMC for wood-based materials.

TABLE 4—*EMC as determined according to standard C 1498 for three building materials, with three variations in the dimensions of the test specimens; the numbers in parenthesis give deviations from the reported mean value.*

Building material	RH,%	Equilibrium moisture content, kg kg^{-1} Thicker specimen	Thinner specimen	Fine particles
Eastern white pine	50.1	0.070(0.001)	0.072(0.001)	0.0653(0.0002)
	70.9	0.099(0.001)	0.100(0.001)	0.0915(0.004)
	88.7	0.164(0.001)	0.166(0.001)	0.162(0.001)
Aerated concrete	50.1	0.024(0.003)	0.021(0.001)	0.018(0.003)
	70.9	0.034(0.005)	0.031(0.003)	0.023(0.003)
	88.7	0.066(0.004)	0.060 (0.003)	0.058(0.001)
Calcium silicate brick	50.1	0.0075(0.0006)	0.0069(0.0008)	0.0072(0.0001)
	70.9	0.0108(0.0010)	0.0104(0.0005)	0.0109(0.0002)
	88.7	0.0246(0.0005)	0.0255(0.0009)	0.0254(0.0003)

When the experimental uncertainties are taken into consideration, for the aerated concrete and calcium silicate brick specimens, the dimensional differences seem to have little effect on the EMCs that are listed above. Here also, the dusts did not attain final equilibrium significantly faster than the block specimens. For each building materials, it is advisable to recommend a representative thickness. For interior gypsum board, this can be the full nominal thickness. For wood, 10-mm-thick slabs appear to be representative. Similarly, 10-mm-thick slabs of aerated concrete and calcium silicate brick appear to be a practical thickness for the test specimens.

Starting Moisture Content for Desorption Measurements

For some materials, the initial moisture content has a measurable influence on the EMC attained after a desorption process. Measurements that are listed below, on interior gypsum board B specimens, illustrate this behavior.

Three batches of six test specimens each, 60 mm × 60 mm and 1/2-in. nominal thickness, were oven dried to constant weight at 50°C. Specimens in one batch were equilibrated at 94 % RH and 23°C. These specimens were left to desorb and equilibrate at 79.5 % RH and 23°C, then at 53 % RH and 23.2°C, and finally at 33 % RH and 23°C. A second batch was allowed to equilibrate initially at 79.5 % RH and 23°C and were left to desorb and equilibrate at 53 % RH and 23.2°C, and finally at 33 % RH and 23°C. The third batch was equilibrated at 53 % RH and 23.2°C and allowed to desorb and equilibrate at 33 % RH and 23°C. The results from these measurements are listed in Table 5.

The results from Table 5 are plotted in Fig. 2. For reference, a sorption curve for the material is included in the figure. It can be seen that the total picture is not as simple as depicted in Fig. 1. The desorption curve for the interior gypsum board is not unique. Depending on where the desorption starts, the EMC attains different values. The higher the starting moisture content (or RH), higher is the EMC attained, as is seen in the last column of Table 5. Currently, no detailed information like this has been generated on other building materials. There may be other materials that show similar behavior. Thus, in order to determine an upper limit of the desorption curve, one has to start the desorption process from the highest possible moisture content that is practically reproducible. The capillary saturation state may be used as that starting point. Then again, this may not be possible for all materials. In such situations the

TABLE 5—*Desorption EMCs of interior gypsum board specimens with different initial moisture contents; the numbers in parenthesis indicate standard deviations.*

Initial conditions	Equilibrium moisture content, kg kg^{-1} At 79.5 % RH and 23°C	At 53 % RH and 23.2°C	At 33 % RH and 23°C
94 % RH and 23°C	0.0166(0.0001)	0.0133(0.0001)	0.0120(0.0001)
79.5 % RH and 23°C		0.00924(0.00006)	0.00548(0.00003)
53 % RH and 23.2°C			0.00465(0.00008)

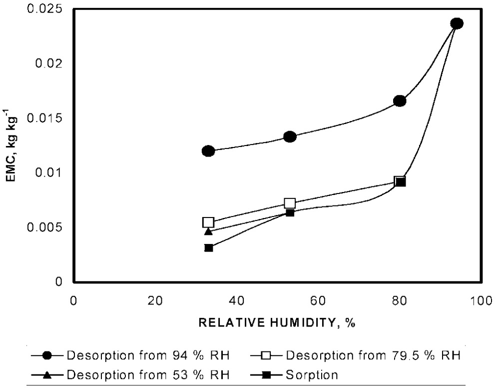

FIG. 2—*Sorption-desorption curves for interior gypsum board B.*

standard should prescribe the starting point explicitly so that data from different sources allow intercomparison. In addition, in practice it may be important to know the intermediate desorption curves, as shown in Fig. 2, of some building products. The Standard should facilitate the generation of such information wherever applicable.

Starting Moisture Content for Pressure Plate (Suction) Measurements

Pressure plate measurements are always desorption measurements. One invariably starts the process from a saturation moisture content. Just as in the case of desorption measurements discussed above, the starting moisture content affects the EMC attained by the specimens at each applied over pressure. This is illustrated with three series of measurements on aerated concrete in Fig. 3.

In one series of measurements shown in Fig. 3, eight 40 mm × 40 mm × 6 mm specimens were vacuum saturated with de-aerated water to attain an average initial moisture content of 1.72 kg kg^{-1}. Measurements on these specimens with the pressure plate apparatus resulted in the uppermost curve in Fig.

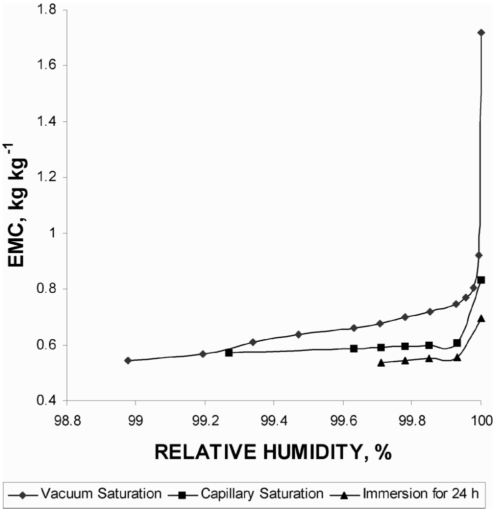

FIG. 3—*EMC of aerated concrete as measured using the pressure plate method, starting from three different initial moisture contents.*

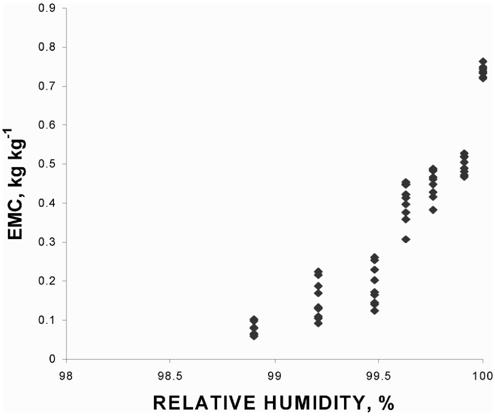

FIG. 4—*EMC of eight test specimens of interior gypsum board A from pressure plate measurements.*

3. In the next series similar, a set of six specimens were immersed in water and allowed to attain capillary saturation. The average initial moisture content was 0.83 kg kg^{-1}. These specimens gave the middle EMC curve shown in Fig. 3. In a third series, the pressure plate measurement were started after 24 h of immersion in water with an average initial moisture content of 0.69 kg kg^{-1}. (Admittedly this was a case of incomplete saturation.) The result was as shown in the lowermost curve in Fig. 3. The need to specify the saturation procedure in the pressure plate method is quite obvious from these results. For practical reasons, it is advisable to start with capillary saturation and a prescription for attaining the capillary saturation for each building material. The vacuum saturation is a hypothetical case that is rarely reached in real buildings. The air at high pressure that is trapped in porous building materials during capillary saturation will resist the attainment of this hypothetical saturation point.

Materials that Disintegrate on Saturation

Some inorganic building materials disintegrate on saturation, when done in the normal way using deaerated pure water. Interior gypsum board is an example. Often this is due to the loss of ionic compounds that dissolve in water. For these materials, it is advisable to use water that is already saturated with the ionic compounds for the initial specimen saturation. A piece of the material can be ground and stirred into the water that subsequently will be used for saturation.[4] As illustrated in Fig. 4, at the Institute this technique has successfully yielded at least an approximate suction curve for the interior gypsum board A, which was otherwise impossible to obtain.

Eight test specimens, each 40 mm × 40 mm at 1/2-in. nominal thickness, were used in these measurements. The reference dry weight was obtained after oven drying at 50°C. The starting point was vacuum saturation. All data are plotted in Fig. 4 to highlight another inherent practical problem in the measurement of EMC. EMC measurements on building products often results in large scatter of the experimental data. In such cases, it is imperative to provide information on the large mean deviation.

Concluding Remarks

In spite of the simple definition of equilibrium moisture content, various results that are presented in the preceding sections show that the experimental determination of this quantity with good precision is a challenging task. Perhaps the greatest challenge is to accommodate the non-homogeneity, as is evident from Fig. 4, of porous building materials. This alone can introduce an uncertainty that is more than 20 %! Thus, it should always be the recommended practice to include the uncertainty in each set of measure-

---

[4] Admittedly, this may affect the equilibrium point due to the difference in the chemical potential of water in the the saturated solution in relation to that of pure water, but the procedure allows an estimate of the desorption curve of materials that disintegrate on saturation.

ments. To assess this uncertainty, as many as eight to ten randomly selected specimens from a material need to be equilibrated at each exposure condition.

For each building material, or at least for each class of building materials, a drying temperature as well as a drying procedure should be explicitly defined, to determine the reference dry weight. Otherwise, results from different laboratories will have different meanings. This may require well-planned round robin series of measurements that involve several laboratories.

It is better to avoid fine particles of building materials for the measurement of EMC, because in certain cases it may affect the pore size distribution of the building material. Use of fine particles is not substantially improving the time that is taken for equilibration. Furthermore, at least in the case of wood, a systematic error is introduced in the EMC data when sawdust is used as the test specimen. It appears that for most materials 40 mm × 40 mm × 10 mm specimens are quite practical dimensions.

It is always advisable to start with the highest possible moisture content to construct upper limits of the desorption isotherms. Practically, capillary saturation is a reasonably reproducible high-moisture-content starting point for many materials. This is true for the suction measurements in the pressure plate apparatus too. It is advisable not to start from the vacuum saturation state, for this rarely happens in building practice. Special procedures need to be developed to saturate those building materials that disintegrate on saturation.

For practical reasons, if the information on the intermediate desorption curves of building materials, as shown in Fig. 2, is needed, the Standard should facilitate the generation of such information. In this regard, further experimental data on other building materials need to be generated.

The ASTM Standard C 1498 should be further refined to accommodate the findings that are reported here. There is a need to develop an ASTM Standard for the use of the pressure plate apparatus to determine the EMC of building materials at high humidity (above 98 % RH) conditions. ASTM C16 Committee should take the initiative in this regard. Efficient interlaboratory collaborations will be necessary to arrive at consensuses and address these recommendations.

References

[1] Kumaran, M. K., Mitalas, G. P., and Bomberg, M. T., "Fundamentals of Transport and Storage of Moisture in Building Materials and Components," *ASTM Manual Series*, MNL 18, H. Trechsel, Ed., 1994, Chap. 1, pp. 3–17.

[2] Tveit, A., "Measurements of Moisture Sorption and Moisture Permeability of Porous Materials," Rapport 45, Norwegian Building Research Institute, 1966, pp. 39.

[3] Hansen, K. K., "Sorption Isotherm, A Catalogue," Technical Report 162/86, The Technical University of Denmark, Lyngby, Denmark, 1986, pp. 80.

[4] Kumaran, M. K., "ASHRAE RP-1018 Research Report: A Thermal and Moisture Transport Property Database for Common Building and Insulating Materials," 2002, pp. 229.

[5] Richards, R. F., Burch, D. M., and Thomas, W. C., "Water Vapor Sorption Measurement of Common Building Materials," *ASHRAE Trans.*, Vol. 98, Pt. 2, 1992, pp. 475.

[6] Kumaran, M. K., "Heat, Air and Moisture Transfer in Insulated Envelope Parts. Final Report, Volume 3, Task 3: Material Properties," International Energy Agency Annex 24, Laboratorium Bouwfysica, K. U. -Leuven, Belgium. 1996, pp. 135.

[7] ASTM C 1498–04, "Standard Test Method for Hygroscopic Sorption Isotherms of Building Materials," *Annual Book of ASTM Standards*, Vol. 4(6), ASTM International, West Conshohocken, PA, 2004.

[8] Hansen, M. H., "Retention Curves Measured Using Pressure Plate and Pressure Membrane," *Nordtest Technical Report* 367, Danish Building Research Institute, 1998, pp. 63.

[9] Nordtest Method: NT BUILD 481, "Building Materials: Retention Curve and Pore Size Distribution," 1997, pp. 8.

[10] ASTM D 2325–68, "Standard Test Method for Capillary-Moisture Relationships for Coarse- and Medium-Textured Soils by Porous-Plate Apparatus," *Annual Book of ASTM Standards*, Vol. 4(8) ASTM International, West Conshohocken, PA, 1991.

[11] ASTM D 3152–72, "Standard Test Method for Capillary-Moisture Relationships for Fine-Textured Soils by Pressure-Membrane Apparatus," *Annual Book of ASTM Standards*, Vol. 4(8) ASTM International, West Conshohocken, PA, 1991.

Journal of ASTM International, Vol. 4, No. 8
Paper ID JAI100332
Available online at www.astm.org

Christopher P. Decareau,[1] *Liyen Kan,*[1] *and Joseph P. Piñon*[1]

Inputs and Analyses: An End User's Perspective of Heat-Air-Moisture Data

---

ABSTRACT: Hygrothermal simulation programs (HSPs) have the potential to help the way building enclosures are designed if end users are convinced the results are reliable. However, HSPs suffer from a lack of manufacturer-specific material data. HSP users often "create" materials by scouring multiple sources for hygrothermal properties. To the less familiar HSP user, significant error can be introduced into simulations by using properties that are calculated from variable sources. Through a series of case studies, this paper illustrates how material properties can make a difference in hygrothermal calculations and, ultimately, material specification.

KEYWORDS: hygrothermal simulation, material data, failure criteria, reliability

Introduction

Promise of Hygrothermal Simulation Programs

Enclosure designers have historically relied on best practice construction techniques that have been established over time specific to a certain climate and building type. However, today's new buildings are pushing the "envelope" in terms of their demands for cost-effective enclosure systems, less use of material and more insulation due to environmental and energy concerns, and less tolerance for water intrusion. Furthermore, recent experience has shown that application of traditional wall systems on taller buildings can result in unsatisfactory performance. For example, the use of cement plaster on high-rise condominiums has resulted in the industry to re-examine the traditional plaster wall system. A case in point is the so called "leaky condo" situation of the Northwest United States.

Experience has shown that as building enclosure systems become more engineering intensive concurrent with less tolerance for leaks or moisture degradation of building materials, there is less tolerance for errors in hygrothermal calculations.

The various commercially-available hygrothermal simulation programs (HSPs) allow the building enclosure designer to determine the effect of enclosure assemblies, material choices, and interior air environment as they relate to the exterior environment. HSPs are a tool which holds the promise of allowing enclosure designers to "engineer" new wall systems, and to better match the performance of walls and roofs to the building interior and exterior climate.

Effect of Material Data on the Results of Hygrothermal Simulation Programs

Commercially-available HSPs rely on an embedded database of materials to create building enclosure assemblies for a hygrothermal simulation. The database is populated with materials that are derived from published literature, such as from ASTM International, ASHRAE, the U.S. Department of Energy, and the Canadian Institute for Research in Construction.

HSPs currently suffer from a lack of manufacturer-specific material data based on standardized tests. Additionally, manufacturers do not readily provide hygrothermal failure criteria for their products. This

---

Manuscript received January 30, 2006; accepted for publication August 23, 2007; published online September 2007. Presented at ASTM Symposium on Heat-Air-Moisture Transport: Measurements on Building Materials on 23 April 2006 in Toronto, Canada; P. Mukhopadhyaya and M. Kumaran, Guest Editors.

[1] Associate Principal and Senior Engineers, respectively, Simpson Gumpertz & Heger, Inc., San Francisco, CA 94105.

lack of manufacturer-specific data and performance failure criteria forces enclosure designers to make hygrothermal assumptions on the importance of various material properties and the likely long-term performance of various materials.

For end users, uncertainty over the exact properties of the materials modeled introduces a perception of uncertainty which may affect the enclosure design and material selection, or both. Some research has shown that other parameters such as weather data and interior climate can have as large an impact on the hygrothermal modeling results than uncertainty in material data [1]. However, more research is needed to evaluate the effect of various material properties on the in-service performance of enclosure systems and on the long-term hygrothermal performance of specific materials.

If there are errors in the material data, end users want to know the effect of those errors so that they do not have to be overly conservative in their designs.

Objective

This study was conducted to accomplish the following two tasks:

- Provide an end user's perspective on how hygrothermal material data can affect calculations.
- Demonstrate the need for manufacturer-supplied hygrothermal performance failure criteria.

Approach

This study uses two case studies to show the effect of varying various material properties on the hygrothermal performance of a wall system. For the computer modeling we used a widely available commercial transient hygrothermal software that is capable of heat transport calculation (thermal conduction, latent heat flow, direct solar radiation and nighttime long-wave radiation), vapor transfer calculation (vapor diffusion), and liquid transport calculation (capillary conduction and surface diffusion) [2].

Scope

The two case studies are of a traditional exterior cement plaster system applied on a high rise residential and low rise hospital building in two different micro-climates in the Western United States. The following material properties were varied in this study in order to quantify their effect on the hygrothermal performance of the wall systems:

- Moisture Isotherm and vapor permeances of glass mat-faced gypsum versus paper-faced gypsum sheathing.
- Vapor permeances of various sheathing membranes.
- Water absorption of cement plaster.

Case Study 1: High Rise Residential Building in San Francisco, California

Background

This project is a 17-story residential building clad with exterior cement plaster. Given the recent concerns and rain water leakage failures of high rises clad with a traditional cement plaster wall system, this case study illustrates the use of a self-adhesive sheet membrane as an enhanced weather resistive barrier (WRB) instead of the traditional two layers of building paper. The proposed wall assembly is as follows (from interior to exterior):

- 16 mm gypsum wallboard with latex paint.
- 152 mm metal stud wall with 140 mm of unfaced, glass fiber blanket insulation (RSI=3.35).
- 16 mm glass mat-faced gypsum sheathing.
- One layer of self-adhesive modified bituminous sheet membrane (SASM) (water/air barrier and vapor retarder).
- One layer of 60 minute building paper, that acts primarily as a bond break between cement plaster and the SASM.
- 22 mm exterior cement plaster (scratch, brown, and finish coat) on the exterior.

TABLE 1—*Comparison of material data for Case Study 1.*

Material	Thickness, m	Bulk Density, kg/m^3	Porosity, m^3/m^3	Specific Heat Capacity, J/kgK	Thermal Conductivity, W/mK	Vapor Diffusion Resistance Factor
Glass mat-faced gypsum sheathing	0.0159	768.8	0.650	870	0.16	18
Paper-faced gypsum sheathing	0.0125	850.0	0.650	870	0.16	6
Self-adhesive sheet membrane (SASM)	0.0010	1441.7	0.002	2300	2.30	68626
Polyethylene membrane	0.0010	130.0	0.001	2300	2.30	50000

Hygrothermal Concerns

This wall assembly was modeled because there was a concern with the use of a waterproof membrane (SASM) on the exterior sheathing that also acts as a vapor retarder. The concern in this climate was with modeling accurately the amount of winter condensation or moisture accumulation within the sheathing.

The glass mat-faced gypsum sheathing modeled (it is used extensively in Western United States) has a patented gypsum core with layers of yellow fibrous glass mat facer sheets on both sides. The glass mat facing is made of nonorganic fiberglass, and therefore is less likely to absorb moisture, especially at elevated relative humidity.

Up until recently, the only published hygrothermal data available were for paper-faced gypsum sheathing. A paper published at the Buildings IX conference presented a moisture isotherm for glass mat-faced gypsum [3] for the first time. Since the material data for glass mat-faced gypsum sheathing have not been readily available, it is of great interest to building enclosure designers to compare the results of hygrothermal modeling using data from glass mat-faced gypsum sheathing versus data from paper-faced gypsum sheathing. See Tables 1 and 2 for a comparison of the material data between glass mat-faced gypsum sheathing and paper-faced gypsum sheathing.

Furthermore, the vapor permeance of many materials that are classified as vapor retarders are not clearly defined or published. Therefore, it was of interest for this project to understand the effect of uncertainty of the vapor permeance of the sheathing membrane on the wall system performance.

TABLE 2—*Comparison of Isotherm.*

Relative Humidity (%)	Paper-faced Gypsum Sheathing (kg/m^3)	Glass Mat-faced Gypsum Sheathing[a] (kg/m^3)
0	0	0
11.3	0.67	0.62
32.8	2.01	
32.9		1.08
43.2	2.68	
53.5		1.69
57.6	3.35	
75.4		2.61
78.6	6.03	
84.3	6.70	
84.6		6.07
93.6	12.73	
94.0		7.84
97.3	18.09	
97.4		11.99
100.0	400.00	173.00

[a] *Note*: Moisture Isotherm taken from Ken Wilkes Buildings IX paper, "Effect of Drying Protocols on Measurement of Sorption Isotherms of Gypsum Building Materials."

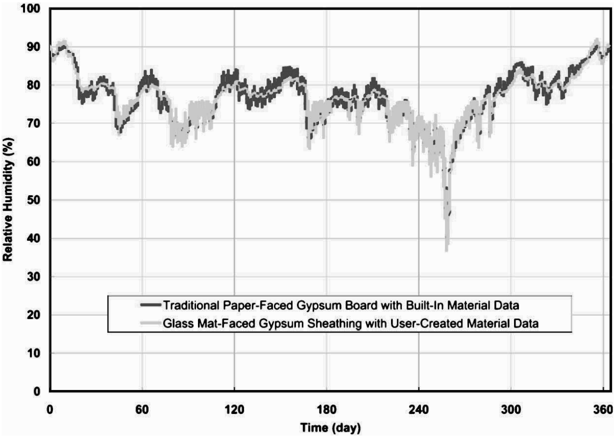

FIG. 1—*Case Study 1—Variation of gypsum sheathing.*

Boundary Conditions

The hygrothermal computer models for this case study were constructed with the following boundary conditions:

- Exposure: North-facing wall on the 10th floor of the building.
- Weather: Built-in weather data in the simulation program software database for San Francisco, cold year.
- Interior Conditions: Medium moisture load as defined in the simulation program.

Material Data Variations

Based on the hygrothermal concerns noted above, for this case study the material properties for the gypsum sheathing and the sheathing membrane were varied to understand what effect uncertainty in the data would have on the hygrothermal performance of the proposed wall system. Tables 1 and 2 list the variations in the material data that were used in the hygrothermal simulations for this case study.

Modeling Results

Figure 1 shows the relative humidity (RH) within the sheathing modeled with glass mat-faced gypsum sheathing as compared with the same wall modeled with paper-faced gypsum sheathing. The results of the two computer modeling analyses show little difference between the expected RH within the wall system. According to the computer simulation, by the end of the second year, both analyses settle into a stable, seasonal (oscillating) pattern that indicates that there are no long-term moisture accumulation concerns. The patterns of these two simulation results using different material data both include a period of high RH (above 80 %) within the wall systems in the winter and spring for three months, and a period of lower RH, below 80 % for the rest of the year.

Figure 2 shows that even varying the vapor permeance of the sheathing membrane by as much as 36 % did not have a significant effect on the moisture accumulation within the glass mat-faced gypsum sheathing. Similar results were found when either glass mat-faced or paper-faced gypsum is modeled as the sheathing.

Case Study 2: Low Rise Hospital Building in Sacramento, California

Background

This project is a five-story hospital building with exterior wall systems that includes exterior cement plaster over light gage metal studs. The wall system is identical to Case Study 1 with the exception that for the WRB two layers of 60 minute building paper is proposed instead of one layer of SASM.

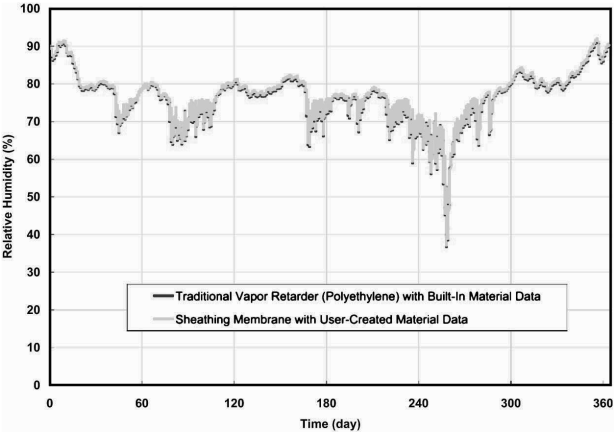

FIG. 2—*Case Study 1—Variation of sheathing membrane.*

Hygrothermal Concerns

This wall was modeled for the following two reasons:

- There was a concern over the large moisture load caused by the rain and sun in Sacramento combined with the absorption of the plaster wall system. Furthermore, with the exception of the plaster, this modern light-framed wall system has very little moisture storage capacity.
- To meet the occupancy cleanliness standards, the hospital ownership was reviewing various low-permeable finishes on the interior gypsum board such as vinyl wall paper or epoxy paint finishes. There was an interest to evaluate the effect of various low-permeance finishes on the interior gypsum board.

Boundary Conditions

The hygrothermal computer models for this case study were constructed with the following boundary conditions:

- Exposure: South-facing wall on the fifth floor of the building.
- Weather: TMY2 (Typical Meteorological Year) weather data for Sacramento were converted to TRY (Test Reference Year); a format compatible with the simulation program.
- Interior Conditions: Low moisture load as defined in the simulation program.

Material Data Variations

Based on the hygrothermal concerns noted above, for this case study the material properties for the cement plaster and the interior low-permeance finish were varied to understand what effect uncertainty in the data would have on the hygrothermal performance of the proposed wall system. Table 3 lists the variations in the material data that were used in the hygrothermal simulations for this case study.

TABLE 3—*Material data varied for Case Study 2.*

Variation	Rain Water Absorption Factor	Vapor Permeance, ng/m^{2}sPa
Traditional cement plaster	0.70	…
Cement plaster with elastomeric coating—Variation 1	0.10	…
Cement plaster with elastomeric coating—Variation 2	0.03	…
Low-permeance interior finish—vinyl wall paper	…	56.56
Very low-permeance interior finish—see text	…	1.98
High-permeance interior finish—latex paint	…	989.85

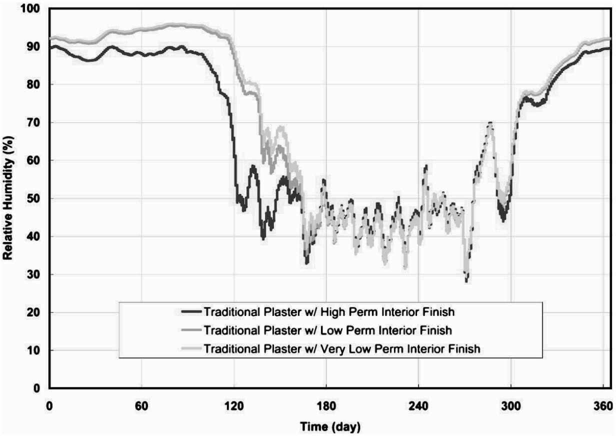

FIG. 3—*Case Study 2—Variation of permeance of interior finish.*

As shown in Table 3, the rain water absorption coefficient of the plaster was varied from 0.03 to 0.7 to model the effect of an elastomeric waterproof coating on the plaster. While more or less vapor permeable, the elastomeric coating adds a layer of some increased vapor resistance; however, the effect of this increase in vapor resistance was found to be negligible for this case study.

Table 3 also shows that the vapor resistance of the interior low-permeable finish was varied by as much as 28 times. This wide variability was given to the interior low-permeable finish to account for the wide variety of interior finish options available, and to account for future coatings applied at a time of remodeling.

Modeling Results

Figure 3 shows that in this traditional plaster wall system over modern framing in this climate and interior conditions the RH within the glass mat-faced gypsum sheathing is predicted to exceed 80 % for 140 days and 85 % for 120 days. This elevated humidity was determined to be primarily caused by sun-driven inward condensation.

Figure 3 also shows that the conditions within the exterior sheathing are made even worse when a low-permeance interior finish such as vinyl wall paper is used on the interior gypsum board. In this variation the RH within the sheathing remained above 90 % for about 120 days. This result is expected because the interior retarder can trap the inward driven moisture within the wall cavity. The variation with a very low-permeance interior finish (refer to Table 3 and Fig. 3) did not significantly worsen the already elevated humidity.

Figure 4 shows that by significantly reducing the rain water absorption (use a rain water absorption factor of 0.03 as shown in Table 3) of the plaster, the RH of the sheathing can be maintained below 80 % for the entire year, and this result does not change significantly even when a low-permeance interior finish is used. However, Fig. 4 also shows that using a higher rain water absorption factor of 0.1, even though it is seven times lower than the case of uncoated plaster, still results in elevated humidity above 90 % within the sheathing.

Discussion

The case studies show how varying material properties can affect the results of the simulation.

Case Study 1 shows that a refinement on the material properties of the exterior sheathing does not have a significant effect on the results of the simulation.

Both Case Studies 1 and 2 show that varying the vapor permeance of a vapor retarder within an assembly does not significantly affect the model results as long as the material is modeled generally as a

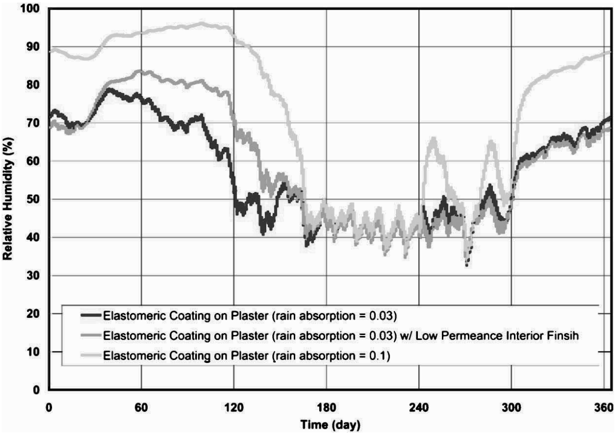

FIG. 4—*Case Study 2—Variation of water absorption of plaster.*

vapor retarder. This finding is in agreement with the common understanding that the placement of the vapor retarder within a wall assembly is more important than an exact knowledge of its permeance.

These findings indicate that for certain materials and material properties, there may be less of a need for manufacturer specific data as long as there is a reliable generic material in the HSP database.

Case 2 shows that changing a material property that moderates the moisture load, such as the rain water absorption factor of the exterior surface, can have a significant effect on the hygrothermal performance of wall systems. In California, there are 16 design climate zones and even more microclimates. There can be high variability of exterior cement plasters, particularly their absorption characteristics. There are also many different water resistant, waterproof coatings and admixtures advertised to reduce or eliminate the rain water absorption of cement plaster. The long-term performance or characteristics of these coatings is not clearly defined or understood. Consequently, in order to understand a building envelope assembly in this region without manufacturer data or other published data; the enclosure designer has to make assumptions on material properties, which can possibly introduce large errors into the results.

Conclusions

In this study, we varied the vapor permeance and the moisture isotherm of an exterior gypsum sheathing, the permeance of a vapor retarder located on both the interior and exterior parts of a wall assembly, and the rain water absorption characteristics of a hygroscopic cladding. The only variation that had a significant effect on the hygrothermal modeling results was the variation of the rain water absorption characteristics of the cladding. The results indicate that at least for some materials and material parameters, generic material data or classification may be adequate for hygrothermal modeling and enclosure design. There is still a need for manufacturers to supply product data to show under which categories their product falls into.

With HSPs, providing end users with ability to "know" the moisture performance of an enclosure, it is necessary for manufacturers to publish both hygrothermal properties and moisture failure criteria so end users can determine if a manufacturer's material can be appropriately used in the enclosure design.

References

[1] Holm, A. and Kuenzel, H. M., "Uncertainty Approaches for Hygrothermal Building Simulations-Drying of an AAC Flat Roof in Different Climates," *Proceedings, 7th International IBPSA Conference*, IBPSA, Rio de Janeiro, Brazil, 2001, 8 pp.

[2] Kuenzel, H., Karagiozis, A., and Holm, A., "Wärme Feuchtetransport Instationär (WUFI) Pro Ver-

sion 3.3.5.93," Transient Hygrothermal Software, Oak Ridge National Laboratory and Fraunhofer Institute for Building Physics, 2004.

[3] Wilkes, K. E., Atchley, J. A., and Childs, P. W., "Effect of Drying Protocols on Measurement of Sorption Isotherms of Gypsum Building Materials," *Proceedings, Performance of Exterior Envelopes of Whole Buildings IX*, American Society of Heating, Refrigerating and Air-Conditioning Engineers, Inc., Atlanta, GA, 2004.

Journal of ASTM International, Vol. 4, No. 1
Paper ID JAI100321
Available online at www.astm.org

Therese K. Stovall[1]

Interlaboratory Comparison of the Thickness of the Destroyed Surface Layer of Closed-cell Foam Insulation Specimens

---

ABSTRACT: The preparation of closed-cell foam insulation test specimens can affect the results of a number of hygrothermal property measurements. In particular, the thickness of the destroyed surface layer affects the measurement of gas diffusion coefficients and thermal conductivity. Multiple specimen preparation methods are in use, as well as multiple methods to measure the thickness of the destroyed surface layer. A ruggedness test, including an interlaboratory comparison, was conducted by an ASTM technical committee to examine the variations due to both of these factors. The results are important in understanding the likely range in values for each preparation technique. The results also demonstrate a sensitivity to the measurement technique.

KEYWORDS: foam insulation, destroyed surface layer, accelerated aging, errors

Introduction

The thermal resistance of any closed-cell foam insulation that relies on the containment of a low-thermal conductivity gas for its thermal properties will change over time due to gas diffusion. An accelerated aging test procedure, ASTM Standard Test Method for Estimating the Long-term Change in the Thermal Resistance of Unfaced Rigid Closed-cell Plastic Foams by Slicing and Scaling Under Controlled Laboratory Conditions (C 1303), was developed to facilitate product development and product labeling. This test procedure calls for the extraction of thin slices of the foam insulation from the full thickness product. These thin slices are typically produced using either a bandsaw or a circular blade (similar to a meat slicer). In the cutting process, these tools cut through cellular walls within the foam, as shown in Fig. 1. This simplified depiction of a foam cross section shows a simulation of a very smooth cut. In a real foam slice, the foam cells are not lined up in an orderly fashion; the cutting tool may dig deeper into the foam structure, and some of the cut cells will be open to interior cells, so that the destroyed cells may reach beyond those cells immediately adjacent to the surface. The interior of the broken surface cells is open to the atmosphere, so that the lower thermal conductivity gas that had been contained within these cells is

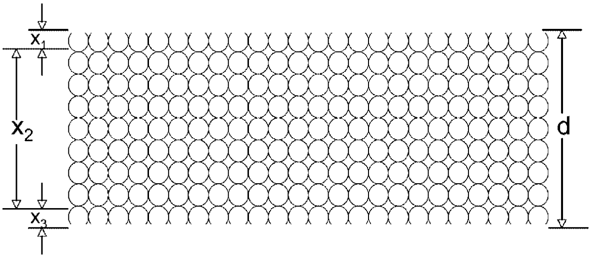

FIG. 1—*Simplified depiction of foam morphology cross section, showing surface cells broken by the cutting process.*

Manuscript received January 25, 2006; accepted for publication November 10, 2006; published online December 2006. Presented at ASTM Symposium on Heat-Air-Moisture Transport: Measurements on Building Materials on 23 April 2006 in Toronto, Canada; P. Mukhopadhyaya and M. Kumaran, Guest Editors.

[1] Senior Research Engineer, Oak Ridge National Laboratory, Oak Ridge, TN 37830.

released and that volume is almost immediately equal in composition to the surrounding air.

A ruggedness test was therefore performed to determine the effect of the cutting parameters and methods on the accelerated aging test procedure results [see ASTM Standard Guide for Conducting Ruggedness Tests (E 1169)]. This test included an interlaboratory comparison of the test methods used to measure the thickness of the destroyed surface layer. The participants included Dow Chemical Company, Holometrix, Inc., National Research Council of Canada, Oak Ridge National Laboratory, OC Celfortec Inc., and Owens Corning.

The thickness of the destroyed surface layer (TDSL) is a function not only of the cutting instruments, but also depends upon the fundamental foam morphology. The foams tested here were produced in 1996, and there have been many changes in the foam manufacturing process in the past ten years.

Basis for Ruggedness Test

The purpose of a ruggedness test is to find the experimental factors that strongly influence the results of a test method and to determine how closely these factors need to be controlled. A mathematical consideration of the accelerated aging procedure shows that the smoothness of the cut surface could have a significant effect on the test results.

Fick's Law for one-dimensional diffusion shows that the rate of diffusion in a thin slab is inversely proportional to the square of the slab thickness [1]. A scaled time parameter in the accelerated aging test procedure is therefore based on the square of the slice thickness, making the test results very sensitive to this parameter. However, because the destroyed surface cells are already at atmospheric conditions, the effective diffusion thickness for the thin slab is less than the full geometric thickness. The correct length scale, i.e., the diffusion thickness, differs from the slice thickness by the total TDSL, as shown in Fig. 1 and Eqs 1 and 2.

$$\text{Scaled time}_{\text{used}} = \frac{d^2}{(\text{product thickness})^2} \times (\text{real time}), \quad \text{where } d = (x_1 + x_2 + x_3) \tag{1}$$

$$\text{Scaled time}_{\text{correct}} = \frac{(d - sd)^2}{(\text{product thickness})^2} \times (\text{real time}), \quad \text{where } s = \frac{(x_1 + x_3)}{(x_1 + x_2 + x_3)} \tag{2}$$

The parameter, s, represents the portion of the thickness that is the total TDSL, because it includes both cut surfaces. The error in the scaled time, shown in Eq 3, is then approximately equal to twice the total TDSL. The error propagation for this factor depends both upon the magnitude of the time error and the rate at which the foam is aging when it reaches that time.

$$\text{Error}_{\text{time}} = \frac{(\text{Scaled time}_{\text{used}} - \text{Scaled time}_{\text{correct}})}{\text{Scaled time}_{\text{correct}}} = \frac{(2s - s^2)}{(1 - 2s + s^2)} \tag{3}$$

The accelerated aging test protocol uses the thin slices to make thermal resistivity measurements. Another error is therefore introduced by the difference between the thermal resistivity in the broken cells, which are already fully aged, and the thermal resistivity in the closed-cell portion of the slice, which is undergoing the aging behavior of interest. Using a series resistance representation, that error is shown in Eq 4. This error is smaller in magnitude than the time error. For example, for an s of 10 % and a C of 1.2, the magnitude of Error_{R} is less than 2 %. This value of C was chosen because it represents a worst case scenario, such as might have been found in the very earliest portion of the aging curve for a previous generation of foams, and was a value that would therefore maximize Error_{R}.

$$\text{Error}_{\text{R}} = \frac{[R_{measured}(t) - R_{cc}(t)]}{R_{cc}(t)} = s\frac{(1 - C)}{C}, \quad \text{where } C = \frac{R_{cc}(t)}{R_{final}} \tag{4}$$

where

$R_{measured}(t)$ = Thermal resistivity measured at time t
R_{final} = Final (time $\rightarrow \infty$) thermal resistivity of fully aged foam, and
$R_{cc}(t)$ = Thermal resistivity of undamaged closed cell foam at time t.

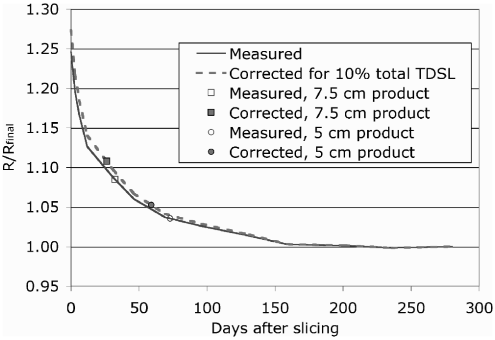

FIG. 2—*Comparison of the measured normalized thermal resistivity to the normalized thermal resistivity of the closed-cell foam portion of the slice for 10 % total TDSL.*

Using actual aging data for a closed-cell foam insulation product produced in 2003, Fig. 2 shows the measured thermal resistance for a stack of 1-cm thick slices, normalized by the thermal resistance measured after 280 days. If there was a TDSL of 0.05 cm on each cut surface, the total TDSL would be 10 %. This figure shows the thermal resistance of the closed-cell portion of the slices that would correspond to a TDSL of 10 %. If the slice thickness was used to predict the thermal resistance of a 7.5-cm thick product at an age of five years, the measurement would be made on the thin slices 32 days after the slices were prepared. If the correct closed-cell diffusion thickness of 0.9 cm were used, that measurement would be made after 26 days. Both of these corrections together make a difference of −2 % in the aged thermal resistance test results. Similarly, for a 5-cm thick product at an age of five years, the measurement would be made after 73 days versus 59 days if the corrected diffusion thickness were used.

Based on Eqs 3 and 4, and as shown in Fig. 2, both of these errors cause the test result to under predict the future thermal resistance of the foam, and thereby introduce a bias into the test procedure. This ruggedness test was performed in an effort to better understand and reduce this bias.

Test Plan

The test plan called for five specimens each of:

- Two classes of foam:
  - Polyisocyanurate (PIR)
  - Extruded Polystyrene (XPS)
- Sliced using four different cutting tools:[2]
  - Slicer
  - Bandsaw with 10 teeth/in
  - Bandsaw with 14 teeth/in
  - Grinder
- Produced for each of three TDSL test laboratories

All PIR foam was taken from a single production batch, as was the XPS foam, to minimize material variability. All specimens from a single tool were prepared in a single batch by a single operator to minimize the variability of the specimens within each tool class. Separate test specimens were prepared for each of the three laboratories making the TDSL measurements. Because the foam types evaluated for accelerated aging are designed to be as near to 100 % closed-cell content as possible, the difference between the geometric volume and the closed-cell volume is proportional to the average TDSL. Two of the laboratories used ASTM Standard Test Method for Open Cell Content of Rigid Cellular Plastics by the Air Pycnometer (D 2856, Method A) and the third laboratory used a related method [2]. Test method D 2856 uses a pycnometer to adjust the variable volumes of two test chambers held at equal pressures, thus

---

[2] Other work had already shown that a hot wire produced an unacceptable "skin" on the finished test specimen (see ASTM C 1303).

TABLE 1—*TDSL test parameters.*

	Cutting Tool	Nominal Geometric Size (cm)	Nominal Active Surface Area/Volume Ratio (1/cm)	Test Method
Lab A	Bandsaw with 14 teeth/in, Bandsaw with 10 teeth/in (PIR), Grinder	2.5 cube	0.8	D 2856, Method A
	Meat slicer	4.5×2.5×0.6	3	
	Bandsaw with 10 teeth/in (EPS)	5×3×2.5	2	
Lab B	Both bandsaws, Meat slicer	15 diameter× 1.0 thick	1	Alternate method, Eight measurements per specimen
Lab C	All four	3×2.5×5	0.8	D 2856, Method A, Five measurements per specimen

revealing the closed-cell volume of the enclosed test specimen. The related method uses two constant volume test chambers and measures the pressure differential before and after the two chambers are connected to produce the closed-cell volume of the enclosed test specimen. Specimen sizes varied among the test labs, as shown in Table 1.

Results

The results are summarized in Fig. 3 and Table 2. The differences between the results for the two foam classes were very small, with a few exceptions. However, it must be remembered that these foams were produced in 1996 and may not be representative of today's foam products.

The differences among the cutting instruments were also less than clear cut. Based on Lab A's results, it would appear that the slicer is far superior to the other tools, but the results from the other two labs show no such advantage. For all three labs, the difference between the two bandsaws was very small. The grinder showed a slightly smaller TDSL than the bandsaws, but that tool was only 6 in wide, and the thin slicing procedure has evolved such that the use of a 12-in by 12-in thin slice is common.

The greatest difference appears to be between the different laboratories, as shown in Fig. 4. A previous interlaboratory study included in D 2856, the test method used by Labs A and C, showed a reproducibility of 1.4 to 11.4 % for measuring open-cell volume. However, it should be noted that we are using that procedure to measure the volume of the broken surface cells in a mostly closed-cell product, which is not the test method's intended application. In D 2856, a linear measurement is used to evaluate the change in volume of a cylinder with a moveable piston. The method used by Lab B relies upon the same ideal gas

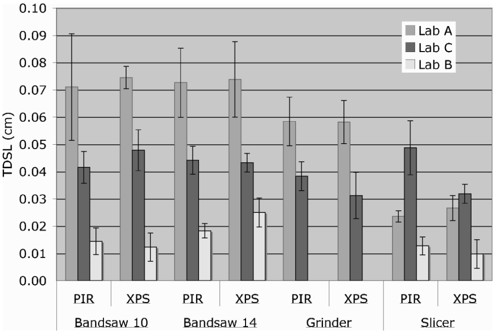

FIG. 3—*Measured TDSL values, showing mean and standard deviation for five specimens for four cutting tools.*

TABLE 2—*TDSL values*[a] *measured by three labs, cm.*

	Cutting Tool	Foam Type	Mean	Minimum	Maximum	STD[d]
Lab A	BS10[b]	PIR	0.071	0.048	0.101	0.020
Lab A	BS10	XPS	0.075	0.070	0.080	0.004
Lab A	BS14[c]	PIR	0.073	0.061	0.094	0.013
Lab A	BS14	XPS	0.074	0.059	0.094	0.014
Lab A	Grinder	PIR	0.058	0.048	0.072	0.009
Lab A	Grinder	XPS	0.058	0.047	0.068	0.008
Lab A	Slicer	PIR	0.024	0.022	0.027	0.002
Lab A	Slicer	XPS	0.027	0.021	0.033	0.005
Lab B	BS10	PIR	0.018	0.013	0.026	0.005
Lab B	BS10	XPS	0.025	0.018	0.031	0.005
Lab B	BS14	PIR	0.014	0.012	0.019	0.003
Lab B	BS14	XPS	0.012	0.007	0.019	0.005
Lab B	Slicer	PIR	0.013	0.010	0.018	0.003
Lab B	Slicer	XPS	0.010	0.005	0.016	0.005
Lab C	BS10	PIR	0.042	0.037	0.052	0.006
Lab C	BS10	XPS	0.048	0.038	0.058	0.008
Lab C	BS14	IR	0.044	0.036	0.050	0.005
Lab C	BS14	XPS	0.043	0.040	0.049	0.003
Lab C	Grinder	PIR	0.038	0.032	0.044	0.005
Lab C	Grinder	XPS	0.031	0.024	0.045	0.009
Lab C	Slicer	PIR	0.049	0.034	0.059	0.010
Lab C	Slicer	XPS	0.032	0.028	0.037	0.003

[a] Statistics based on five specimens each.

[b] BS10 is a bandsaw with ~4 teeth/cm (10 teeth/in).

[c] BS14 is a bandsaw with ~6 teeth/cm (14 teeth/in).

[d] Standard deviation of the sample [based on $(n-1)$].

relationships as D 2856, but measures differential pressures rather than volume. The size and shape of the test specimens also varied between the two methods, as was shown in Table 1, but the definition of active surface area was the same.

Discussion and Conclusions

The error in the scaled accelerated aging time was shown to be approximately proportional to twice the total TDSL fraction. That is, a total TDSL of 5 % will produce an error in the calculated aging time of about 10 %. The degree to which this error propagates into the C 1303 test results depends on the rate of foam aging at the time the measurement is made, and is therefore likely to be greater for the test results produced for thicker products. The error in the measured thermal resistivity due to TDSL is less, and is

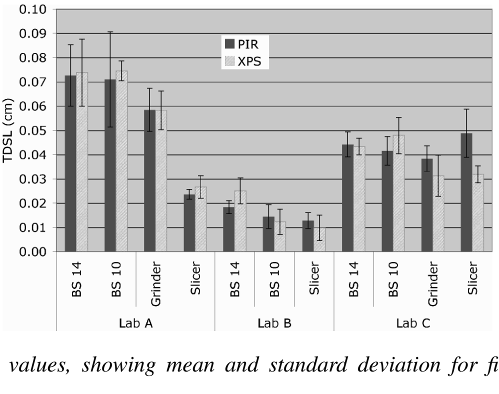

FIG. 4—*Measured TDSL values, showing mean and standard deviation for five specimens from three laboratories.*

approximately proportional to the total TDSL fraction. Both of these errors are conservative; that is, they both lead to an under prediction of the aged thermal resistivity.

Based on the test results, the bandsaws, grinder, and slicer all produced comparable TDSL on the foam specimens examined. The TDSL for these tools when used with the foams tested was in the 0.01 to 0.07 cm range. It should be recognized that all specimen preparation was performed by experienced personnel and that appropriate care must be taken in the cutting process to meet the specimen smoothness and flatness requirements.

Unfortunately, no standard specimen exists to determine which TDSL measurement technique is most accurate. For future work, it would be desirable to evaluate the accuracy of the instrumentation used at each TDSL measurement laboratory in order to calculate a likely error bound for each measurement.

Acknowledgments

Funding for this project was provided by the U.S. Department of Energy, Office of Building Technology, State, and Community Programs under contract number DE-AC05-00OR22725 with the Oak Ridge National Laboratory, managed by UT-Battelle, LLC.

References

[1] Crank, J., *The Mathematics of Diffusion*, 2nd ed., Oxford University Press, New York, 1995.

[2] Normandin, N. and Kumaran, M. K., "A Pressure-Volume Apparatus to Measure the Effective Thickness of Cellular Plastic Test Specimens," *J. Therm. Insul.*, Vol. 15, 1992, pp. 217–225.

Journal of ASTM International, Vol. 4, No. 5
Paper ID JAI100607
Available online at www.astm.org

David W. Yarbrough[1] *and Ronald S. Graves*[1]

The Effect of Air Flow on Measured Heat Transport through Wall Cavity Insulation

ABSTRACT: The methods commonly used for determining the thermal resistance of insulations in wall cavities do not include the effect of air movement through the insulation. Contributions to the total building heating or cooling load include the change in enthalpy of air moving through an insulation and the heat flux through the insulation due to the imposed thermal gradient. The two effects are not independent since the air movement affects the temperature distribution in the insulation. A heat-flow-meter apparatus meeting the requirements of the Standard Test Method for Steady-State Thermal Transmission Properties by Means of the Heat Flow Meter Apparatus ASTM C 518 has been configured to allow uniform air flow across thermal test specimens. The air flow is parallel to the heat flow direction. Air is introduced into the specimen chamber of the heat-flow-meter apparatus from an external source. The heat-flow-meter with controlled air flow has been used to determine total heat-flow rates as a function of air-flow rate, air-flow direction, and temperature for commonly used wall cavity insulation.

KEYWORDS: thermal resistance, fiberglass, convection, convection in porous insulation, fiberglass batts

Introduction

Wall cavity insulation is conventionally measured and labeled for thermal performance under specific steady-state conditions with solid isothermal bounding surfaces [1]. This configuration, as a result, does not include air flow through the insulation that can occur in actual applications. Walls of low-rise residences, for example, have leakage paths through which air can move due to small pressure differences between the interior and exterior of a residence [2]. This movement of air has an effect on the heating and cooling loads of the building. One approach to the determination of the load added to a building due to air leakage adds the heat load resulting from air flow to the heat flow through the envelope without forced convection [3]. The assumption that the heat flow through insulation without air flow and the heat transfer resulting from air flow can be added is not valid if the temperature distribution in the wall cavity insulation is affected by the movement of air through the insulation. If wall cavity insulation is tight in a cavity, then air leakage will be through the insulation and the temperature profile in the insulation will be disturbed. Anderlind and Johansson [4] have provided a theoretical analysis of the effect of air flow through thermal insulation that predicts heat-flow changes that depend on the direction of air flow relative to the direction of air movement. Anderlind and Johansson used the terms contraflux insulation and proflux insulation for the cases where the heat flow is opposite the air-flow direction (contra) or heat flow is in the same direction as the air flow (pro). The purpose of the present research is to measure the effective thermal resistance (RE) of wall cavity insulation with an imposed air flow through the insulation

$$RE = \Delta T/(Q_{\mathrm{net}}/A) \qquad (1)$$

where Q_{net} is the heat loss or gain from the conditioned space with area A. Q_{net} is the sum of the measured heat flow through the test specimen and the change in enthalpy of the air moving across the test specimen, Q_{air}. The RE defined by Eq 1 is a system value that depends on the air flow.

Manuscript received April 19, 2006; accepted for publication May 2, 2007; published online September 2007. Presented at ASTM Symposium on Heat-Air-Moisture Transport: Measurements on Building Materials on 23 April 2006 in Toronto, Canada; P. Mukhopadhyaya and M. Kumaran, Guest Editors.

[1] R&D Services, Inc., Cookeville, TN 38502-2400.

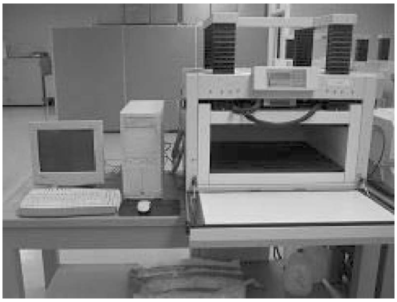

FIG. 1—*Photograph of the heat-flow-meter apparatus.*

Experimental Apparatus

The apparatus used in this research is a customized heat-flow meter designed to meet the requirements of ASTM C 518 when used in the normal configuration without air flow [5]. Figure 1 is a photograph of the heat-flow-meter apparatus designed for 61 by 61 cm test specimens. The basic apparatus has been modified to provide for measured amounts of air flow through a test specimen. This is accomplished by an air-tight specimen box containing the insulation to be tested with air flow constructed to fit the test specimen space in the heat-flow meter. The specimen box has air inlet/outlet channels on each side of the box. One set of five inlet channels is on the warm side of the test specimen while the second set of five air channels is on the cold side of the test specimen. The selection of five inlets and five outlets was a compromise between an ideal uniform distribution of air flow and a practical design. There was no determination of air flow velocity profiles. Air enters and leaves the test box at five locations on each side that includes one inlet/outlet in the center and one inlet/outlet in each quadrant. Thermocouples have been

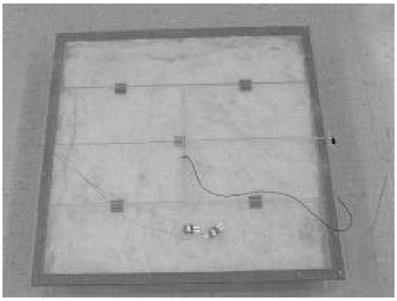

FIG. 2—*Photograph of the test box used to enclose the test specimen.*

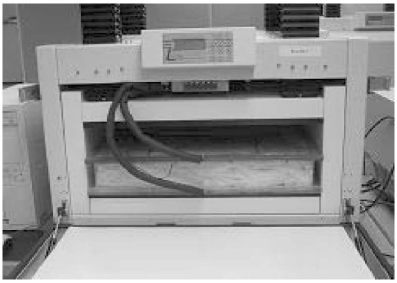

FIG. 3—*Photograph of the test box positioned in the heat-flow-meter apparatus.*

TABLE 1—*Heat-flow meter control temperatures.*

Test Sequence	Type	Cold Plate (°C)	Hot Plate (°C)
1	contraflux	31.4	51.4
2	contraflux	31.4	51.4
3	proflux	31.4	51.4

TABLE 2—*Thermal results for test sequence 1.*

Air Rate (SLM)	T_{cold} (°C)	T_{hot} (°C)	T_{mean} (°C)	Q_{in} (W/m^2)	Q_{out} (W/m^2)	Q_{air} (W/m^2)	Heat Balance Closure (%)
0.067	32.31	50.81	41.56	3.647	3.713	0.029	−2.6
1.093	31.85	50.80	41.32	3.860	3.534	0.562	−5.8
2.156	31.67	50.79	41.23	4.046	3.197	1.136	−6.7
3.371	31.46	50.76	41.11	4.281	2.806	1.773	−6.5
4.433	31.25	50.76	41.05	4.529	2.435	2.327	−4.9
5.302	31.20	50.76	40.98	4.625	2.267	2.795	−8.6
5.668	31.02	50.72	40.87	4.839	1.883	3.039	−1.7
6.973	30.81	50.66	40.74	5.305	1.363	3.702	4.7

TABLE 3—*Thermal results for test sequence 2.*

Air Rate (SLM)	T_{cold} (°C)	T_{hot} (°C)	Q_{in} (W/m^2)	Q_{out} (W/m^2)	Q_{air} (W/m^2)	Heat Balance Closure (%)
0.068	32.08	50.75	3.705	3.689	0.030	−0.5
1.114	31.83	50.78	3.802	3.567	0.574	−8.2
2.281	31.72	50.79	4.025	3.246	1.184	−9.1
3.551	31.47	50.77	4.333	2.698	1.873	−5.2
4.725	31.28	50.76	4.565	2.340	2.520	−6.1
6.088	31.07	50.71	5.008	1.840	3.150	0.4
7.273	30.88	50.66	5.330	1.432	3.859	0.7
7.751	30.84	50.65	5.414	1.286	4.116	0.2

TABLE 4—*Thermal results for test sequence 3.*

Air Rate (SLM)	T_{cold} (°C)	T_{hot} (°C)	T_{mean} (°C)	Q_{in} (W/m^2)	Q_{out} (W/m^2)	Q_{air} (W/m^2)	Heat Balance Closure (%)
0.068	26.12	50.79	38.46	3.593	3.779	0.031	−4.2
1.045	26.95	50.73	38.84	3.674	3.995	0.548	5.4
2.145	26.53	50.00	38.27	4.520	4.184	1.131	−15.0
3.342	26.47	48.96	37.72	5.856	4.459	1.694	−4.8
4.530	26.45	48.04	37.25	7.025	4.716	2.260	0.7
5.664	26.42	47.20	36.81	8.349	5.047	2.709	7.6
8.247	26.19	45.92	36.06	10.959	5.816	3.805	13.9

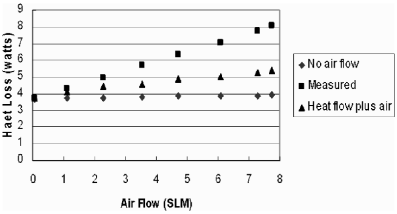

FIG. 4—*Heat flow rates determined with and without air flow (contraflux).*

added to the basic design of the heat-flow meter to measure the hot and cold surface temperatures at the surface of the insulation in the test box. This is necessary because there is a small thermal resistance and resulting temperature difference between the temperature set points of the heat-flow meter and the surface of the test specimen. Figure 2 is a photograph of the test box. Figure 3 is a photograph of test box inserted in the heat-flow-meter apparatus.

Air flow from a tank of compressed air is controlled by a microvalve in the tubing connected to the inlet of the specimen box. The volumetric air flows in and out of the test box are measured by TSI Series 4000/4100 High Performance Linear OEM Mass Flowmeters. Heat-flux data, temperatures, and air-flow data are collected by a computer data acquisition system.

Experimental Data

Three sets of experimental data are included in this paper. Each dataset contains heat fluxes, temperatures, and air-flow rates for a range of air-flow rates from zero to about eight standard litres per minute, SLM. Two of the datasets are for contraflux operation while the third set is for proflux operation. The data that are included in this paper are the heat flows across the hot and cold surfaces, bounding temperatures, air-flow rates, and the change in enthalpy of the air moving through the test specimen, and the inlet and outlet air temperatures. The enthalpy change of the dry air is based on data from NBS Circular 564 [6]. The flow-meter control temperatures for the three datasets are shown in Table 1. In all cases, the test specimen was a nominal RSI 1.937 $m^2 \cdot W/K$ fiberglass batt insulation with a thickness of 88.9 mm. The measured bulk density for the test specimen was 9.6 kg/m^3. The same test specimen was used for all of the data that follow. Inlet air to the heat-flow meter was at the laboratory temperature in the range of 22 to 26°C.

The data in Tables 2–4 contain air rate, temperatures in °C, heat flows with Q_{in} being the hot side and Q_{out} being the cold side. The T_{mean} entries in the tables are the average specimen temperatures. The mean specimen temperatures for the measurements in this study are greater than the mean specimen temperature used to develop labels. The present study is not related to evaluation of products. The term Q_{air} is calculated from T_{hot} and T_{cold}. T_{cold} is the temperature of the incoming air. The heat flow rates Q_{in} and Q_{out} are based on the temperature difference across the insulation. The temperature differences across the insulation are less than the temperature differences for the heat-flow meter set points because of the thermal resistance of the test box material.

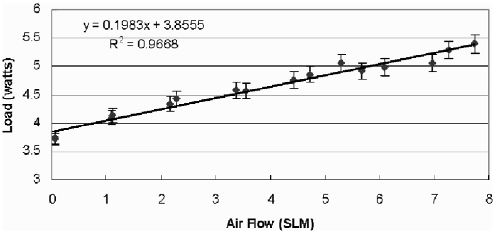

FIG. 5—*Comparison of measured heat losses from two contraflux datasets.*

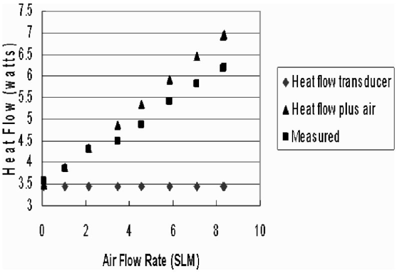

FIG. 6—*Heat flow rates determined with and without air flow (proflux).*

The "Heat Balance Closures" for the contraflux tests were calculated using Eq 2 with the heat loss from the hot side, L_c, calculated using Eq 3.

$$\text{Closure } \% = 100^{*}(Q_{\text{in}} - Q_{\text{out}} - Q_{\text{air}})/(Q_{\text{out}} + Q_{\text{air}}) \tag{2}$$

$$L_c = Q_{\text{out}} + Q_{\text{air}} \tag{3}$$

Closure for the proflux test was calculated using Eq 4 with the heat loss, L_p, calculated using Eq 5.

$$\text{Closure } \% = 100^{*}(Q_{\text{out}} - Q_{\text{in}} - Q_{\text{air}})/(Q_{\text{in}} + Q_{\text{air}}) \tag{4}$$

$$L_p = Q_{\text{in}} + Q_{\text{air}} \tag{5}$$

The contraflux configuration represents air infiltration in the winter or air exfiltration in the summer. The proflux configuration represents air infiltration in the summer or air exfiltration in the winter.

Discussion of Results

The data summarized above has been used to make comparisons of the heat loss from the warm side of the system determined three ways. The heat loss can be calculated from the apparent thermal conductivity of the insulation in the test box and the temperature difference across the insulation. This will be denoted as the "no air flow" case. A second heat loss rate calculated by adding the heat flow without air flow and Q_{air} is denoted as the "additive" case. The additive case could be viewed as a "standard" estimation for the total heat flow in the presence of net air flow through an insulated cavity. A third heat loss rate which is the measured heat loss with air flow is denoted as the "measured" case. Figure 4 compares the three heat transfer rates for the data from sequence one which is representative of the contraflux observations. The

TABLE 5—*Performance factors for contraflux tests.*

Air Flow (SLM)	L_c (watts)	$L_c - L_0$	RE (m^2·K/W)	RE/RE_0
0.067	3.742		1.688	
1.093	4.096	0.354	1.579	0.94
2.156	4.333	0.591	1.506	0.89
3.371	4.579	0.837	1.439	0.85
4.433	4.762	1.020	1.399	0.83
5.302	5.062	1.320	1.319	0.78
5.668	4.922	1.180	1.366	0.81
6.973	5.065	1.323	1.338	0.79
0.068	3.719		1.714	
1.114	4.141	0.422	1.563	0.91
2.281	4.430	0.711	1.469	0.86
3.551	4.571	0.852	1.441	0.84
4.725	4.860	1.141	1.368	0.80
6.088	4.990	1.271	1.344	0.78
7.273	5.291	1.572	1.276	0.74
7.751	5.402	1.683	1.252	0.73

TABLE 6—*Performance factors for proflux test.*

Air Flow (SLM)	L_p (watts)	L_p-L_0	RE ($m^2 \cdot K/W$)	RE/RE_0
0.068	3.624		2.036	
1.045	4.222	0.598	1.922	0.94
2.145	5.651	2.027	1.417	0.70
3.342	7.550	3.926	1.017	0.50
4.530	9.285	5.661	0.794	0.39
5.664	11.058	7.434	0.642	0.32
8.247	14.764	11.140	0.456	0.22

bottom curve in the figure is for "no air flow," the middle curve is the measured heat loss, and the top curve is the additive case. The present study does not provide a determination of the air flow rates likely to be observed in buildings. Actual air flow rates depend on the design of the structure and the quality of the workmanship. "Typical" air flow rates have not been established because of the large number of factors involved.

Test sequences 1 and 2 provide data at the same conditions. Figure 4 contains a comparison of the measured heat losses for the two contraflux sequences and provides a measure of the repeatability of the measurement. The vertical error bars in Fig. 5 show ±3 % about the data points. The line shown in the figure is a linear fit to the composite dataset consisting of 16 steady-state thermal measurements.

Figure 6 shows the three heat flow rates for the sequence 3, the proflux example. The bottom curve is the heat flow without air, the middle curve is the additive case, and the top curve is the measured heat loss from the warm side.

The contraflux measurements show the measured heat loss to be less than the sum of the heat flow without air movement and the heat carried by air. The proflux measurements show the measured heat loss to be greater than that obtained by adding the heat flow without air movement and the heat carried by the air. This is qualitatively consistent with the observation that contraflux reduces the temperature gradient on the cold side of the wall, thus reducing the conductive transfer while the temperature gradient is increased on the cold side of the wall in the proflux case [4].

The heat flow results were used to calculate RE from Eq 1 and either L_c or L_p. The RE were used to calculate the ratio RE/RE_0 where RE_0 is the zero air flow case. This ratio is associated with an efficiency. The difference, $RE-RE_0$, is a measure of the thermal performance improvement to be achieved by stopping air leakage. The difference, $L-L_0$, where L_0 is the no air-flow case is a measure of the energy savings to be realized by stopping air flow through the 0.3414 m^2 test section. Table 5 contains the performance factors for the contraflux tests while Table 6 contains the performance factors for the proflux test.

The loss of efficiency represented by the ratio RE/RE_0 approaches 25 % for the contraflux measurements. The loss of efficiency for the proflux case approaches 80 %.

Summary

The usefulness of a modified heat-flow-meter apparatus to study the effect of air flow through porous insulation has been demonstrated.

The measured total heat loss from the high temperature side of a test specimen with air flow differs from the sum of the no-air flow thermal resistance and the enthalpy change of the air. For contraflux measurements the measured heat flow was less than the sum of the two heat flows while in the case of the proflux measurement the measured heat flow was greater than the sum of the two flows.

The loss of thermal effectiveness of the insulation was reduced as much as 25 % for the contraflux measurements and up to about 80 % for the proflux measurement.

Acknowledgments

This project is being supported by Guardian Building Products, Inc., headquartered in Greenville, SC. Guardian's interest and support for the project are appreciated.

References

[1] ASTM Standard C 518-04, “Standard Test Method for Steady-State Thermal Transmission Properties by Means of the Heat Flow Meter Apparatus,” *Annual Book of ASTM Standards*, Vol 04.06, ASTM International, West Conshohocken, PA, 2005.

[2] *2001 ASHRAE Handbook of Fundamentals*, “Infiltration and Ventilation Heat Gain,” Section 29.18, American Society of Heating, Refrigerating and Air-Conditioning Engineers, Inc., Atlanta, GA, 1993.

[3] *2001 AHRAE Handbook of Fundamentals*, “Infiltration and Ventilation,” Chapter 26, American Society of Heating, Refrigerating and Air-Conditioning Engineers, Inc., Atlanta, GA, 2001.

[4] Anderlind, G. and Johansson, B., “Dynamic Insulation,” Swedish Council for Building Research, Document *D8:1983*, 1983.

[5] Flowmeter manufactured by TSI, Inc., St. Paul, MN.

[6] National Bureau of Standards Circular 564, “Tables of Thermal Properties of Gases” taken from Table 1.1 in *Handbook of Tables for Engineering Science*, R. E. Bolz and G. L. Tuve, Eds., The Chemical Rubber Company, Cleveland, OH, 1970.

Journal of ASTM International, Vol. 4, No. 1
Paper ID JAI100323
Available online at www.astm.org

Yoshihiko Kishimoto, D. Eng.,[1] *Shuichi Hokoi, D. Eng.,*[2] *Kazunori Harada, D. Eng.,*[3] *and Satoru Takada, D. Eng.*[4]

The Effect of Vertical Distribution of Water Permeability on the Modeled Neutralization Process in Concrete Walls

ABSTRACT: The aim of this paper was to predict the durability of concrete walls. Because liquid movement is important in discussing the neutralization process, the vertical distribution of the permeability in a concrete wall was measured. In a 20 cm high sample, the permeability clearly showed a nonuniform vertical distribution. Next, an analytical model was proposed to predict the neutralization process taking into account the influence of acid rain. Based on this model, the simulation was carried out with permeability as a parameter. The results showed that neutralization was accelerated due to acid rain in regions with a high permeability and retarded in regions with a low permeability. Thus, it can be concluded that the influence of acid rain on the neutralization process may differ depending on the position in the concrete structure.

KEYWORDS: durability of concrete structure, neutralization, acid rain, water permeability

Nomenclature

C = concentration of substance in material $[\mathrm{kg/m^3}]$
D = diffusion coefficient $[\mathrm{m^2/s}]$
M = molecular weight [kg/mol]
$[CO_2]$, $[Ca(OH)_2]$ = molar concentration $[\mathrm{mol/m^3}]$
α_{VL} = dissolution rate coefficient from gas phase to liquid phase [l/s]
k = reaction rate coefficient $[\mathrm{m^3/mol \cdot s}]$
v = water velocity of liquid in porous material [m/s]
T = temperature [K]
μ = water chemical potential (relative to free water) [J/kg]
c = specific heat [J/kg·K]
ρ, ρ_w = densities of concrete and water, respectively $[\mathrm{kg/m^3}]$
ψ_w = volumetric water content $[\mathrm{m^3/m^3}]$
R = latent heat of vaporization [J/kg]
λ = thermal conductivity [W/m·K]
λ'_T = moisture conductivity due to temperature gradient [kg/m·s·K]
λ'_{TV} = moisture conductivity in gas phase due to temperature gradient [kg/m·s·K]
λ'_μ = moisture conductivity due to water chemical potential gradient [kg/m·s(J/kg)]
$\lambda'_{\mu V}$ = moisture transfer in gas phase due to water chemical potential gradient [kg/m·s(J/kg)]

Subscripts

V = gas phase

Manuscript received January 26, 2006; accepted for publication November 20, 2006; published online September 2007. Presented at ASTM Symposium on Heat-Air-Moisture Transport: Measurements on Building Materials on 23 April 2006 in Toronto, Canada; P. Mukhopadhyaya and M. Kumaran, Guest Editors.

[1] Postdoctoral fellow, Hokkaido University, Kita 13 Nishi 8, Kita-ku, Sapporo 060-8628, Japan.

[2] Professor, Kyoto University, Kyotodaigaku-Katsura, Nishikyo-ku, Kyoto 615-8540, Japan.

[3] Associate Professor, Kyoto University, Kyotodaigaku-Katsura, Nishikyo-ku, Kyoto 615-8540, Japan.

[4] Associate Professor, Kobe University, 1-1 Rokkodai, Nada-ku, Kobe 654-8507, Japan.

L = liquid phase
CO_2 = carbon dioxide
$Ca(OH)_2$ = calcium hydroxide
$CaCO_3$ = calcium carbonate
H_2O = water

Introduction

Deterioration of concrete walls is currently a serious problem despite the significant development in concrete R&D, production, and maintenance technology.

Concrete walls deteriorate due to many external and internal factors, such as alkali aggregate reaction, repetition of drying and wetting processes, and neutralization due to acid substances such as carbon dioxide (CO_2).

Neutralization of concrete occurs as a result of CO_2 gas from the air dissolving in the absorbed water, which contains alkali materials such as calcium hydroxide ($Ca(OH)_2$) [1]. Therefore, the ad- or absorbed water is essential to neutralization, and the rate of the neutralization strongly depends upon the moisture regime. Because CO_2 gas cannot diffuse into concrete, it is generally believed that the neutralization is slow when the concrete wall is exposed to rain [2]. Although rain is assumed to be pure water, rain in Japan is usually acid with a pH less than 5.6 [3]. In this situation, neutralization may proceed faster because CO_2 has already dissolved in the atmosphere, and the acid substances can move due to advection of pure water. Therefore, in order to evaluate the influence of acid rain on the neutralization process, liquid movement in a concrete wall must be taken into account.

From this point of view, permeability is one of the important parameters in discussing the neutralization of a concrete wall. Furthermore, if the permeability varies depending upon the position in the wall, the neutralization rate may also differ from place to place.

In this paper, concrete permeability is measured at atmospheric pressure in order to clarify the vertical distribution. Next, an analytical model is proposed for predicting the neutralization process coupled with heat and moisture transfer, with an emphasis on liquid movement. Based on this model, a neutralization process in a small-scale concrete wall is simulated under cyclic infiltration of rain and drying, with an assumed vertical distribution of water permeability.

Measurement of Water Permeability

Introduction

In the acid solution experiment reported elsewhere [4], the test pieces (water cement ratio 0.715) were split after the infiltration process. Photo 1 shows the moisture content distributions in the two samples that had been compression tested, one with a strength of 30 MPa and the other with a strength 50 MPa (written as P50 MPa in the caption). They showed clear differences in the infiltration depth between the upper and lower parts of the sample. The area inside the solid line in Photo 1 is the area judged by visual observation to have high moisture content. The nonuniform vertical moisture distribution is thought to be caused by the difference in pore structure between the upper and lower parts. This difference in pore structure may be due to bleeding in the curing period since air bubbles tend to concentrate in the upper part of the sample [1]. Although it is known that the permeability of concrete strongly depends upon the strength (water-cement ratio) [5], the vertical distribution of permeability has not been investigated adequately.

Liquid movement in concrete walls influences the transport of various substances related to the neutralization process, and affects the history of moisture distribution. Moreover, the moisture content in concrete walls influences the diffusion of acid substances and the neutralization rate. Thus, permeability is one of the important parameters in discussing the neutralization process of concrete walls.

In this study, the permeability of concrete walls was measured in order to clarify possible vertical differences.

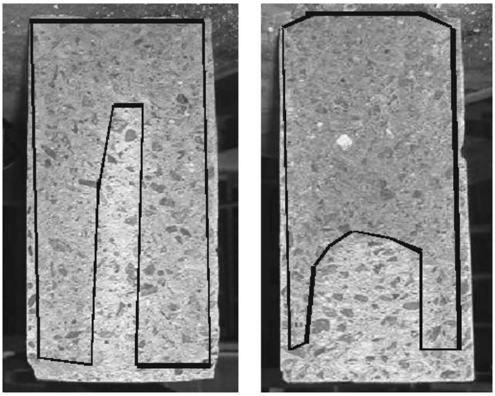

(a) 30 MPa. (b) P50 MPa.

PHOTO 1 -- Sections immediately after splitting.

Test Samples

Three 20-mm-high slices were prepared. These slices were cut from a concrete cylinder with a strength of 30 MPa (∅100 mm by 200 mm).This cylinder had been cast at the same time as the specimens for the acid solution experiment (Photo 2).

The smoothness of the upper and lower surfaces differed due to the mold. Therefore, slice Nos. 2, 4, and 6 in Photo 2 were used as samples of the upper, middle, and lower parts, respectively.

PHOTO 2 -- Slices measured.

Experimental Apparatus

Figure 1 shows the experimental apparatus. After the side surface of the sample was sealed with a rubber band, the sample was plugged into a rubber tube, and tightened with a clamp ring.

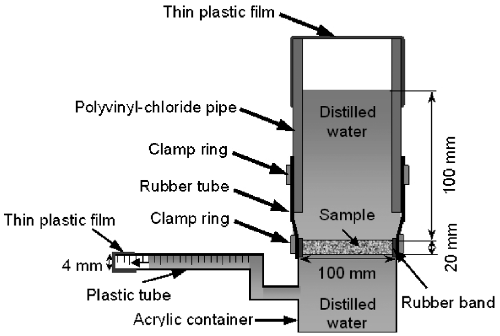

FIG. 1—*Experimental apparatus.*

The other end of the rubber tube was connected to the bottom of a polyvinyl-chloride pipe, and also tightened with a clamp ring. Distilled water was poured into the pipe to 100 mm above the upper surface of the sample. Evaporation of water was prevented by covering the upper open end of the polyvinyl-chloride pipe with a thin plastic film with a 1 mm ⊘ hole. For making the water saturated condition of the specimen, before the bottom of the specimen was connected to the acrylic container, the specimen had been attached to the water container (top surface of the specimen in contact with distilled water in the container), and had been kept until the water that penetrated and flowed through the specimen was observed at the bottom surface. Three to five days were needed for it.

After confirming the specimen saturated with water, the bottom of the specimen was placed in contact with water in an acrylic container. A plastic tube (4 mm ⊘) was connected to the side of the acrylic container and kept horizontal. The evaporation from the other open end of the plastic tube was also prevented by using a thin plastic film with a small hole.

Experimental Procedures

The position of the water meniscus in the plastic tube was recorded over time. The permeability of the sample was calculated from these results.

Experimental Conditions

Although the experiments should be carried out under constant climatic conditions, they were carried out in a non-air-conditioned room under natural conditions for unavoidable reasons. However, since the fluctuation of the temperature and moisture in the room was small, the influence on the experimental results was regarded as insignificant.

Results and Discussion

Figure 2 shows the results. If the permeability of the sample was 4.5×10^{-9} cm/s, a typical value from Ref. [6] that is widely used in Japan, the speed of movement of the meniscus in the tube would have been 1.3 cm/day. However, the measured average speed was 13 cm/day for the upper sample and 5.4 cm/day for the lower sample. These were, respectively, 10 and 4 times faster than the reference value. The measurement was not successfully carried out for the lower sample, due to instability of liquid movement in the tube. However, in a preliminary unpublished experiment where the evaporation rate from the bottom of the sample was measured, the evaporation rate decreased from the upper to the lower sample.

Estimated permeability values giving moisture content distributions in good agreement with those shown in Photo 1, were about 20 times and 10 to 15 times higher than the reference value in the upper and the lower parts, respectively. Although the values measured are lower than the estimated values, they show a qualitative agreement in that the permeability in the upper part is about twice as large as that in the middle part.

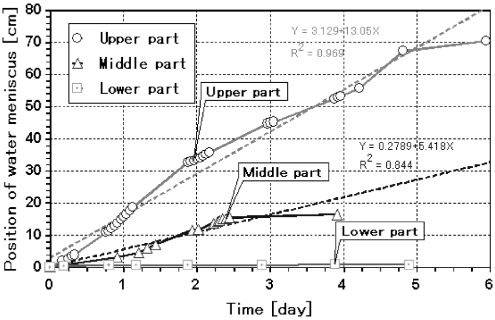

FIG. 2—*Permeability measurements.*

Analytical Model for Predicting the Neutralization Process Taking Into Account Liquid Movement

Introduction

The state of liquid water in concrete walls influences the transport of various substances related to the neutralization process and affects the history of the moisture content distribution. Thus, it is important to take into account liquid movement in discussing the neutralization process of concrete walls.

In this study, an analytical model is proposed which predicts the neutralization process coupled with heat and moisture transfer, particularly emphasizing liquid movement.

Fundamental Equations

In this study, it was assumed that the neutralization reaction occurs between $Ca(OH)_2$ in the concrete walls and CO_2 from the air.

Figure 3 shows a schematic model of the neutralization process in the concrete wall.

In this model, the following assumptions were made. The material is composed of three phases: gas, liquid, and solid. CO_2 exists in the gas and liquid phases, $Ca(OH)_2$ in the liquid and solid phases. The thickness of the liquid phase is determined by the moisture content, while that of the solid phase is not affected by the neutralization process. The concentration of diffusive substances in each phase is uniform in a small control volume.

Based on these assumptions, the one-dimensional balance equation of each diffusive substance in each phase is given as follows:

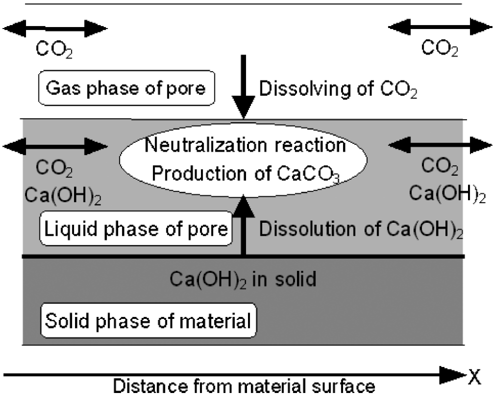

FIG. 3—*Analytical model.*

$$\frac{\partial C_{\mathrm{VCO_2}}}{\partial t} = D_{\mathrm{VCO_2}} \frac{\partial^2 C_{\mathrm{VCO_2}}}{\partial x^2} + \alpha_{\mathrm{VL}}\left(f(C_{\mathrm{LCO_2}}) - C_{\mathrm{VCO_2}}\right) \tag{1}$$

$$\frac{\partial C_{\mathrm{LCO_2}}}{\partial t} = D_{\mathrm{LCO_2}} \frac{\partial^2 C_{\mathrm{LCO_2}}}{\partial x^2} - \alpha_{\mathrm{VL}}\left(f(C_{\mathrm{LCO_2}}) - C_{\mathrm{VCO_2}}\right) - \frac{\partial v_{\mathrm{L}} C_{\mathrm{LCO_2}}}{\partial x} - M_{\mathrm{CO_2}} k [\mathrm{CO_2}]_{\mathrm{L}} [\mathrm{Ca(OH)_2}]_{\mathrm{L}} \tag{2}$$

$$\begin{aligned}\frac{\partial C_{\mathrm{LCa(OH)_2}}}{\partial t} = {} & D_{\mathrm{LCa(OH)_2}} \frac{\partial^2 C_{\mathrm{LCa(OH)_2}}}{\partial x^2} - D_{\mathrm{LCa(OH)_2}} \left.\frac{\partial C_{\mathrm{LCa(OH)_2}}}{\partial y}\right|_{y=l_{\mathrm{LS}}} - \frac{\partial v_{\mathrm{L}} C_{\mathrm{LCa(OH)_2}}}{\partial x} \\ & - M_{\mathrm{Ca(OH)_2}} k [\mathrm{CO_2}]_{\mathrm{L}} [\mathrm{Ca(OH)_2}]_{\mathrm{L}}\end{aligned} \tag{3}$$

$$\frac{\partial C_{\mathrm{LCaCO_3}}}{\partial t} = M_{\mathrm{CaCO_3}} [\mathrm{CO_2}]_{\mathrm{L}} [\mathrm{Ca(OH)_2}]_{\mathrm{L}} \tag{4}$$

The simultaneous equations of heat and moisture transfer are used for heat and moisture balance. The source term in the moisture balance equation is the liquid water produced by the neutralization reaction. Since the amount of reaction heat is small, it is ignored:

$$c\rho \frac{\partial T}{\partial t} = \frac{\partial}{\partial x}\left(\lambda \frac{\partial T}{\partial x}\right) + R \frac{\partial}{\partial x}\left(\lambda'_{\mu \mathrm{V}} \frac{\partial \mu}{\partial x} + \lambda'_{\mathrm{TV}} \frac{\partial T}{\partial x}\right) \tag{5}$$

$$\rho_W \frac{\partial \psi_{\mathrm{W}}}{\partial \mu} \frac{\partial \mu}{\partial t} = \frac{\partial}{\partial x}\left(\lambda'_{\mu} \frac{\partial \mu}{\partial x}\right) + \frac{\partial}{\partial x}\left(\lambda'_{\mathrm{T}} \frac{\partial T}{\partial x}\right) + M_{\mathrm{H_2O}} k [\mathrm{CO_2}]_{\mathrm{L}} [\mathrm{Ca(OH)_2}]_{\mathrm{L}} \tag{6}$$

The third term on the right-hand side of Eqs 2 and 3 expresses diffusive substance transfer due to an advection of the liquid water (rain). The advection rate v_{L} is calculated by Eq 6. These terms are very important in the proposed model.

In Eqs 1 and 2, $f(C_{\mathrm{LCO_2}})$ expresses the CO_2 concentration in the gas phase which equilibrates with the CO_2 in the liquid phase. In the following analysis, a local equilibrium is assumed between gaseous and dissolved CO_2 because CO_2 dissolves faster than the diffusion rate of gaseous CO_2. The concentration of CO_2 in the gas phase, which is in equilibrium with the CO_2 dissolved in the liquid phase, is assumed to be given by Henry's equation:

$$H_{\mathrm{CO_2}} C_{\mathrm{VCO_2}} = C_{\mathrm{LCO_2}} \tag{7}$$

Definition of Neutralization Depth

The dissolution rate of solid $Ca(OH)_2$ into the liquid phase is assumed to be faster than that of CO_2 gas into the liquid phase. Therefore, the liquid phase is regarded as saturated with dissolved $Ca(OH)_2$ until the neutralization is finished in an area of interest. Until the completion of neutralization, the $Ca(OH)_2$ in the solid phase remains available for neutralization. Based on the result of Saeki et al. [7], the maximum amount of soluble $Ca(OH)_2$ in the solid phase is set at 29.6 $\mathrm{kg/m^3}$ (1.56×10^3 $\mathrm{mol/m^3}$). Here, the neutralization depth is defined as the largest distance from the material surface to the position where the neutralization has finished.

Transfer Properties Used in the Analysis

The transfer coefficients of moisture used in the simulation are mainly from Ogura [8], which are based on vapor conductivity and sorption isotherms measured by Hedenblad [9]. Our results were used for the water permeability at saturation. The vapor conductivity from 98 % relative humidity (RH) to saturation was estimated by interpolation because there is no measured data in this region. For RH higher than 90 %, the vapor conductivity measured by Hedenblad increases very sharply with RH. This must be caused by liquid movement. Thus, the vapor conductivity was assumed to be constant throughout the whole region of the relative humidity at 1.25×10^{-12} $\mathrm{kg/m \cdot s \cdot Pa}$ (measured value at low RH region), while the difference between the measured and this constant value was regarded as the liquid water transfer coefficient.

TABLE 1—*Physical properties.*

	Density, kg/m^3	Specific heat, kJ/kg·K	Thermal conductivity, W/m·K	Diffusion coefficient m^2/s
Concrete	2300	0.933	1.624	…
CO_2	1.964	…	…	1.73×10^{-7} [a] 1.80×10^{-9} [b]
$Ca(OH)_2$	2.24	…	…	1.80×10^{-9}

[a] In gas phase.
[b] In liquid phases [14].

In previous papers [10,11], we simulated the existing experimental results [4,12] with the coefficients as parameter in order to estimate the CO_2 diffusivity. The simulated results with the diffusion coefficient 1/80 of that in air [13] agreed reasonably well with the measured results. It was not dependent upon water infiltration and CO_2 concentration in atmosphere. Thus, this value was used for the present calculation. These physical properties are listed in Table 1. The equilibrium moisture content is from Hedenblad. Figure 4 shows the equilibrium moisture content at 20°C. In the calculation, this curve was transformed into the relation between the chemical potential of water μ and the volumetric moisture content ψ.

Influence of Permeability on the Neutralization Process

In this section the influence of permeability on the neutralization process is investigated by using the analytical model described previously. The neutralization process of a small-scale concrete wall was simulated under cyclic raining and drying, where the vertical distribution of water permeability in the concrete wall was assumed based on measured results (Measurement of Water Permeability section) and Ref. [15].

Computational Conditions

Analyzed Object—A two-dimensional area, 150 mm thick and 5 m high from the surface of the concrete wall, was analyzed.

Boundary Conditions—A cyclic change of precipitation with a period of 10 days, a 6-h rain (infiltration) period, and 9 days and 18-h dry period was assumed. Fluxes of heat and moisture occur at the surface of the concrete wall ($x=0$ mm). The temperature and relative humidity of the ambient air were set at 20°C and 60 % RH during the drying period and 20°C and 100 % RH during the raining period. The CO_2 concentration at the sample surface was set at 0.035 % (the same as air) during the drying period and 3.5 % for the raining period, corresponding to pH 4.6 for acid rain. It was assumed that there was no flux of heat, moisture, or chemical substances at the other surface of the concrete wall ($x=150$ mm).

Initial Conditions—It was assumed that initially there was a uniform temperature and relative humidity of 20°C and 60 % RH. The moisture content that equilibrates with these conditions is given. The CO_2

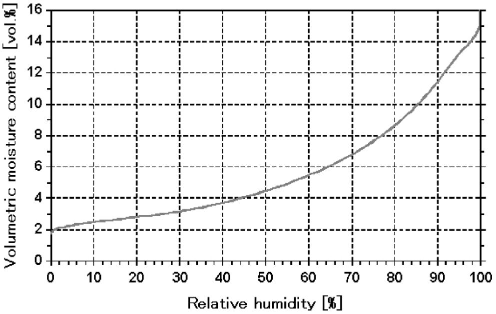

FIG. 4—*Equilibrium moisture content from Hedenblad [8].*

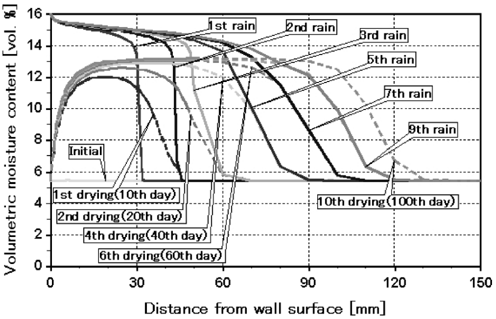

FIG. 5—*History of moisture content distribution in upper part (y = 5 m).*

concentration was set at 0 %. The concentration of $Ca(OH)_2$ was assumed to be 100 % in the not-neutralized region and 0 % in the region already neutralized. Calculations were for initial neutralization depths of 5 and 20 mm.

Calculation Method—Numerical calculations were performed by the finite difference method. The sample was divided into 1-mm slices. The time increment was set at 0.5 s during the drying process, and 0.01 s during the infiltration process. A simulation was performed for 100 days after a start-up period of one day.

Vertical Distribution of Permeability—The above result (Measurement of Water Permeability section) shows that the permeability is about 2 times larger than that in the lower part by 10 cm. Furthermore, it is reported that the permeability at the height of 3 m was 1.4 times lager than that at 1 m height in an actual concrete wall [15]. Based on these results, the permeability was assumed to increase vertically 2 times larger every 1 m height, and the influence of permeability on neutralization was investigated. The permeability, given as a ratio to the standard value (4.5×10^{-9} cm/s, from Ref. [6]) was set at 0.25, 0.5, 1, 2.5, 5, 10 at a height of 0, 1, 2, 3, 4, 5 m, respectively.

Results and Discussion

Figures 5 and 6 show the history of the moisture content distribution in the upper part and lower part of the concrete wall, respectively. Figure 7 shows the moisture content distribution in the concrete wall at the 100th day.

Comparison of Figs. 5 and 6 shows that the infiltration depth of the rain reached only 40 mm in the lower region and about 120 mm in the upper part after 100 days. Even under the same precipitation condition, the difference in the infiltration depth is significant. As shown in Fig. 7, the infiltration depth in the region lower than 2 m reached only 20 mm after 100 days.

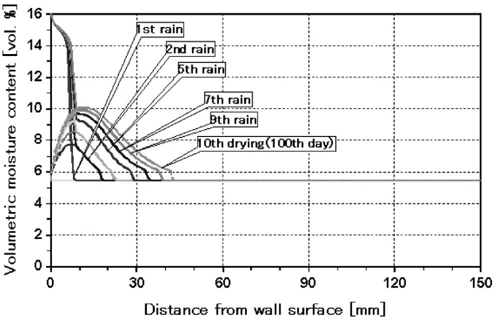

FIG. 6—*History of moisture content distribution in lower part (y = 0 m).*

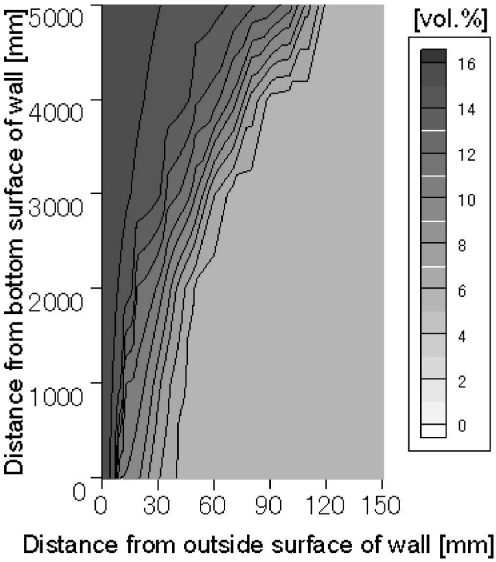

FIG. 7—*Moisture content distribution after 100 days.*

The total amount of $Ca(OH)_2$ dissolved from the solid phase into the liquid phase is shown in Figs. 8 and 9. Figures 8 and 9 are for a 5-mm and 20-mm initial neutralization depth, respectively.

When the initial neutralization depth was 5 mm (Fig. 8), the neutralization during infiltration was accelerated in the upper region with higher permeability and retarded in the lower region with no infiltration and lower permeability. This is because the amount of acid rain transferred to the neutralization depth is small. In addition, for an initial 20 mm neutralization depth (Fig. 9), the situation was almost the same as in the 5-mm initial depth. Since the acid rain does not reach the initial neutralization depth in the region below 2 m, the amount of dissolved $Ca(OH)_2$ does not show a stepwise change. This is because the diffusion of CO_2 gas is suppressed by an increase in the moisture content near the surface. Thus, it can be seen that the influence of acid rain on the neutralization progress may differ depending on the height of the concrete wall.

At a height of 5 m, where the neutralization process is most accelerated, the amount of dissolved $Ca(OH)_2$ after 100 days is about 1.6 times greater than that without rain for an initial neutralization depth of 5 mm, and about 3.1 times greater for an initial neutralization depth of 20 mm.

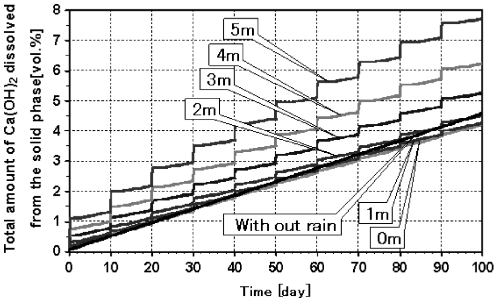

FIG. 8—*History of total amount of* $Ca(OH)_2$ *dissolved from the solid phase (initial neutralization depth is 5 mm).*

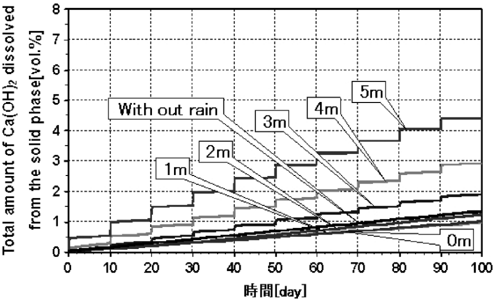

FIG. 9—*History of total amount of $Ca(OH)_2$ dissolved from the solid phase (initial neutralization depth is 20 mm).*

Therefore, in an actual concrete wall, although the neutralization due to acid rain is not accelerated in a normal part, it may be accelerated in a weak region with higher permeability.

There has not been an integrated evaluation of the influence of acid rain on the neutralization process [16–18]. Therefore, the mechanism of neutralization has not been clarified yet. This paper shows that neutralization due to acid rain is accelerated or retarded depending on the permeability of the concrete. Therefore, varying permeability of concrete walls may explain the range of results on the effect of acid rain.

Conclusion

On the assumption that liquid movement is important for discussing the neutralization process, the vertical distribution of permeability in a concrete wall was measured. Next, the simulation was carried out with permeability as a parameter in order to investigate the influence of acid rain on the neutralization process.

The results were as follows.

1. In a 20-cm-high sample, the permeability clearly showed a nonuniform vertical distribution. The water permeability in the upper part was about twice as high as that in the middle part. Much larger difference may occur in concrete walls, since they are usually up to 5 m high.
2. In the region of the wall with the highest permeability neutralization is accelerated by acid rain. In contrast, in a region with a lower permeability, neutralization is retarded by acid rain because the CO_2 gas diffusion is suppressed by an increase in the moisture content near the surface. It can be concluded that the influence of acid rain on the neutralization process may differ depending on the position in the concrete structure. Predictions using the average permeability value may underestimate the rate of the neutralization. Real concrete walls may have parts where the permeability is higher making them more susceptible to neutralization.
3. The results of this study will lead to a better evaluation of the durability of concrete walls. Although rain is believed to delay neutralization, the neutralization of parts with a high permeability is accelerated by acid rain.

References

[1] Mehta, P. K. and Monteiro, P., *Concrete Structure, Properties, and Materials*, Second Ed., Prentice Hall, New Jersey, 1993.

[2] Neville, A. M., *Properties of Concrete*, Fourth Ed., Longman, Edinburgh, 1995.

[3] Environment Agency of Japan (dir.), *Acid Rain—Whereabouts of Global Environment*, Chuohoki Publishers, Tokyo, Japan, 1998 (in Japanese).

[4] Kishimoto, Y., Hokoi, S., Harada, K., and Takada, S., “Influence of Acid Rain on Carbonation of Concrete Wall,” *Summaries of Technical Papers of Annual Meeting*, Architectural Institute of Japan, Tokyo, Japan, D-2, 2001, pp. 293–294 (in Japanese).

[5] Bamforth, P. B., “The Water Permeability of Concrete and its Relationship With Strength,” *Mag.*

Concrete Res., Vol. 43, No. 157, 1991, pp. 233–241.

[6] *Concrete Manual*, Second Ed., Japan Concrete Institute, Gihodo Shuppan, Tokyo, Japan, 1996.

[7] Saeki, T., Oga, H., and Nagataki, S., "Mechanism of Carbonation and Prediction of Carbonation Process of Concrete," *J. Japan. Soc. Civ. Eng.*, Vol. 12, No. 414, 1990, pp. 99–108 (in Japanese).

[8] Ogura, D. and Matsumoto, M., "An Analysis of Heat and Moisture Behavior in Underground Space by Qua-silinearized Method," *Proceedings of CIB W40 meeting*, Kyoto, Japan, 1997, 313–328.

[9] Hedenblad, G., "Moisture Permeability of Mature Concrete, Cement and Cement Paste," Ph.thesis, Division of Building Materials, Lund Institute of Technology, Sweden, 1993.

[10] Kishimoto, Y., Hokoi, S., Harada, K., Takada, S., and Watanabe, F., "Prediction Model for Carbonation of Concrete Structure Considering Heat and Moisture Transfer," *J. Struct. Constr. Eng.*, No. 595, 2005, pp. 17–23. (in Japanese).

[11] Kishimoto, Y., Hokoi, S., Harada, K., and Takada, S., "Influence of Water Movement on Neutralization of Concrete Structure," Summaries of Technical Papers of Annual Meeting, Architectural Institute of Japan, D-2, 2005, pp. 463–464 (in Japanese).

[12] Uomoto, T. and Takada, Y., "Factors Affecting Concrete Carbonation Ratio," *J. Japan. Soc. Civ. Eng.*, Vol. 17, No. 451, 1992, pp. 119–128 (in Japanese).

[13] *Chronological Scientific Tables*, National Astronomical Observatory, Maruzen, Tokyo, Japan, 1999 (in Japanese).

[14] Iyoda, T., Yajima, T., and Uomoto, T., "Effect of Existence of Cracks in Concrete on Carbonation Rate," *Proceedings of the Japan Concrete Institute*, Vol. 20, No. 2, 1998, pp. 979–984 (in Japanese).

[15] Ogishi, S., Tanahashi, I., Ono, H., and Mizutani, K., "An Evaluation of Concrete Durability Based on Tightness to Water Measured by Permeability Test," *Proceedings of the Japan Concrete Institute*, 1986, Vol. 8, pp. 113–116 (in Japanese).

[16] Japan Cement Association Committee on Durability of Concrete, "Effects of Acid Rain on Deterioration of Concrete, Accelerating Test due to Artificial Acid Rain," *Cement and Concrete*, No. 562, 1994, pp. 25–35 (in Japanese).

[17] Kobayashi, K., Uno, Y., and Mori, Y., "Deterioration Process of Concrete Structures Affected by Acid Deposition," *J. Japan. Soc. Civ. Eng.*, Vol. 35, No. 564, 1997, pp. 243–251 (in Japanese).

[18] Sato, T., Takewaka, K., Kamata, S., and Kuwahara, M., "Experimental Study on Deterioration of Concrete due to Acid Rain and Deterioration Control by Surface Coating," *J. Japan. Soc. Civ. Eng.*, Vol. 45, No. 634, 1999, pp. 11–25 (in Japanese).

www.astm.org

ISBN: 978-0-8031-3422-5
STOCK #: STP1495